博士論文

Clarifying catalysis of nitrogen-substituted mesoporous SBA-15 in CO_2 transformation

（CO_2 変換反応における窒素置換 SBA-15 の触媒作用解明）

山﨑　清行

1 Utilization of CO_2

1.1 Utilization of CO_2

Increasing the concentration of carbon dioxide (CO_2) emissions has been thought to trigger worldwide environmental problems, which disturb sustainable development of our society.[1] The methods of reducing CO_2 concentration in the atmosphere is divided into three: 1) conversion for relieving the amount of CO_2 emission or reduction of CO_2 emission in the atmosphere, 2) preservation of CO_2 in the deep seabed, which is said carbon capture and storage(CCS) in other word. 3) Utilization of CO_2 into chemical products which is said carbon capture and utilization (CCU) in other words.

1.1.1 Conversion for relieving the amount of CO_2 emission or reduction of CO_2 emission in the atmosphere

It is thought that a major problem in the world caused by greenhouse gas emission is climate change. Measures for climate change have been divided into three types; mitigation, adaptation and compensation. Mitigation is reduction of greenhouse gas emission to prevent further climate change in the future. Adaptation is relieving damage of climate change that is already happened. Compensation is supports by money, insurance and human for irreversible damage of climate change that adaptation cannot recover. Now, mitigation and adaptation is required to be enhanced for preventing irreversible damage.

Paris agreement mainly discussed about mitigation. The agreement set long term goal that increase of annual average temperature is suppressed under 2 K and Both emission and absorption of greenhouse gas is balanced until latter half of this century. To achieve this scenario, the greenhouse gas concentration converted to CO_2 been had to suppress under about 450 ppm until 2100. And greenhouse gas emission is required to reduce 40 to 70% of the

amount of CO_2 emission in 2010.

Various measures are considered for huge CO_2 emission reduction and divided into four types: 1) reduction of energy consumption, 2) conversion to energy derived from low carbon or non-carbon energy carrier, 3) diversification of energy resource and 4) reduction of greenhouse gas emission except the one derived from combustion of carbon resource and increase of forest for CO_2 adsorption. Type 1) is tried to be achieved by reduction of energy demand and improvement of energy efficiency. Cellulose nanofiber is one of the materials that achieve weight saving of automobiles and improvement of fuel efficiency[2]. Mean for achievement of type 2) is expansion of utilizing renewable resource. Policies for achievement of type 3) are, for example, alternation from gasoline-powered vehicle to electrically-powered vehicle and utilization heat pump for air conditioning and hot water supply system.

1.1.2 Preservation of CO_2 in the deep seabed.

The amount of CO_2 emission in the world is about 33 billion ton, and 3.5% of it is occupied in Japan. According to Paris agreement, it is expected that 4.2 billion ton of CO_2 emission, which is 13% of required CO_2 reduction per year is reduced by CCS until 2050.

Technology of CCS is closely related to Enhanced Oil Recovery (EOR)[3-5]. Most of oil in oil well is penetrated in small pore in rocks. The methods of oil recovery are divided into three stages; the primary recovery is oil recovery by self-injection and pump. This method is simple and not required complex equipment. But only 25% of buried oil is recovered at most. In the secondary recovery, remained oil is pushed out by water flooding or natural gas injection. Oil layer in crude oil is pressurized by injection water or natural gas and remained oil is recovered. Oil yield improves up to 60% by this operation. The third recovery attempts to recover remained oil even by secondary recovery and is said enhanced oil recovery in other word. Remained oil is

high viscosity and low fluidity. Therefore, to improve liquidity of remained oil, Steam, CO_2 or surfactant is injected into crude oil. According to impregnant, they are called Steam flooding, Carbon dioxide flooding, detergent flooding, respectively. Especially, carbon dioxide flooding is attractive as realizing CO_2 utilization and improving oil yield. Part of this technology has been used in CCS.

Currently, space of CO_2 storage is limited to oil layer in thin sandstone because EOR technology can apply. However, Most of lands and sea in Japan is located at fluctuation zone where earth's crust drastically change, and they are unsuitable for CO_2 storage because leakage can be occur with change of earth's crust. For achieving required CO_2 reduction, larger space for CO_2 storage should be needed. Therefore, searching the candidate sites is carried out frequently and huge space under the seabed or plateau in the sea is proposed. CO_2 reacts with minerals especially quartz in the seabed and forms silicate mineral. Silicate mineral can trap CO_2 firmly. Therefore mineral layer in the seabed can be one of the candidates. And, if searching area is extended to Exclusive Economic Zone of Japan, sea mountain and sea plateau is suitable for CO_2 storage. Major problem is remoteness from main land. It is expected to overcome the cost of transportation for huge CO_2 storage.

1.1.3 Utilization of CO_2 for chemical products

CCU is the main topic for chemical industry to contribute to reduction of CO_2 emission. CO_2 can be considered as one of the sustainable C1 resources to form complex organic products.[6, 7] If a high-valued chemical product is able to be produced by CO_2 insertion, utilization of CO_2 is attractive. This process is required to be superior to the conventional manufacturing process of chemical products in CO_2 emission in order to replace it as the method of CO_2 reduction.

CO_2 transformation is divided into two types of reactions; reduction and acid-base reactions.

Low carbon products include about ten carbon atoms at most and are mainly produced by the reduction of CO_2. Low carbon products such as alkane and alcohol are used as an energy carrier. On the other hand, high value-added chemical compounds, such as carbonate, carboxylic acid, and lactone, have been produced by the acid-base reactions. The carbon atom in CO_2 is polarized positively by the adjacent oxygen atoms and CO_2 could be activated by a nucleophilic attack against the carbon atom. Therefore, an electron-donating base catalyst could be applied for CO_2 transformation.

Dimethyl carbonate (DMC) works as a methylating agent, a carbonylating agent, and an octane booster.[6] DMC forms from methanol and CO_2 by ZrO_2.[8] Water also forms as a by-product via this reaction. Therefore, the conversion is low by 1 % because the equilibrium leans to materials without any treatment. The conversion is improved to 95 % by adding dehydrating agent.[9]

Diethyl carbonate (DEC) works as an alkylating agent and a fuel additive. DEC formation from ethanol and CO_2 is an ideal reaction without by-products. Base catalyst CeO_2-ZrO_2（Ce/（Ce+Zr）=0.2） is a solid solution and found to catalyze the reaction for the first time.[10] After the report, the yield is improved to 42 % by CeO_2 and adding acetonitrile as dehydrating agent.[9]

1.2 Solid base catalyst

Solid catalysts, such as transition metal, transition metal oxide and typical element oxide, are classified into a heterogeneous catalyst. The heterogeneous catalyst is advantageous to a homogeneous catalyst in respect of separation of the catalyst and reaction products. On the other hand, a metal complex, dissolved cation, and anion works as a homogeneous catalyst. Reaction rate of homogeneous catalyst is generally superior to that of a heterogeneous catalyst because a contact area between materials and heterogeneous catalyst is limited. Characters of both catalysts are shown in Table 1-1.

Table 1-1. Rough classification heterogeneous and homogeneous catalyst.

	Heterogeneous	Homogeneous
Form of catalyst	Supported metal, metal oxide and porous materials	Solved anion, cation and metal complex
Reaction phase	solid phase / fixed bed	liquid phase
Catalytic activity	High	Low
Selectivity	Low	High
Separation of catalyst and product	Easy	Difficult
Recycle of catalyst	Easy	Difficult

In acid-base reaction by the heterogeneous catalyst, solid acid catalyst is widely used in chemical industries. Synthetic zeolite is the representative example of solid acid catalyst. Zeolite Y brought an innovation in fluid catalytic cracking (FCC) process. [11, 12] In 1962, Mobil applied rare-earth exchanged form Zeolite X and Y for FCC catalyst. In 1972, ultrastable Y zeolite was produced by dealumination and used as the catalyst that improved octane number.[13] Currently, Almost all FCC catalyst is based on rare earth exchanged form ultrastable Y zeolite.

On the other hand, few solid base catalysts have been industrized. The main problem has been deactivation of the catalyst by water and CO_2. Water and CO_2 adsorb on the basic site of the catalyst and the catalytic activity is retarded because these molecules have a high affinity to the basic site. However, in organic chemistry, various high carbon number and high value-added chemical compounds, such as carbonate, carboxylic acid, and lactone, have been produced by base reactions. If the problem is overcome, the potential of solid base catalyst is able to be opened up. Typical solid base catalysts are summarized in table 1-2.[14]

Table 1-2. Typical solid base catalysts[14].

Metal oxides	MgO, CaO, Al_2O_3 ZrO_2 La_2O_3, Rb_2O
Mixed oxides	SiO_2･MgO, SiO_2･CaO, MgO･La_2O_3, MgO･Al_2O_3(calcined hydrotalcite)
Alkali or alkaline earth oxides on support	Na_2O/SiO_2, MgO/SiO_2, Cs oxides supported on zeolites
Metal oxynitrides and metal nitrides	AlPON, partially nitrided zeolites and mesoporous silica
Alkali compounds on support	KF/Al_2O_3, K_2CO_3/Al_2O_3, KNO_3/Al_2O_3, $NaOH/Al_2O_3$, KOH/ Al_2O_3
Amides, imines on support	KNH_2/Al_2O_3, K, Y, Eu supported on zeolites from the ammoniacal solution
Alkali metals on support	Na/Al_2O_3, K/Al_2O_3, K/MgO, Na/zeolite
Anion exchangers	Anion exchange resins, hydrotalcite and modified hydrotalcite
Zeolites	K, Rb, Cs-exchanged X,Y zeolite, ETS10
Clays	Sepiolite, Talc
Phosphates	Hydroxyapatite, metal phosphates, natural phosphates
Amines or ammonium ions tethered to a support	Aminopropyl group / Silica, MCM41, SBA15 Alkylammonium group/MCM41

Solid base catalyst is superior to a homogeneous one in respect to flexibility of solvent selectivity. When a homogeneous catalyst is applied for a certain reaction, solvent is normally required to dissolve both reactants and catalysts. The candidate for the solvent is a polar one, such as ethyl chloride and dimethyl sulfoxide. However, such a polar organic solvent is not environmentally friendly and is required not to be used. Furthermore, the boiling point of the polar solvent is usually low. It is unsuitable for reactions that need high temperature. A solid base catalyst has a potential to overcome these problems, because solid base catalyst does not have to be dissolved.

A solid catalyst is normally superior to a homogeneous catalyst in respect to economy. It takes a lot of time and efforts for separation of products, such as distillation, recrystallization, and chromatography over a homogeneous catalyst because products, reactants, and catalysts are included in the solution. On the other hand, it is easy to separate products over solid catalyst because filtration is available. It is afraid an acid or basic homogeneous catalyst corrodes reaction equipment. Solid catalyst is hard to corrode because a contact area of wall and catalyst is limited.

1.2.1 Well-studied solid base catalysts

1.2.1.1 Alkaline earth metal oxides

Alkaline earth metal oxides have been known for a long time as one of solid base catalysts. Some of them have been applied for organic synthesis. For example, MgO, which is one of the solid base catalysts, synthesized by pyrolysis of $Mg(OH)_2$ at 873 K in vacuum. MgO catalyzes Henry reaction[15] (Figure 1-1) and Michael reaction[16](Figure 1-2).

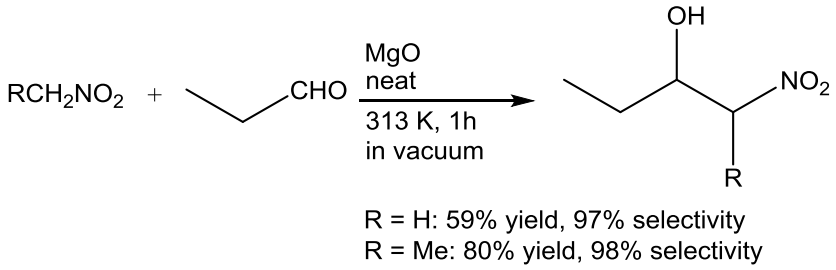

Figure 1-1. The Henry reaction on MgO

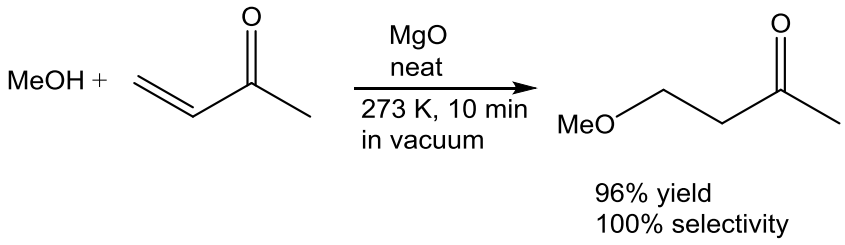

Figure 1-2. The Micheal reaction on MgO

A solid base catalyst is in general easy to be deactivated by water and CO_2. However, MgO maintained its activity to these two reactions even if it was left in the air. Furthermore, it was reported that formation of 3-methoxy-1-propanol from methanol and ally alcohol on MgO occurred in anti-Markownikov fashion[17](Figure 1-3). It is considered that the surface structure of MgO is related to the phenomena. However, the detail reaction mechanism is unclear.

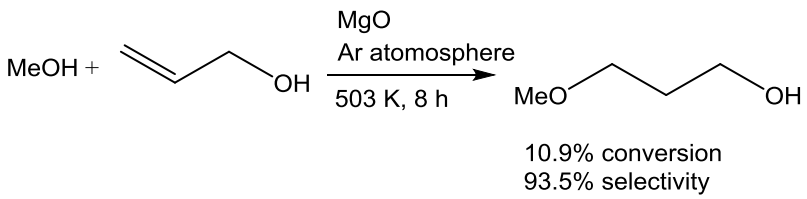

Figure 1-3. Formation of 3-methoxy-1-propanol from methanol and ally alcohol on MgO

1.2.1.2 Hydrotalcite

Hydrotalcite is one of the layered clay minerals. It is formed by substituting aluminium ion (Al^{3+}) for a part of magnesium ion (Mg^{2+}) in structure of Brucite, whose chemical formula is $[Mg_3(OH)_6]$. Brucite is charged positively and carbonate anion is inserted between layers so as to keep electrical neutrality (left side of Figure 1-4). The width of a layer is 0.48 nm and the distance of layers is 0.34 nm. Mg-Al mixed oxide is formed by calcination of hydrotalcite and works as base. It was reported that hydration of the formed Mg-Al mixed oxide led to recover the layered structure and hydroxide ion is introduced between layers with enhancing the basicity.[18, 19](Fig. 1-5)

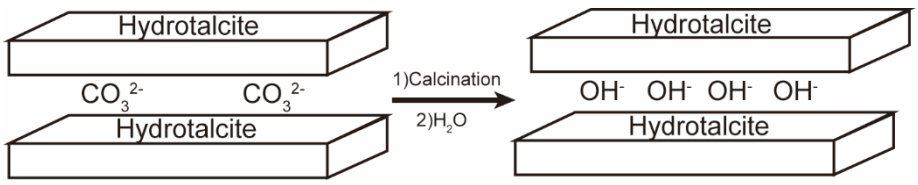

Figure 1-4. Preparation of hydroxide-exchanged hydroxytalcite.

Hydrotalcite synthesized by hydration of the mixed oxide formed from $Mg(NO_3)_2 \cdot 6H_2O$ and $Al(NO_3)_3 \cdot 9H_2O$ catalyzed Claisen-Schmidt condensation with high yield and selectivity[20]. 2',4,4'-trimethoxychalcone, which is known to helpful pharmaceuticals, is synthesized via this reaction.(Figure 1-5)

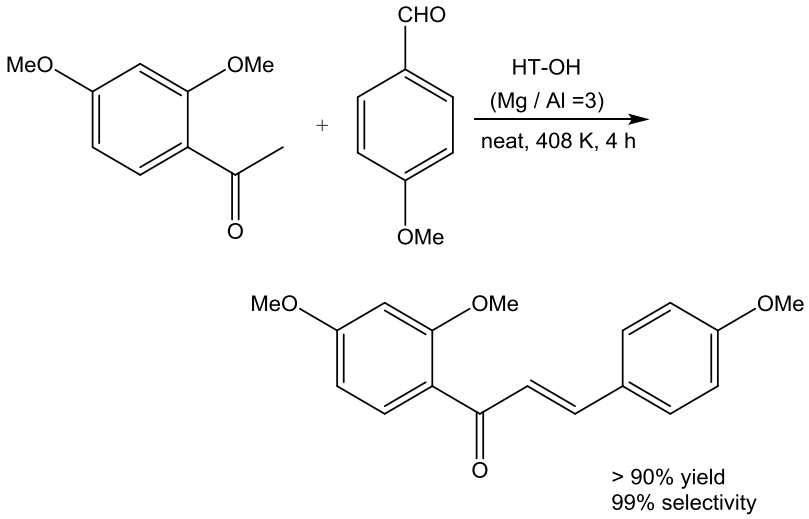

Figure 1-5. Formation of 2',4,4'-trimethoxychalcone (Claisen-Schmidt condensation).

1.2.1.3 Supported potassium fluoride and potassium hydroxide

Alumina supported potassium fluoride is conventionally used in organic synthesis as a solid base catalyst. It catalyzes reduction of benzaldehyde by triethylsilane[21], protection of phenolic hydroxyl group by 2-(trimethylsilyl)ethoxymethyl chloride (SEM-Cl)[22], and selective deprotection[23].

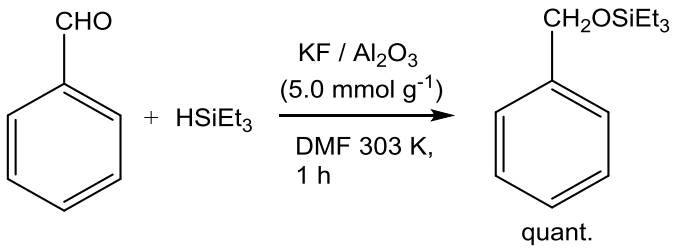

Figure 1-6. Reduction of benzaldehyde by triethylsilane.

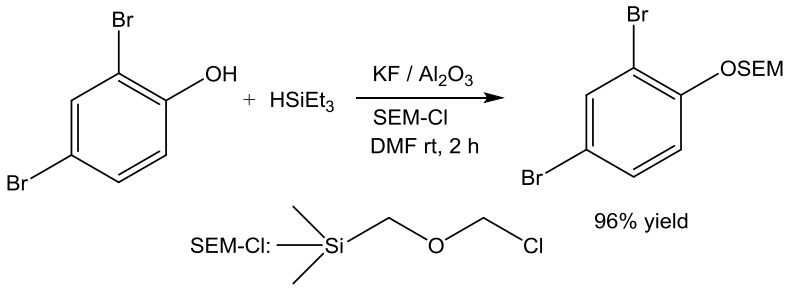

Figure 1-7. Protection of phenolic hydroxyl group by SEM-Cl.

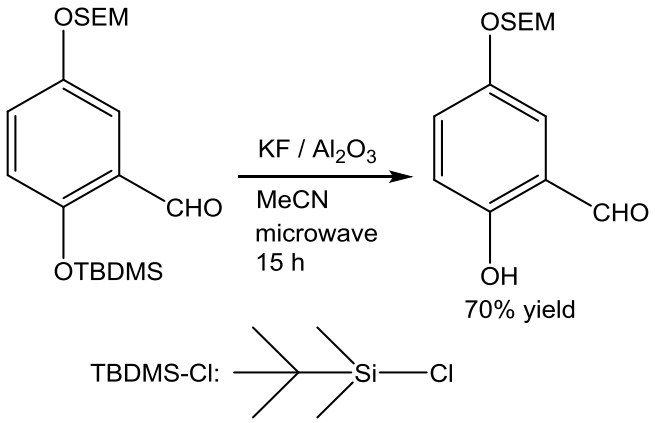

Figure 1-8. Selective deprotection.

KOH / Fe_2O_3 is one of the solid base catalysts supported metal oxide. It was reported that the asymmetric P−C bond formation over KOH / Fe_2O_3 was achieved for the first time via a Fe_2O_3-mediated conjugate addition of a chiral phosphite to alkylidene malonates[24]. It was unique that the yield and diastereomeric excess decreased when other supports, such as Al_2O_3 and ZnO, used instead of Fe_2O_3

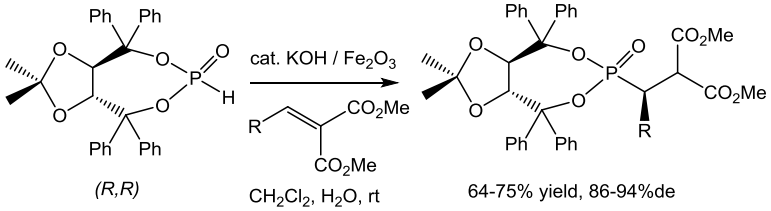

Figure 1-9. Selective deprotection

1.3 Nitrogen-substituted mesoporous silica

Mesoporous silica materials, which is proposed in the 1990s,[25, 26] have attracted a lot of interest because of their unique porous frameworks with wide applications.[27-29] It is expected that large molecules adsorb inside the mesopores larger than micropores zeolite has.

Nitrogen-substituted mesoporous silicas, such as NMCM41 and NSBA15, have been proposed as a solid base catalyst.[30, 31] NSBA15 possesses 2D hexagonal mesoporous structure, uniform pore size, and high surface area. It is synthesized by substitution of nitrogen atom for oxygen atom in the silica framework via nitridation.[32] Nitridation is applied to mesoporous silica for the first time is synthesis of ICMUV6 in 2001[33]. Since the first report, some groups have investigated the nature of nitrogen substituted mesoporous silica in terms of nitridation mechanism[34-37], catalysis[34, 38-40], characterization[41-46], and applications[47].

1.3.1 Synthesis of nitrogen-substituted mesoporous silica

Most of nitrogen–substituted silica materials are prepared by nitridation of them. Silica materials are zeolites (FAU[44, 48-58], MFI[40, 49, 58-64], BEA[65], FER[44, 61]), zeolite analogs (Aluminophosphates[40, 49, 66, 67], SAPO34[42]) , mesoporous silica (MCM41[36, 47, 68-70], MCM48[39, 45, 69], SBA15[34, 35, 40, 43, 46, 47, 69], ICMUV6[33]) and fibrous silica (KCC1[38, 41, 47]). Oxygen atoms of silica materials are substituted by nitridation under flow of ammonia gas at high temperature. Nitrogen substitution rates of silica samples are controlled by the amount of ammonia supply per sample weight and temperature. The amount of nitrogen substitution depends on the total surface area derived from structure of silica materials.

Nitridation setup is shown in Figure 1-10.[36] Silica sample is put on ceramic boat and inside quarts tube. This sample is then kept in a temperature programmable furnace under N_2 gas flow for several tens of minutes. Next, the temperature is raised and when the temperature rise over

643 K, the material is flushed with NH_3 gas. After the temperature is maintained at designated one for several hours, the furnace and sample are allowed to cool. When the temperature decreases below 643 K, the flush gas is switched to N_2. The sample is left inside the furnace to cool to room temperature.

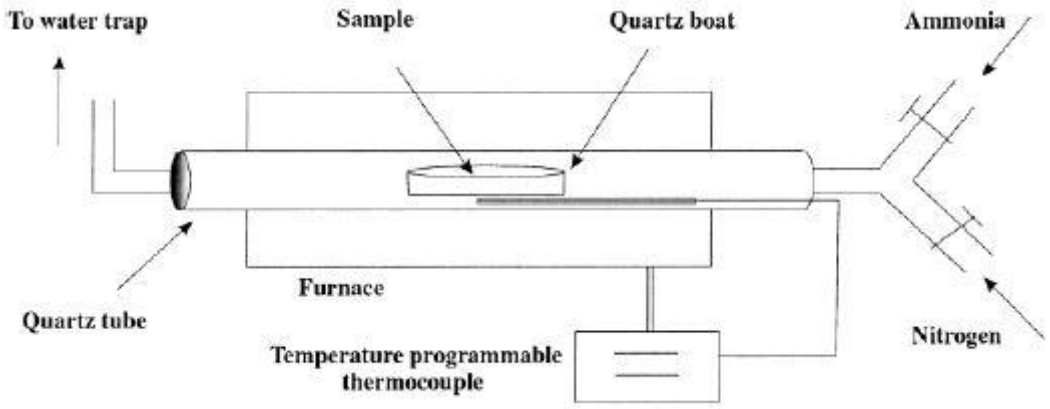

Figure 1-10. Nitridation experimental set–up[36]

The nitrogen substitution process is changed by temperature (Scheme 1). Nitridation starts over 643 K and the rate of nitrogen substitution increase with increasing of temperature. Chino and Okubo investigated nitrogen substitution mechanism of SBA15 by varing temperatures between 873 and 1273 K.[35] the following reactions (1)–(6) may take place on the surface at 873 K. Primary amine forms from silanol and NH_3 by direct dehydration (1). Dehydration of silanols also proceeds and oxy–radicals generates according to reaction (2). The oxy–radicals (≡Si−O· and ≡Si·) are located next to each other and primary amine also forms by reactions (3) and (4) or reactions (5) and (6).In addition to reactions (1)–(6), secondary amine forms by reaction (7) at 973 K.

At 1073 K, decomposition of NH_3 creates radical atomic hydrogen according to reaction (5) and radical atomic hydrogen decomposes siloxane bridging bonds. Net reaction of reaction (5) and (8) is reaction (9). Primary amine forms from siloxane bridging bond. Therefore, the amount of

nitrogen substitution at 1073 K is more than that at 973 K.

Polshettiwar, et al. referred to similar tendency.[34] They investigated nitrogen substitution content of SBA15 between 500 K and 1200 K. They claim that if the nitrogen substitution involves only replaced silanol to the primary amine, the number of effective silanols on the surface of SBA15 is the limiting factor for the content of nitrogen substitution. The same concentration is available on the calcined SBA-15 if the nitrogen substitution condition is same. Hence, the limit content of nitrogen substitution is irrespective of nitrogen substitution temperature. However, the content of nitrogen substitution increases with increasing reaction temperature, meaning that nitrogen substitution would take place through other mechanism, the attack of NH_3 on the siloxane bridging bond.

At 1173 K, reaction (7) proceeded more than at 1073 K. Secondary amine increases with decreasing primary amine by net reaction of reactions (1), (7), (9) rewritten as reaction (10). At 1273 K, tertially amine is formed from secondary and primary amine according to reaction (11). The bridging bond (secondary amine) decomposes and the mesoporous structure is condensed.

The content of nitrogen substitution relates to the total gas flow of ammonia supplied per sample weight. Hayashi, et al. examined effects of nitrogen substitution condition over various MCM41 samples (pM41s).[69] The nitrogen substitution condition and the characters of the MCM41 samples (nM41s) are summarized in Table 1-3. Subscripts of CS and WG mean colloidal silica and water glass, respectively, which were used as silica source.

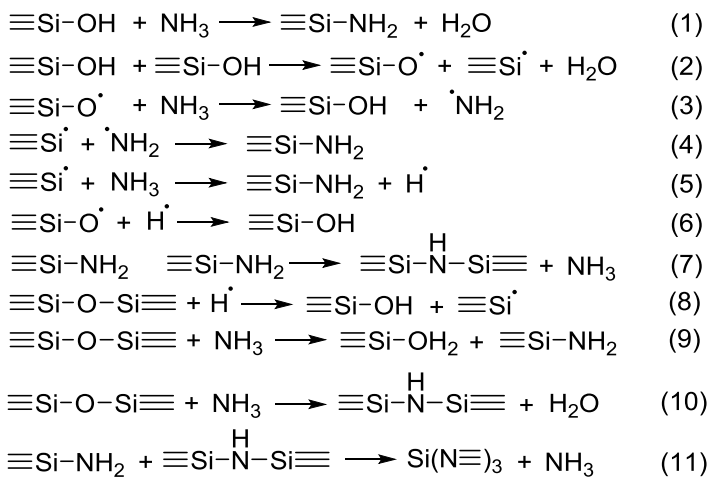

Scheme 1-1. The nitrogen substitution reaction.[35]

Figure 1-11 shows that correlation between the content of nitrogen of nM41s and the total gas flow of NH_3 supplied at 1273 K. The nitrogen amount increased gradually at 0–2000 L_{NH3} g^{-1}, and saturated above 2000 L_{NH3} g^{-1}. The maximum content was about 38 wt%, which is Si_3N_4. This means nitrogen substitution of MCM41 almost complete above 2000 L_{NH3} g^{-1}. The substitution rate was independent of pore size of pM41 as the nitrogen content of all nM41s formed from pM41s increases linearly with increasing the total amount of NH_3 supplied. An effect of pore structure was also investigated.

Figure 1-12 summarizes the dependencies of the amount of nitrogen substitution of SBA15(nSBA15), MCM48 (nM48s) and silica gel (n–silica gels). It shows the linear correlation is observed on all examined silica samples. The maximum content of mesoporous silica is similar but the minimum total amounts of NH_3 supplied by which nitrogen content reach maximum is different from pore size and structure.

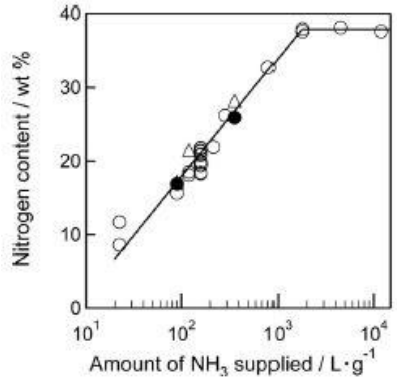

Figure 1-11. The nitrogen amount of nM41–16_{CS} (white circle), nM41–16_{WG} (white triangle), and nM41–22 (black circle) on the total gas flow of NH_3 supplied per weight at 1273 K. the subscripts of CS and WG mean colloidal silica and water glass, respectively, which were used as silica source.[69]

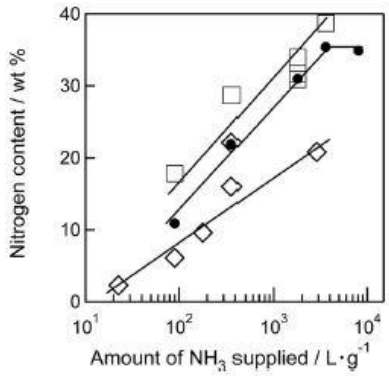

Figure 1-12. The nitrogen contents of nSBA15 (black circle), nM48–16 (white square), and n–silica gel (white diamond) as a function of the amount of NH_3 supplied per weight at 1273 K[69]

Table 1-3. Characters of parent (p), heated (h), and nitrogen–substituted (n) mesoporous silica(MS).[69]

Entry	Sample	Nitridation conditions				Nitrogen content	a	D	T	S_{int}		S_{ext}	V		ρ
		Weight / g	t / h	NH_3 flow rate / L·min^{-1}	Total NH_3 / L·g^{-1}	/ wt.-%	/ nm	/ nm	/ nm	Measd. / m^2·g^{-1}	Theor. / m^2·g^{-1}	/ m^2·g^{-1}	Measd. / mL·g^{-1}	Theor. / mL·g^{-1}	/ g·cm^{-3}
1	n-M41-16$_{CS}$	0.2	0.25	0.3	22.5	11.7	–[a]	–[b]	–[b]	654	–[b]	92	0.53	–[b]	2.49
2	n-M41-16$_{CS}$	0.2	1	0.3	90	15.4	3.87	2.92	0.95	576	592	148	0.41	0.42	2.59
3	n-M41-16$_{CS}$	1.5	4	1	160[c]	21.3	3.91	2.85	1.06	555	501	48	0.34	0.34	2.73
4	n-M41-16$_{CS}$	0.2	4	0.3	360	27.5	3.90	2.87	1.03	563	487	69	0.33	0.34	2.89
5	n-M41-16$_{CS}$	0.2	10	0.6	1800	37.9	3.75	2.60	1.15	412	397	138	0.25	0.25	3.15
6	n-M41-16$_{CS}$	0.2	50	0.8	12000	37.6[d]	3.87	2.55	1.32	303	341	204	0.21	0.21	3.14
7	p-M41-16$_{CS}$[e]	–	–	–	0	0	4.64	3.81	0.83	826	–	115	0.72	–	2.20
8	h-M41-16$_{CS}$[f]	0.2	0	0	0	0	4.44	3.57	0.87	758	–	141	0.65	–	2.20
9	n-M41-16$_{WG}$	0.2	1	0.3	90	16.8	3.78	2.73	0.92	597	573	44	0.34	0.36	2.62
10	n-M41-16$_{WG}$	0.6	4	0.3	120[c]	19.3	3.74	2.71	1.03	622	573	45	0.34	0.36	2.68
11	n-M41-16$_{WG}$	0.2	4	0.3	360	27.9	3.68	2.79	0.89	610	613	35	0.38	0.40	2.90
12	p-M41-16$_{WG}$[e]	–	–	–	0	0	4.57	3.86	0.71	967	–	52	0.83	–	2.20
13	h-M41-16$_{WG}$[f]	0.2	0	0	0	0	4.49	3.71	0.78	913	–	39	0.74	–	2.20
14	n-M41–22	0.2	1	0.3	90	16.9	4.59	3.39	1.20	482	472	109	0.37	0.38	2.62
15	n-M41–22	0.2	4	0.3	360	25.9	4.46	3.24	1.22	450	427	104	0.32	0.32	2.85
16	p-M41–22[e]	–	–	–	0	0	5.76	4.94	0.82	804	–	223	0.91	–	2.20
17	h-M41–22[f]	0.2	0	0	0	0	5.54	4.73	0.81	804	–	215	0.89	–	2.20
18	n-SBA15	0.2	1	0.3	90	10.9	10.54	8.88	1.66	436	456	55	0.73	0.73	2.47
19	n-SBA15	0.2	4	0.3	360	21.9	10.20	8.63	1.56	406	434	37	0.68	0.68	2.75
20	n-SBA15	0.2	10	0.6	1800	31.0	10.03	8.42	1.61	338	393	72	0.64	0.60	2.98
21	n-SBA15	0.2	20	0.6	3600	35.2	9.88	8.05	1.83	303	339	60	0.60	0.49	3.08
22	n-SBA15	0.2	30	0.6	8100	34.9	9.52	7.72	1.80	298	345	58	0.60	0.48	3.07
23	p-SBA15[e]	–	–	–	0	0	11.66	10.24	1.42	668	–	103	1.02	–	2.20
24	h-SBA15[f]	0.2	0	0	0	0	10.99	9.33	1.66	511	–	87	0.86	–	2.20
25	n-M48–16	0.2	1	0.3	90	17.8	7.64	2.70	1.12	743	723	44	0.45	0.45	2.65
26	n-M48–16	0.2	4	0.3	360	28.6	7.27	2.51	1.10	686	671	46	0.39	0.39	2.92
27	n-M48–16	0.2	10	0.6	1800	34.0	7.27	2.35	1.18	610	598	84	0.33	0.32	3.05
28	n-M48–16	0.2	20	0.6	3600	38.7	7.12	1.95	1.33	408	510	107	0.23	0.23	3.17
29	p-M48-16[e]	–	–	–	0	0	8.59	3.69	0.93	1051	–	65	0.90	–	2.20
30	h-M48-16[f]	0.2	0	0	0	0	8.37	3.21	1.10	887	–	78	0.66	–	2.20
31	n-silica gel	0.2	1	0.3	90	6.1	–	–[b]	–	–[b]	–	–[b]	–[b]	–	2.35
32	n-silica gel	0.2	4	0.3	360	16.0	–	10.4	–	156	–	32	0.47	–	2.60
33	n-silica gel	0.1	8	0.6	2880	20.8	–	–[b]	–	–[b]	–	–[b]	–[b]	–	2.72
34	p-silica gel[e]	–	–	–	0	0	–	11.3	–	215	–	25	0.63	–	2.20
35	h-silica gel[f]	0.2	0	0	0	0	–	10.8	–	149	–	32	0.53	–	2.20

[a] Not measured. [b] Not calculated because of no measurement of the lattice constant using XRD. [c] NH_3 was started to flow onto the sample at 973 K and the sample was heated at 1273 K in NH_3 and treated under the conditions listed in the table. [d] Nitrogen and oxygen contents determined by the nitrogen/oxygen analyzer were 37.8 and 5.7 wt.-%. [e] Parent silica samples. [f] Samples after heating p-MS at 1273 K in a flow of N_2.

In Figure 1-13, the content of nitrogen substitution at 100 L_{NH3} g^{-1} were plotted as a function of the surface areas of silica samples heated for the nitrogen substitution to identify the reasons for differences of the amount of substitution derived from various silica samples. Linear correlation observed and showed that the amount of substitution was related to surface area of the parent silicas.

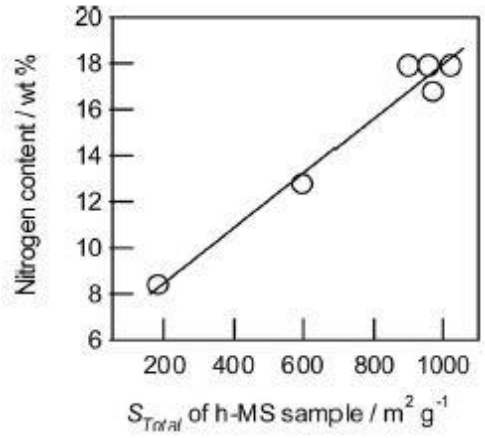

Figure 1-13. Correlation between the nitrogen amount of n–MS at 100 L_{NH3} g^{-1} and the total surface area of h–MS.[69]

1.3.2 Characterization of nitrogen-substituted mesoporous silica

Various analyses, such as powder X-ray diffraction (XRD), nitrogen adsorption measurement, Fourier transform infrared (FT-IR) spectroscopy, elemental analysis, X-ray photoelectron spectroscopy (XPS), and magic angle spinning nuclear magnetic resonance (MAS-NMR) is utilized for characterization of nitrogen-substituted mesoporous silica.

1.3.2.1 Nitrogen adsorption/desorption isotherms

Figure 1-14, 15, 16 is nitrogen adsorption measurement of SBA15, MCM41, ZSM5 and nitrogen–substituted materials of these (NSBA15, NMCM41, NZSM5).[46, 64, 68] The parent SBA15 possessed mesopores. This porous structure was maintained even after the nitrogen substitution process.

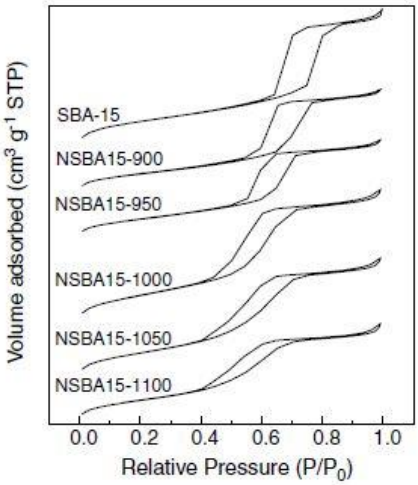

Figure 1-14. Nitrogen adsorption measurement over pure SBA15 and NSBA15[46]

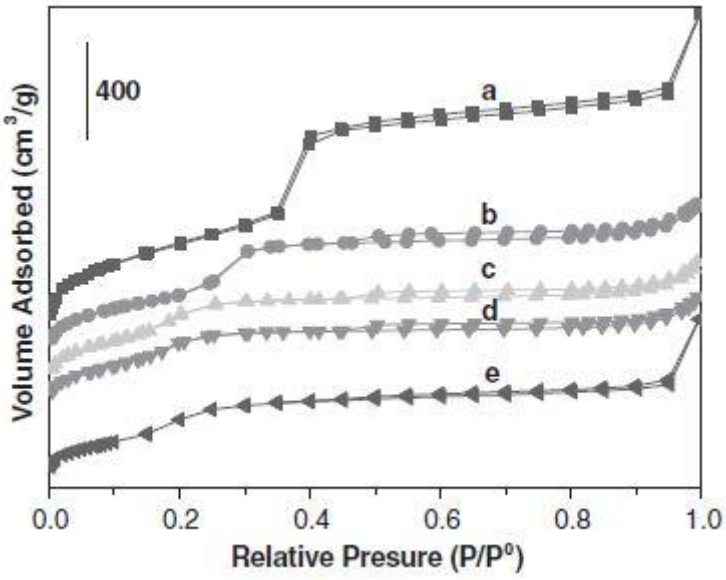

Figure 1-15. Nitrogen adsorption measurement of MCM-41 (a), nitrogen—substituted MCM-41 at 873 K (b), at 1073 K (c), at 1173 K (d) and at 1223 K (e). in constant NH_3 flow (0.4 L min^{-1}) for 12 h [68]

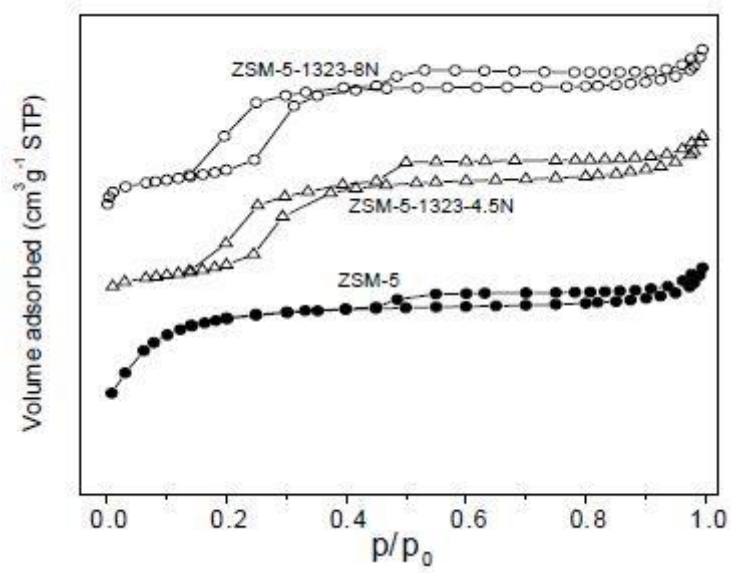

Figure 1-16. Nitrogen adsorption–desorption isotherms of ZSM–5 and nitrogen–substituted ZSM–5 at 1323 K for 4.5–8 h in constant NH_3 flow (0.5 L min^{-1})[64]

1.3.2.2 X-ray diffraction patterns

Figures 1-17 and 18 are low–angle XRD patterns of parent and nitrogen-substituted SBA-15 and MCM-41. Three characteristic peaks attributed to (100), (110), and (200) planes of 2D-hexagonal periodic structure were observed in all the samples. After nitrogen substitution, the three peaks were shifted to a larger angle, which suggests that the high–temperature nitrogen substitution process causes the shrinking of the mesoporous structure without collapsing the periodic structure.

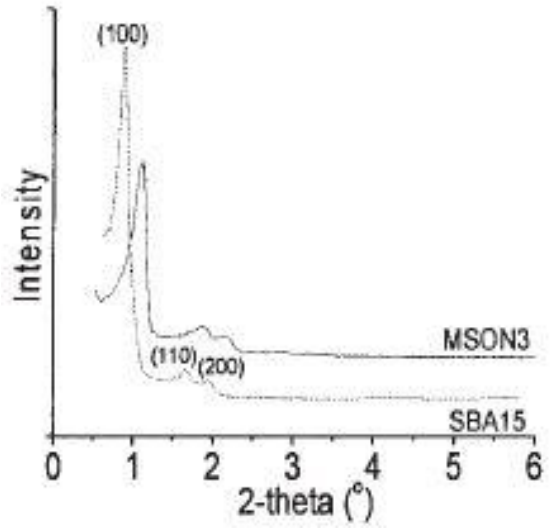

Figure 1-17. Low–angle XRD measurement over SBA15 and NSBA15 (MSON3) in constant NH_3 flow (0.5 L min^{-1}) nitrogen–substituted at 1323 K for 18 h[40]

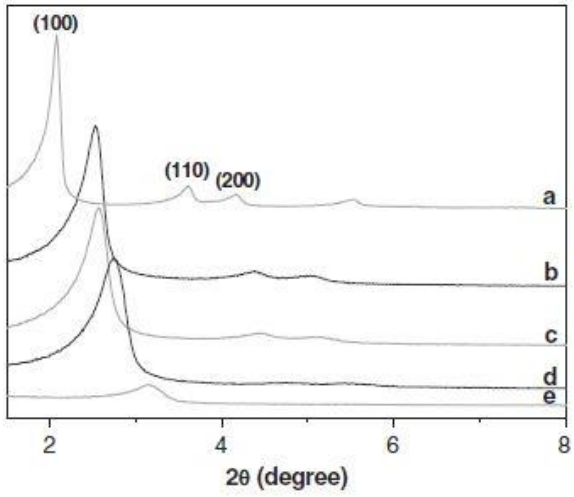

Figure 1-18. XRD measurement over MCM41 and of nitrogen–substituted MCM41 at 1073–1273 K: MCM41 (a), nitrogen–substituted MCM41 at 1073 K (b), at 1173 K (c), at 1223 K (d) and at1273 K (e) in constant NH_3 flow (0.4 L min^{-1}) for 12 h [68]

1.3.2.3 Fourier transform infrared (FT-IR) spectra

The surface groups formed by nitrogen substitution at 873-1273 K were observed by FT–IR. Figures 1-19, 20 and 21 show FT–IR spectra of calcined, nitrogen–substituted SBA15, and

KCC–1.[35, 38, 46] The type of formed surface groups on nitrogen–substitution was studied by identifying three surface groups, the HOSi≡, H_2NSi≡ and ≡SiHNSi≡. The IR spectrum of SBA15 shows a OH peak due to a silanol group at 3750 cm^{-1}. The intensity of the silanol peaks of NSBA15–873 was lower than the silanol of parent SBA15, and new peaks observed at 3452 and 3530 cm^{-1} that are due to $\nu_s(H_2N)$ and ν_{as} (H_2N) of the H_2NSi≡ surface group, respectively. These results indicate that the H_2NSi≡ group was formed according to the reaction (1) After nitrogen substitution at 973 K, the silanol groups become more intense than that of NSBA15–873, and a new broad band observed at 3396 cm^{-1} that is due to ν (HN) of ≡SiHNSi≡. This result indicates that the ≡SiHNSi≡ was formed by the reaction (2), which is the dehydration of H_2NSi≡ and HOSi≡. The IR spectrum obtained after the nitrogen substitution at 1073 K is like that of NSBA15–973. The difference between NSBA15–973 and 1073 is just the intensity of the silanol. In the case of NSBA15–1173, the IR peaks at 3452 cm^{-1} and 3530 cm^{-1} were not observed. Furthermore, the IR peak due to ν (NH) of ≡SiHNSi≡ in NSBA15–1273 was much more intense than that of NSBA15–1173.

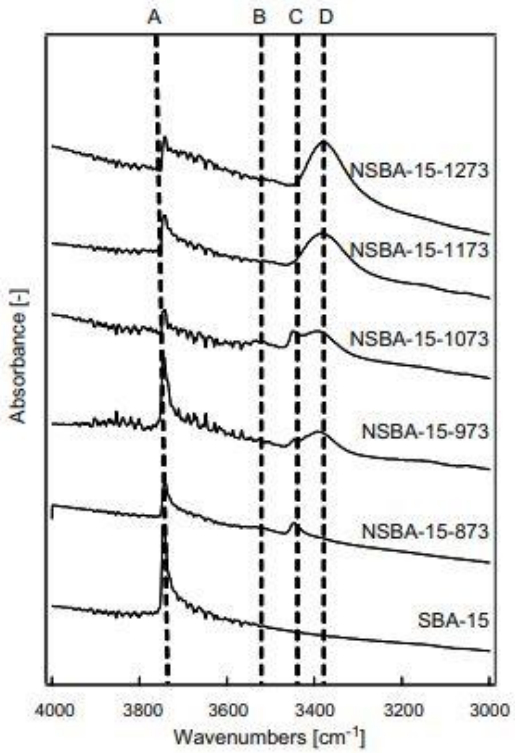

Figure 1-19. IR spectra of SBA15 and NSBA15 samples. The peak positions of (A) ν (HOSi), (B) ν_s (H_2N), (C) ν_{as} (H_2N), and (D) ν(NH)[35]. The end number of NSBA15 is nitrogen substitution temperature (K).[46]

Figure 1-20 shows FT–IR spectra of SBA15 and nitrogen–substituted SBA15 under 2000 cm^{-1}. In the SBA15, main IR peaks related to SBA15 framework are assigned to the asymmetric and symmetric stretching vibration of Si–O–Si at 1086 cm^{-1} and 804 cm^{-1} respectively. The peaks at 966 cm^{-1} and 1635 cm^{-1} corresponded to the O–H stretching of the surface silanols. The asymmetric Si−O−Si stretching vibration at 1086 cm^{-1} became broad and shifted to a lower wave number (1060 cm^{-1}) by nitrogen substitution in Figure 1-20 (A). With increasing temperatures, the Si–O–Si (ν_s) peak at 804 cm^{-1} and the Si–OH (ν_s) peak at 966 cm^{-1} gradually disappeared, and a new peak at 948 cm^{-1} appeared and became clear.

The broadening and shifting of the peak of the 948 cm^{-1} and the stretching peak at 1086 cm^{-1} with increasing nitrogen substitution temperature can reflect disorder of the framework and a bond strain by the substitution of nitrogen into the framework. Along with that the peak observed at 1200 cm^{-1} is due to N–H in Si–HN–Si.[46] In Fig. 1-20(B), the peak at 1547 cm^{-1} is due to the vibration of $–NH_2$ groups (δ_s(NH) in H_2NSi) on the nitrogen—substituted materials. The peaks at 1405 cm^{-1} and 1460 cm^{-1} are ascribed to the δ_{as}(NH) of the surface quarternary ammonium ion, which is the ammonia added to on the silanol. The peak in Fig. 1-20(B) at 1635 cm^{-1} in SBA15 spectrum is due to the δ_{as}(OH) peak of adsorbed water. And a peak at neighborhood (about 1650 cm^{-1}) in the nitrogen-substituted SBA15 spectrum also correspond to the δ(OH) vibration of adsorbed water and or the vibration of silicon coordinated ammonia. From the results of FT–IR, there exist terminal amino $–NH_2$, bridged amino(imido) –NH– species, quarternary ammonium ion, and adsorbed ammonia on the surface of the nitrogen–substituted SBA15.

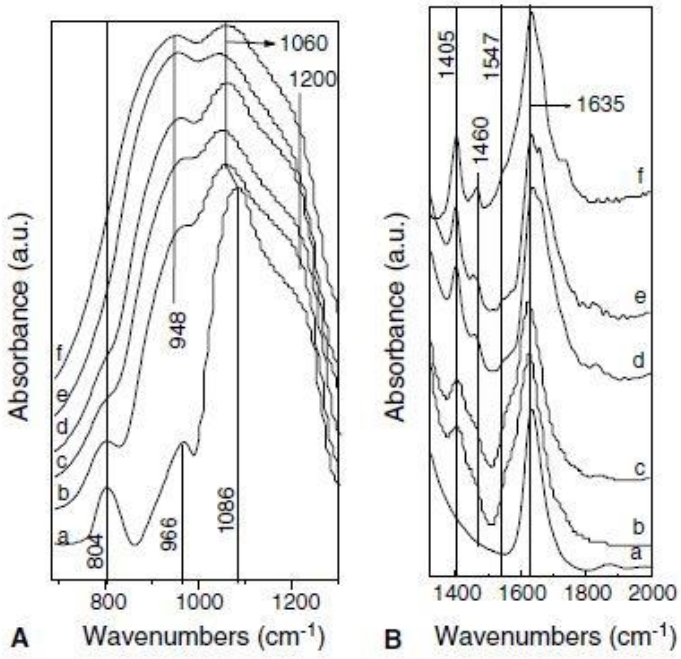

Figure 1-20. FT–IR spectra of SBA15 (a) and NSBA15 and b, c, d, e, f are corresponding to NSBA15–900, NSBA15–950, NSBA15–1000, NSBA15–1050 and NSBA15–1100, respectively. The end number of NSBA15 is nitrogen substitution temperature (K). (A) 690–1330 cm^{-1} and (B) 1340–2000 cm^{-1}

Figure 1-21 is the FT–IR spectra of KCC–1 and nitrogen–substituted KCC–1 material under various conditions. The intensity of the IR peak for silanol at 3741 cm^{-1} decrease with increasing temperature of nitridation and new peaks were observed corresponding to NH_2 stretching vibration at 3516 and 3444 cm^{-1} and NH_2 bending vibration at 1552 cm^{-1}. The intensity of these peaks except peak for silanol at 3741 cm^{-1} increased with nitrogen substitution temperature, indicating progressive nitridation of silanol to amines. Thus, this FT–IR spectra gives a crucial evidence to prove the nitrogen substitution mechanism showed above.

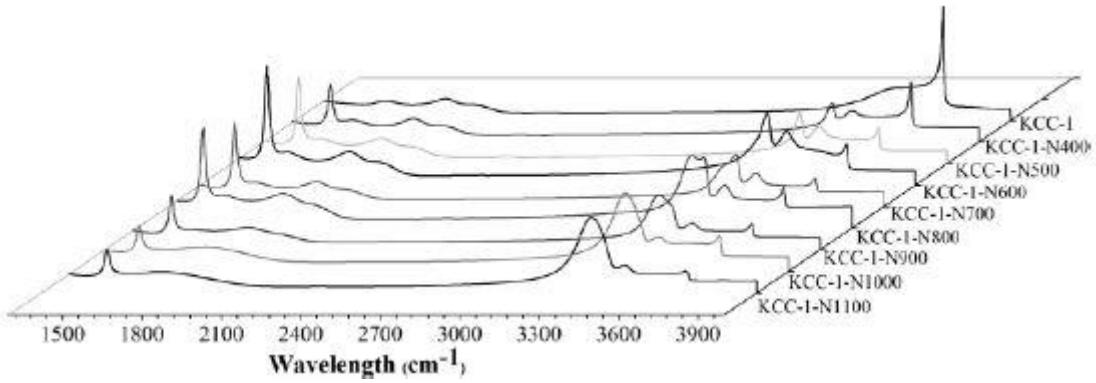

Figure 1-21. FT–IR spectra of KCC–1 [38]

1.3.2.4 Scanning electron microscopy (SEM) and transmission electron microscopy (TEM)

Figures 1-22, 23 and 24 are field–emission scanning electron microscopy (FE–SEM) and transmission electron microscopy (FE–TEM) images of SBA15, MCM48, MCM41, ZSM5 and nitrogen–substituted these materials. [64, 69, 70] Figure 1-22 displays the FE–SEM images of pSBA15 and nSBA15–3600. The end number is total NH_3 (L g^{-1}). The particle of pSBA15 had cylindrical morphology and uniform channels (Fig. 1-22a), which was like those of the SBA15. As shown in Fig. 1-22b, c, the linear and bending pores were maintained even after nitridation for 20 h (Table 1, Entry 21). The morphologies of pMCM48–16 were spherical and their size was reduced by nitridation (Fig. 1-22d–f). The following number of sample name is the amount of carbon in the main chain of surfactant. The average particle diameters of pMCM48–16 and nMCM48–16–3600 were 565 and 430 nm, respectively. The morphology and pore structures of pMCM48–16 didn't changed even after nitrogen substitution.

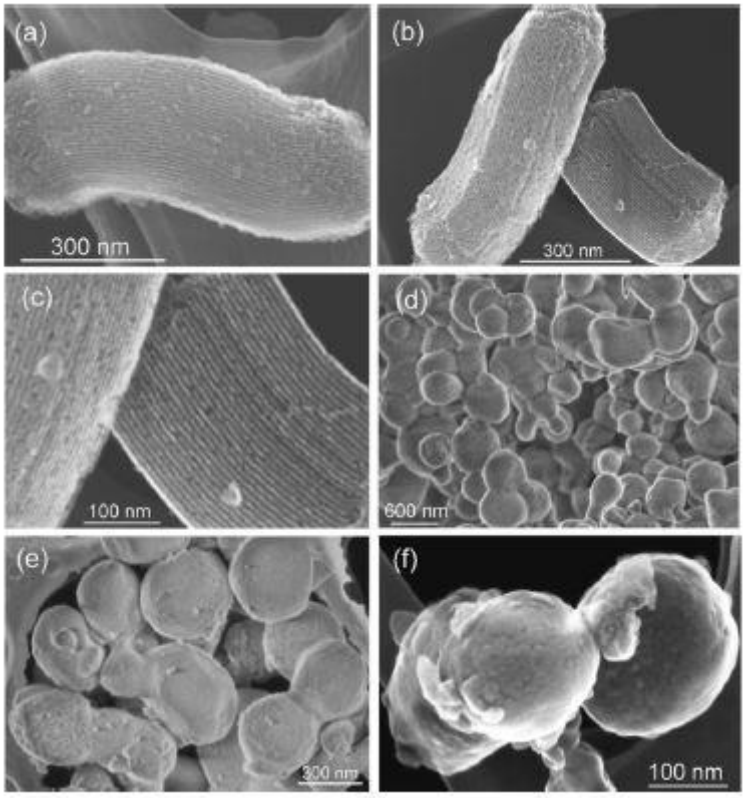

Figure 1-22. Field–emission scanning electron microscopy (FE–SEM) images of pSBA15 (a), nSBA15–3600 (b, c), p–MCM48–16 (d), and n–MCM48–16–3600 (e, f). Images correspond to Entries 23, 21, 29, and 28 in Table 1, respectively. The following number of sample name is the amount of carbon in the main chain of surfactant. The end number is total NH_3 (L g^{-1}). [69]

Figure 1-23 is the FE–SEM and TEM images of MCM–41 and NMCM–41. The morphology of NMCM–41 was almost the same as that of MCM–41, though the particle sizes decreased to 280–400 nm of NMCM–41 from 350–500 nm of MCM–41. Fig. 1-23 (c) and (d) clearly indicated that the preservation of the hexagonally arranged channels.

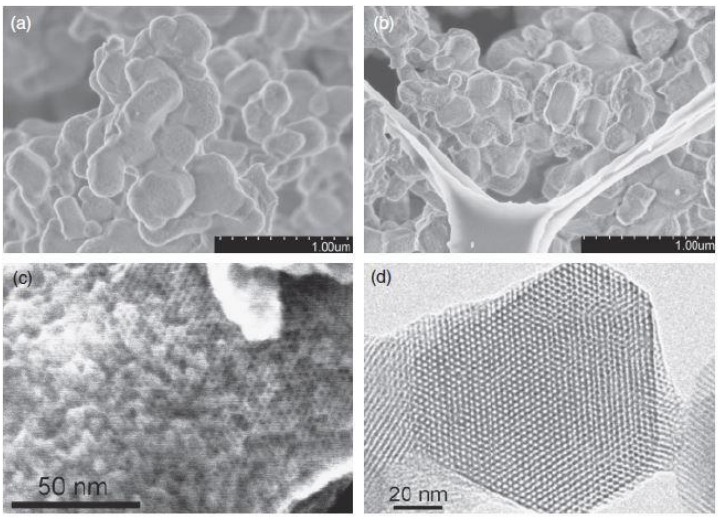

Figure 1-23. FE–SEM and field–emission transmission electron microscopy images of MCM—41 (a) and NMCM—41 (nitrogen—substituted at 1273 K) (b–d).[70]

SEM images of ZSM–5 and NZSM–5 in Figure 1-24 show that growth of crystal grains was going even after treating 2.5 h in air at 1273 K and again nitrogen–substituted 8 h in NH_3 gas at 1323 K. However, a few smaller grains whose crystallinity was bad still existed. Comparing Figure 15 (A) and (B), one sees that these smaller grains could be derived from parent materials.

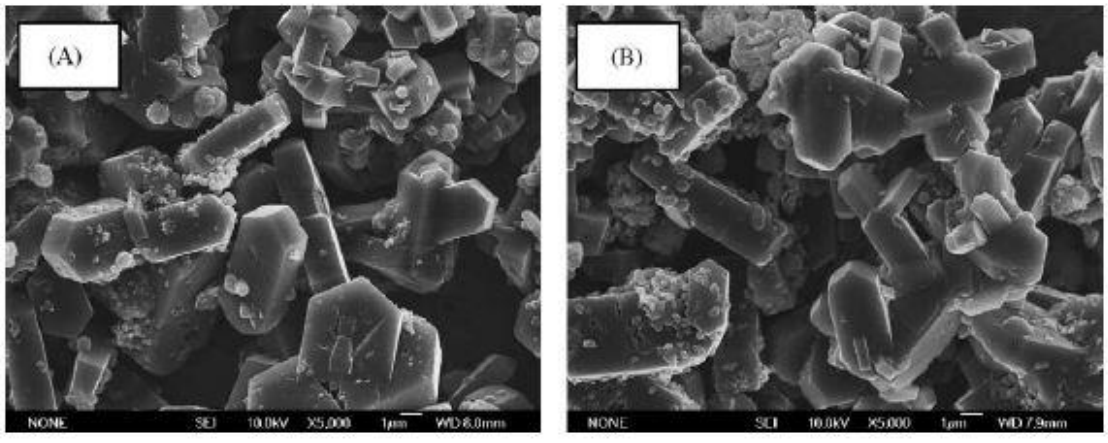

Figure 1-24. SEM images of some samples: (A) ZSM–5 and (B) NZSM–5 (nitrogen-substituted at 1273 K for 8 hours).[64]

1.3.2.5 Magic angle spinning nuclear magnetic resonance (MAS–NMR)

^{29}Si–MAS–NMR is a useful technique for the determination of the chemical environment of Si atoms in materials.[68] As shown in Figure 1-25, the parent MCM41 shows a primary peak at –109 ppm, a shoulder at –99 to –105 ppm and a little peak at –90 ppm, which are assigned to $Si(OSi)_4$, $(SiO)_3SiOH$ and $(SiO)_2Si(OH)_2$, respectively. After nitrogen substitution, the intense peaks became broader at the expense of the original signals. New peaks are ascribed to $SiNO_3$, SiN_2O_2, SiN_3O, and SiN_4. The primary peak of nitrogen-substituted sample at 873 K was divided into two peaks (at –115 ppm assigned to Si $(OSi)_4$ and at –105 ppm assigned to $(SiO)_3SiOH$), indicating the formation of $(SiO)_3SiOH$ by nitrogen substitution. When the nitrogen substitution temperature is raised to 1073 K, the peak due to $(SiO)_3SiOH$ becomes primary, while a new peak at –63 ppm due to SiN_3O appeared. In the spectrum of MCM41–900N, Peaks assigned to Si $(OSi)_4$ and $(SiO)_3SiOH$ decreased and the nitrogen-containing species became clear. When the temperature increased to 1223 K, the peaks of Si $(OSi)_4$ and $(SiO)_3SiOH$ almost disappeared and the SiN_4 species was formed. The nitrogen-containing species are primary in the spectrum of MCM41–950N. This confirms that the N atoms have been inserted into the framework of MCM41 by nitrogen substitution.

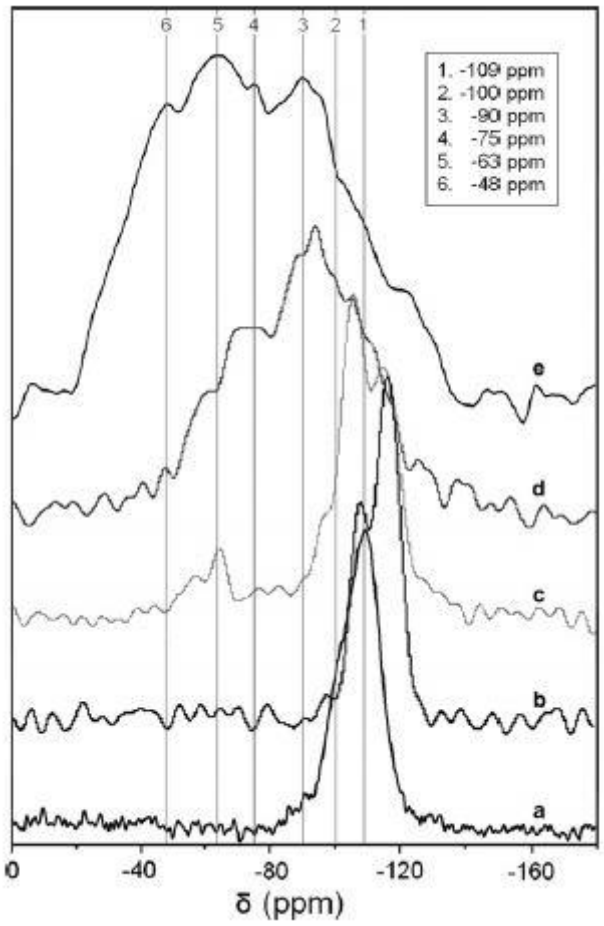

Figure 1-25. ^{29}Si MAS–NMR spectra of MCM–41 (a), MCM–41–600N (b), MCM–41–800N (c), MCM–41–900N (d) and MCM–41–950N (e). The end number is nitrogen substitution temperature (ºC). [68]

1.3.3 Methylated nitrogen-substituted SBA15

Alkylation of substituted nitrogen aims at preventing deactivation by adsorbent (such as H_2O, CO_2) and strengthening basicity and nucleophilicity. Alkylation of substituted nitrogen strengthens its basicity and nucleophilicity because alkyl group donate electron to nitrogen atom of nitrogen–containing silica.

Methylation is the simplest alkylation. Hydrogen atom bound to substituted nitrogen is substituted by methyl group. Methylation is performed by methyl iodide under N_2 atmosphere

and base condition.[30, 31] Methylated nitrogen–substituted silica is a more active catalyst than non–methylated nitrogen–substituted silica for Knoevenagel condensation,[30] Morita–Baylis–Hillman reaction,[31] and cyclic carbonate synthesis. Methylated N–substituted SBA15 (MeNSBA15) can promote Knoevenagel condensation using benzaldehyde and diethyl malonate, non–methylated nitrogen–substituted SBA15 (NSBA15) cannot catalyze this reaction. Catalysts for Knoevenagel condensation extract a proton from active methylene compounds and create carbanion. The index of extraction of a proton is acidity constant (p*Ka*). NSBA15 and MeNSBA15 can extract a proton from ethyl cyanoacetate (p*Ka* = 13.1 in DMSO) and only MeNSBA15 can extract it from diethyl malonate (p*Ka* = 16.4 in DMSO). This means that methylation improves basicity of substituted nitrogen. NSBA15 and MeNSBA15 also catalyze Morita–Baylis–Hillman reaction. The yield of this reaction over MeNSBA15 is higher than over NSBA15. Morita–Baylis–Hillman reaction is nucleophilic reaction; therefore methylation also improves nucleophilicity of substituted nitrogen. MeNSBA15 adsorbed CO_2 and cyclic ether on the surface substituted nitrogen and carbamate and ring–opened cyclic ether (alkoxide) forms for cyclic carbonate synthesis. Cyclic carbonate forms by nucleophilic attack from carbamate to alkoxide. Thus, methylation improves catalytic activity of NSBA15.

Alkylation can also change to other alkyl groups such as ethyl, propyl, and isopropyl group etc. Alkylation of nitrogen–substituted SBA15 is performed by following procedures. Nitrogen–substituted SBA15 and potassium carbonate and a stirrer are put into two–necked flask. Then the flask was evacuated and flushed with nitrogen gas. Under N_2 atmosphere, dehydrous ethanol and alkyl bromide are injected by a syringe. The flask is heated by 350 K for several hours. Next, the flask is cooled and the product is filtered and washed with ethanol and water. Dried residue is alkylated nitrogen–substituted SBA15. The strength of electro–donating depends on the number of carbon atom of alkyl group and ordinal number (primary, secondary, tertiary) .

However the amount of alkylation decreases with increasing size of alkyl group.

1.4 Purpose of this thesis

In this dissertation, methylated nitrogen-substituted SBA15(MeNSBA15) was applied as a catalyst in some cyclic carbonate syntheses. The catalysis of MeNSBA15 in the CO_2 transformation is clarified in order to elucidate mechanisms of CO_2 activation and lay out theoretical plan for development of catalyst for CO_2 transformation. Plans let us select an optimal catalyst for each CO_2 transformation catalyzed by base function.

The framework of this dissertation is shown in Figure 1-26. The background and the objective are described in the Chapter 1. Experimental procedures and characterization of catalyst are described in the Chapter 2. In the Chapters 3 and 4, the catalysis of MeNSA-15 in cyclic carbonate synthesis led by consideration of the turnover frequency dependence as a function of reactant concentration is described. Consideration of the cyclic carbonate synthesis by quantum chemical calculation in terms of the heat of reaction and stability of the reaction intermediates is described in the Chapter 5. Finally, the general conclusions and future perspectives are summarized in the Chapter 6.

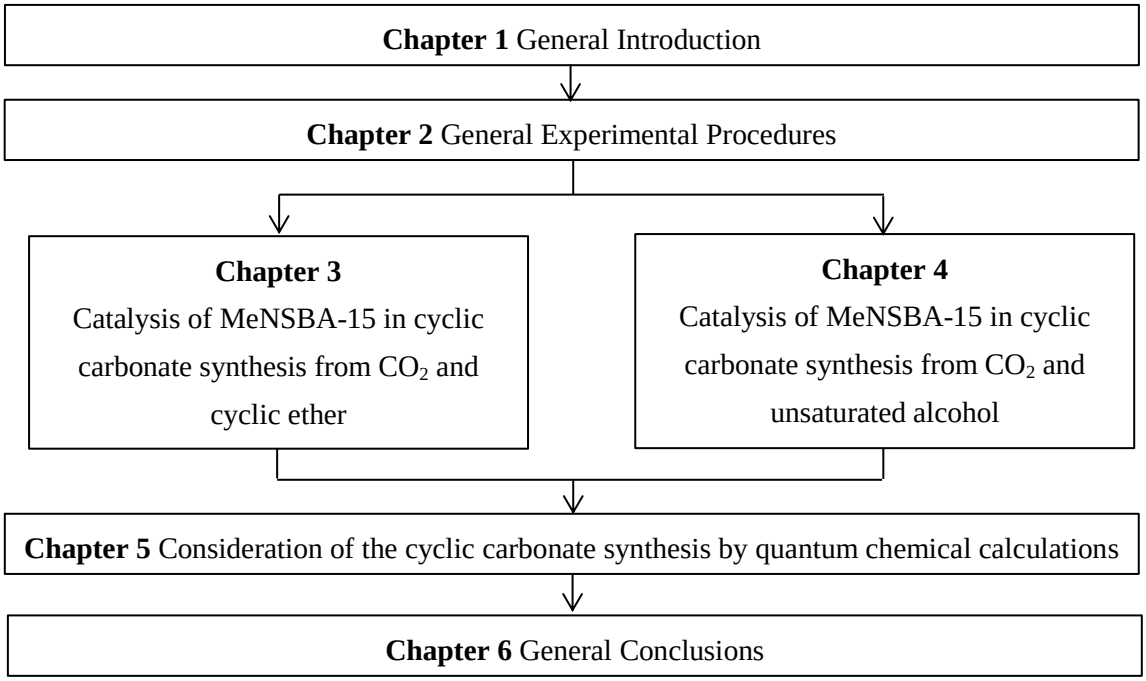

Figure 1-26. Framework of this dissertation

1. Cox, P. M.; Betts, R. A.; Jones, C. D.; Spall, S. A.; Totterdell, I. J., *Nature* **2000,** 408 (6809), 184-187.

2. Ji, S.; Hyun, B. G.; Kim, K.; Lee, S. Y.; Kim, S. H.; Kim, J. Y.; Song, M. H.; Park, J. U., *Npg Asia Materials* **2016,** 8, 9.

3. Bachu, S., *Progress in Energy and Combustion Science* **2008,** 34 (2), 254-273.

4. Thomas, S., *Oil & Gas Science and Technology-Revue D Ifp Energies Nouvelles* **2008,** 63 (1), 9-19.

5. Rocha, C. C.; Onfroy, T.; Pilme, J.; Denicourt-Nowicki, A.; Roucoux, A.; Launay, F., *Journal of Catalysis* **2016,** 333, 29-39.

6. Sakakura, T.; Choi, J. C.; Yasuda, H., *Chemical Reviews* **2007,** 107 (6), 2365-2387.

7. Aresta, M., Carbon dioxide as chemical feedstock. WileyVCH: Weinheim, 2012.

8. Tomishige, K.; Sakaihori, T.; Ikeda, Y.; Fujimoto, K., *Catalysis Letters* **1999,** 58 (4), 225-229.

9. Honda, M.; Tamura, M.; Nakagawa, Y.; Sonehara, S.; Suzuki, K.; Fujimoto, K.; Tomishige, K., *Chemsuschem* **2013,** 6 (8), 1341-1344.

10. Tomishige, K.; Kunimori, K., *Applied Catalysis a-General* **2002,** 237 (1-2), 103-109.

11. Biswas, J.; Maxwell, I. E., *Applied Catalysis* **1990,** 63 (2), 197-258.

12. Scherzer, J., *Applied Catalysis* **1991,** 75 (1), 1-32.

13. Meier, W. M.; Uytterho.Jb, *Advances in Chemistry Series* **1973,** (121), R11-R13.

14. Ono, Y.; Hattori, H., *Solid Base Catalysis* **2011,** 101, 1-421.

15. Akutu, K.; Kabashima, H.; Seki, T.; Hattori, H., *Applied Catalysis a-General* **2003,** 247 (1), 65-74.

16. Kabashima, H.; Katou, T.; Hattori, H., *Applied Catalysis a-General* **2001,** 214 (1), 121-124.

17. Yamakawa, T.; Takizawa, M.; Ohnishi, T.; Koyama, H.; Shinoda, S., *Catalysis Communications* **2001,** 2 (6-7), 191-194.

18. Cavani, F.; Trifiro, F.; Vaccari, A., *Catalysis Today* **1991,** 11 (2), 173-301.

19. Rao, K. K.; Gravelle, M.; Valente, J. S.; Figueras, F., *Journal of Catalysis* **1998,** 173 (1), 115-121.

20. Climent, M. J.; Corma, A.; Iborra, S.; Velty, A., *Journal of Catalysis* **2004,** 221 (2), 474-482.

21. Kawanami, Y.; Yuasa, H.; Toriyama, F.; Yoshida, S.; Baba, T., *Catalysis Communications* **2003,** 4 (9), 455-459.

22. Blass, B. E.; Harris, C. L.; Portlock, D. E., *Tetrahedron Letters* **2001,** 42 (9), 1611-1613.

23. Schmittling, E. A.; Sawyer, J. S., *Tetrahedron Letters* **1991,** 32 (49), 7207-7210.

24. Tedeschi, L.; Enders, D., *Organic Letters* **2001,** 3 (22), 3515-3517.

25. Kresge, C. T.; Leonowicz, M. E.; Roth, W. J.; Vartuli, J. C.; Beck, J. S., *Nature* **1992,** 359 (6397), 710-712.

26. Wan, Y.; Zhao, D. Y., *Chemical Reviews* **2007,** 107 (7), 2821-2860.

27. Taguchi, A.; Schuth, F., *Microporous and Mesoporous Materials* **2005,** 77 (1), 1-45.

28. Vallet-Regi, M.; Ramila, A.; del Real, R. P.; Perez-Pariente, J., *Chemistry of Materials* **2001,** 13 (2), 308-311.

29. Radu, D. R.; Lai, C. Y.; Jeftinija, K.; Rowe, E. W.; Jeftinija, S.; Lin, V. S. Y., *Journal of the American Chemical Society* **2004,** 126 (41), 13216-13217.

30. Sugino, K.; Oya, N.; Yoshie, N.; Ogura, M., *Journal of the American Chemical Society* **2011,** 133 (50), 20030-20032.

31. Furukawa, Y.; Ogura, M., *Journal of the American Chemical Society* **2014,** 136 (1), 119-121.

32. Hasegawa, T.; Krishnan, C. K.; Ogura, M., *Microporous and Mesoporous Materials* **2010,** 132 (1-2), 290-295.

33. El Haskouri, J.; Cabrera, S.; Sapina, F.; Latorre, J.; Guillem, C.; Beltran-Porter, A.; Beltran-Porter, D.; Marcos, M. D.; Amoros, P., *Advanced Materials* **2001,** 13 (3), 192-195.

34. Singh, B.; Mote, K. R.; Gopinath, C. S.; Madhu, P. K.; Polshettiwar, V., *Angewandte Chemie-International Edition* **2015,** 54 (20), 5985-5989.

35. Chino, N.; Okubo, T., *Microporous and Mesoporous Materials* **2005,** 87 (1), 15-22.

36. Asefa, T.; Kruk, M.; Coombs, N.; Grondey, H.; MacLachlan, M. J.; Jaroniec, M.; Ozin, G. A., *Journal of the American Chemical Society* **2003,** 125 (38), 11662-11673.

37. Ishizu, K. I.; Hayashi, F.; Iwamoto, M., *Chemistry Letters* **2007,** 36 (12), 1416-1417.

38. Bouhrara, M.; Ranga, C.; Fihri, A.; Shaikh, R. R.; Sarawade, P.; Emwas, A. H.; Hedhili, M. N.; Polshettiwar, V., *Acs Sustainable Chemistry & Engineering* **2013,** 1 (9), 1192-1199.

39. Xia, Y. D.; Mokaya, R., *Angewandte Chemie-International Edition* **2003,** 42 (23), 2639-2644.

40. Wan, K.; Liu, Q.; Zhang, C. M.; Wang, J. C., *Bulletin of the Chemical Society of Japan* **2004,** 77 (7), 1409-1414.

41. Thankamony, A. S. L.; Lion, C.; Pourpoint, F.; Singh, B.; Linde, A. J. P.; Carnevale, D.; Bodenhausen, G.; Vezin, H.; Lafon, O.; Polshettiwar, V., *Angewandte Chemie-International Edition* **2015,** 54 (7), 2190-2193.

42. Guan, X. X.; Zhang, F. X.; Wu, G. J.; Guan, N. J., *Materials Letters* **2006,** 60 (25-26), 3141-3144.

43. Bendjeriou-Sedjerari, A.; Pelletier, J. D. A.; Abou-Hamad, E.; Emsley, L.; Basset, J.

M., *Chemical Communications* **2012,** 48 (25), 3067-3069.

44. Hammond, K. D.; Dogan, F.; Tompsett, G. A.; Agarwal, V.; Conner, W. C.; Grey, C. P.; Auerbach, S. M., *Journal of the American Chemical Society* **2008,** 130 (45), 14912-+.

45. Xia, Y. D.; Mokaya, R., *Journal of Physical Chemistry C* **2008,** 112 (5), 1455-1462.

46. Wang, J. C.; Liu, Q., *Microporous and Mesoporous Materials* **2005,** 83 (1-3), 225-232.

47. Patil, U.; Fihri, A.; Emwas, A. H.; Polshettiwar, V., *Chemical Science* **2012,** 3 (7), 2224-2229.

48. Kerr, G. T.; Shipman, G. F., *Journal of Physical Chemistry* **1968,** 72 (8), 3071-&.

49. Ernst, S.; Hartmann, M.; Sauerbeck, S.; Bongers, T., *Applied Catalysis a-General* **2000,** 200 (1-2), 117-123.

50. Dogan, F.; Hammond, K. D.; Tompsett, G. A.; Huo, H.; Conner, W. C.; Auerbach, S. M.; Grey, C. P., *Journal of the American Chemical Society* **2009,** 131 (31), 11062-11079.

51. Srasra, M.; Delsarte, S.; Gaigneaux, E. M., *Topics in Catalysis* **2009,** 52 (11), 1541-1548.

52. Agarwal, V.; Huber, G. W.; Conner, W. C.; Auerbach, S. M., *Journal of Catalysis* **2010,** 269 (1), 53-63.

53. Agarwal, V.; Huber, G. W.; Conner, W. C.; Auerbach, S. M., *Journal of Catalysis* **2010,** 270 (2), 249-255.

54. Srasra, M.; Delsarte, S.; Gaigneaux, E. M., *Journal of Physical Chemistry C* **2010,** 114 (10), 4527-4535.

55. Agarwal, V.; Conner, W. C.; Auerbach, S. M., *Journal of Physical Chemistry C* **2011,** 115 (1), 188-194.

56. Verboekend, D.; Keller, T. C.; Mitchell, S.; Perez-Ramirez, J., *Advanced Functional Materials* **2013,** 23 (15), 1923-1934.

57. Chen, X. C.; Guo, J.; Fu, Z. W.; He, H. Y.; Long, Y. C., *Journal of Porous Materials* **2013,** 20 (5), 1271-1281.

58. Min, H. K.; Cha, S. H.; Hong, S. B., *Chemical Communications* **2013,** 49 (11), 1115-1117.

59. Wu, G. J.; Wang, X.; Yang, Y. L.; Li, L. D.; Wang, G. C.; Guan, N. J., *Microporous and Mesoporous Materials* **2010,** 127 (1-2), 25-31.

60. Han, A. J.; He, H. Y.; Guo, J.; Yu, H.; Huang, Y. F.; Long, Y. C., *Microporous and Mesoporous Materials* **2005,** 79 (1-3), 177-184.

61. Han, A. J.; Guo, J. G.; Yu, H.; Zeng, Y.; Huang, Y. F.; He, H. Y.; Long, Y. C., *Chemphyschem* **2006,** 7 (3), 607-613.

62. Guo, J.; Han, A. J.; Yu, H.; Dong, J. P.; He, H. Y.; Long, Y. C., *Microporous and*

Mesoporous Materials **2006,** 94 (1-3), 166-172.

63. Lyu, J. H.; Hu, H. L.; Rui, J. Y.; Zhang, Q. F.; Cen, J.; Han, W. W.; Wang, Q. T.; Chen, X. K.; Pan, Z. Y.; Li, X. N., *Chinese Chemical Letters* **2017,** 28 (2), 482-486.

64. Zhang, C. M.; Xu, Z.; Wan, K.; Liu, Q., *Applied Catalysis a-General* **2004,** 258 (1), 55-61.

65. Narasimharao, K.; Hartmann, M.; Thiel, H. H.; Ernst, S., *Microporous and Mesoporous Materials* **2006,** 90 (1-3), 377-383.

66. Climent, M. J.; Corma, A.; Fornes, V.; Frau, A.; GuilLopez, R.; Iborra, S.; Primo, J., *Journal of Catalysis* **1996,** 163 (2), 392-398.

67. Corma, A.; Pedro, V.; Fernandez, L., *Journal of Molecular Catalysis a-Chemical* **1998,** 133 (3), 241-250.

68. Wu, G. J.; Jiang, S. L.; Li, L. D.; Zhang, F. X.; Yang, Y. L.; Guan, N. J.; Mihaylov, M.; Knozinger, H., *Microporous and Mesoporous Materials* **2010,** 135 (1-3), 2-8.

69. Hayashi, F.; Ishizu, K.; Iwamoto, M., *European Journal of Inorganic Chemistry* **2010,** (15), 2235-2243.

70. Hayashi, F.; Ishizu, K.; Iwamoto, M., *Journal of the American Ceramic Society* **2010,** 93 (1), 104-110.

2 General experimental procedures

2.1 Gases and Chemicals

Carbon dioxide and ammonia gas (liquefied gas) with 99.5% and 99.999% purity, respectively, was obtained from Jyotou Gas. Pluronic P-123 is obtained from Aldrich (PEG 30 wt.%, average M_n of 5800). Hydrochloric acid solution (volumetric analysis grade), tetraethyl orthosilicate (TEOS, >95.0%), potassium carbonate (K_2CO_3 >99.5%), anhydrous ethanol (>99.5%, water <0.001%) methyl iodide (CH_3I, >99.5%), tetrabutylammonium bromide (TBABr, >98.0%) N,N-dimethylformamide (DMF, >99.5%), and diethyl ether (>99.5%) were obtained from Wako Pure Chemical Industries, Ltd. and they were used without purification. Trimethylamine (NMe3, 25% in isopropyl alcohol), 2-methyl-3-butyn-2-ol (>98.0%), and 3-methyl-1-pentyn-3-ol (>98.0%) were obtained from Tokyo Chemical Industry Co. Ltd. and they were used without purification.

2.2 Synthesis of methylated nitrogen-substituted mesoporous silica

MeNSBA-15 was synthesized by methylation of nitrided SBA-15, as described elsewhere.[1, 2] (Figure 2-1) SBA-15 was synthesized by hydrothermal treatment.[3] (Figure 2-1) Specifically, triblock copolymer surfactant, Pluronic P-123, was dissolved in 2 M aqueous hydrochloric acid solution under stirring at 313 K for 3 h. TEOS was then dripped to the solution, and hydrolyzed at 313 K for 24 h under stirring. The resultant solution was placed in an electric oven for hydrothermal treatment at 373 K for 24 h. The chemical composition of the synthetic solution was SiO_2/0.017P123/6HCl/190H_2O. The precipitated sample was filtered and washed with distilled water. The sample was calcined at 823 K for 6 h to remove the template surfactants.

Nitrogen substitution of the synthesized SBA-15 was performed by flowing 99.999% ammonia gas at 1173 K for 10 h with a flow rate of 1 L min^{-1}.(Figure 2-1)

The obtained NSBA-15 and K_2CO_3 were placed in a two-neck flask equipped with a reflux condenser. The flask was flashed and filled with inert gas (house nitrogen). Anhydrous ethanol was added as a solvent, and then CH_3I was added. Molar ratios of CH_3I to N-atom in NSBA-15 and CH_3I to K_2CO_3 were 15 and 3, respectively. The reaction was conducted at 350 K for 24 h under reflux conditions. The product was filtered, washed with 50 vol.% ethanol aqueous solution, and dried at 373 K for 12 h to remove potential iodide salts (methyl iodide and potassium iodide).

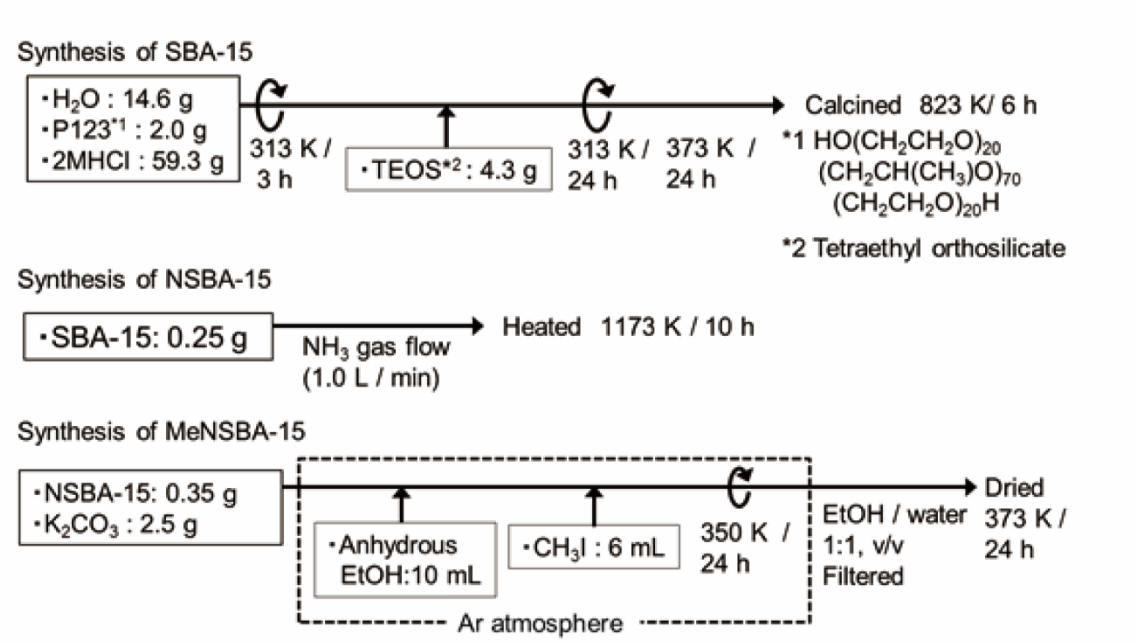

Figure 2-1. Synthesis methods of SBA-15 series

2.3 Characterization

2.3.1 X-ray diffraction (XRD)

Powder X-ray diffraction (XRD) patterns were collected on a Rigaku RINT2100 using Cu Kα radiation (λ = 0.1542 nm, 40 kV, 40 mA) between 0.05° and 3° (2θ) with a scanning step of 0.02° and a scanning speed of 1° min^{-1}. Figure 2-2 shows the XRD patterns of synthesized SBA-15, NSBA-15, and MeNSBA-15 samples. Three characteristic peaks attributed to (100), (110), and (200) planes of 2D-hexagonal periodic structure were observed in all the samples (Figure 2-2). After nitrogen substitution, the three peaks shifted to a larger angle (Fig. 2-2), which suggests that the high-temperature nitrogen substitution process caused the shrinking of the mesoporous structure without collapsing the periodic structure. The methylation process also maintained the periodic mesoporous structure (Fig. 2-2).

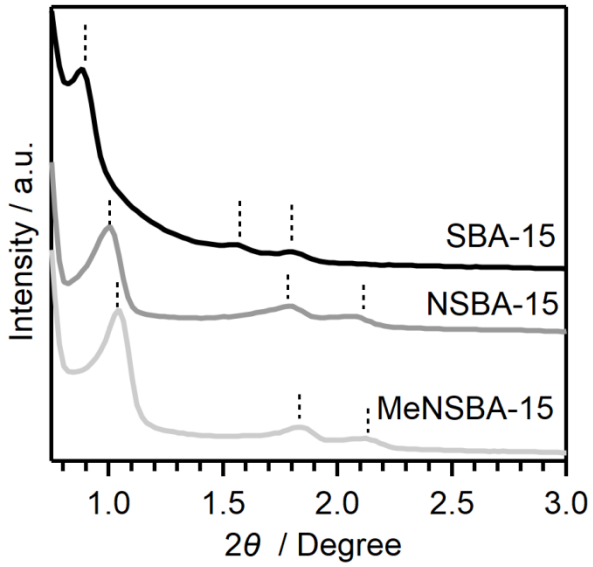

Figure 2-2. XRD patterns of (black line) as-synthesized, (blue line) nitrogen-substituted, and (red line) methylated mesoporous silica materials, SBA-15, NSBA-15, and MeNSBA-15, respectively.

2.3.2 Nitrogen adsorption measurement

Nitrogen adsorption isotherms were collected on a Quantachrome Quadrasorb Evo. Samples were pretreated at 573 K for 3 h under evacuation. Figure 2-3 shows the nitrogen adsorption-desorption isotherms of the series of SBA-15 samples, and Table 2-1 summarizes their sorption properties. The synthesized SBA-15 possessed accessible pores originated from the 2D-hexagonal structure. This porous structure was maintained even after the nitrogen substitution and methylation. However, micropores, which initially existed inside the wall of mesopores, were collapsed by high-temperature thermal treatment (i.e., nitridation) as shown in the drastic decrease of micropore volume from 0.20 to <0.01 cm^3g^{-1} (Table 2-1). The nitrogen substitution process caused pore shrinkage, which agrees with the results of XRD measurement (Figure 2-2). The diameters of the mesopores of all the SBA-15 samples were large enough for reactants and products (cyclic ethers, unsaturated alcohol, cyclic carbonates, respectively) to go through.

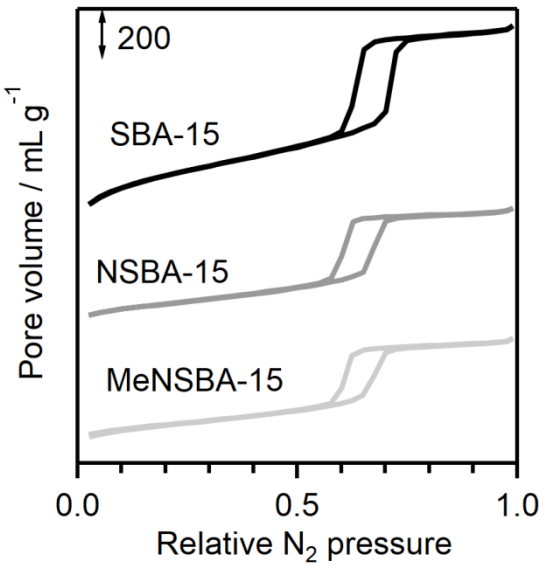

Figure 2-2. Nitrogen sorption isotherms of as-synthesized, nitrogen-substituted, and methylated mesoporous silica materials, SBA-15, NSBA-15, and MeNSBA-15, respectively.

Table 2-1. Summary of nitrogen adsorption properties of synthesized mesoporous silica materials

Sample	BJH pore diameter [nm]	BJH pore volume [$cm^3\ g^{-1}$]	BET surface area [$m^2\ g^{-1}$]	Micropore volume[a] [$cm^3\ g^{-1}$]
SBA-15	5.80	1.30	962	0.197
NSBA-15	5.41	0.829	600	<0.001
MeNSBA-15	5.41	0.752	537	<0.001

a: calculated by t-plot method.

2.3.3 Elemental analysis

The chemical composition of the series of SBA-15 were analyzed by an Elementar Analysensysteme GmbH Vario Micro Cube and summarized in Table 2-2. The amount of nitrogen (20 ± 2.5 mmol g^{-1}) and carbon (1.5±0.052 mmol g^{-1}) atoms was measured after the nitrogen substitution and methylation, respectively, which also supported successful modifications. Comparison of N- and C-atom amounts revealed that about one-tenth of N-atoms were methylated. The decrease in the N-atom content after methylation (from 20±2.5 to 15±0.47 mmol g^{-1}) would be caused by the hydrolysis of weak Si–N bonds during the nitrogen substitution and methylation,[1, 2] thus forming surface silanol groups (Si–OH) and releasing ammonia. The change in the H-atom amount also indicates successful methylation. Methylation of 10% of framework NH groups (Si–NH–Si → Si–(N–CH_3)–Si) would cause a roughly 20% increase in H-atoms, which would explain the experimental results (from 9.9 ± 3.1 to 13 ± 1.7 mmol g^{-1}). Here, it is important to estimate the amount of surface sites on the solid catalyst. On the MeNSBA-15 sample, the amount of measured N-atoms is about 15 mmol g^{-1} (Table 2-2), whereas the maximum amount of O-atoms originally existing on the pore surface is calculated to be 12.6 mmol g^{-1}.[4] Because nitridation is a gas-solid reaction, it is considered to proceed

initially from the accessible surface O-atoms. Therefore, it could be assumed that, because of the larger amount of introduced N-atoms, most of the surface O-atoms are replaced by N-atoms; in contrast, most of the O-atoms embedded in the pore walls would stay as they are. The above discussion further implies that the number of surface methylated nitrogen atoms should be larger than 10% of the number of surface nitrogen atoms (the value is simply calculated by elemental analysis data above).

Table 2-2. Chemical compositions of synthesized mesoporous silica materials

Sample	N [mmol g^{-1}]	C [mmol g^{-1}]	H [mmol g^{-1}]
SBA-15	0.022±0.015	0.10±0.038	11±15
NSBA-15	20±2.5	0.061±0.061	9.9±6.2
MeNSBA-15	15±0.47	1.5±0.052	13±3.3

2.3.4 Fourier transform infrared (FT-IR) spectroscopy

Fourier transform infrared (FT-IR) spectra were collected on a JASCO FT/IR 4100 with an MCT detector. Samples were pretreated at 423 K for 10 min under evacuation, and the spectra were measured at 323 K. This low functionalization percentage agrees with the FT-IR studies (Figure 2-4), which showed no measurable change in the N–H stretching band after methylation. The nitrogen substitution and the subsequent methylation were confirmed by FT-IR spectroscopy and elemental analysis. Fig 2-4 shows the FT-IR spectra of the series of SBA-15 samples. An IR band at 3740 cm^{-1} was observed in the SBA-15 sample, which is attributed to the O–H stretching vibration of surface silanol groups.[5] A broad peak at around 3365 cm^{-1} observed on both NSBA-15 and MeNSBA-15 samples corresponds to the N–H stretching

vibration, indicating the formation of Si–*NH*–Si structures.[6, 7] There was no IR band corresponding to primary amines (Si–*NH_2*), which agrees with the known relationship between the nitridation temperature and the formed amine structure (i.e., primary amines form at nitridation temperatures under 1173 K).[8] After methylation, a sharp band appeared at 2970 cm^{-1}. It can be assigned to C–H stretching of the N–CH_3 group,[9] indicating successful methylation on the substituted N-atom to form the Si–(*N–CH_3*)–Si group. The N–H stretching band, however, did not show a drastic decrease after methylation, which suggests that most of the NH groups remained as they were, and only a small number of N-atoms were functionalized. The abovementioned FT-IR studies allowed us to conclude that the two-step modifications were successfully applied on the mother SBA-15 material.

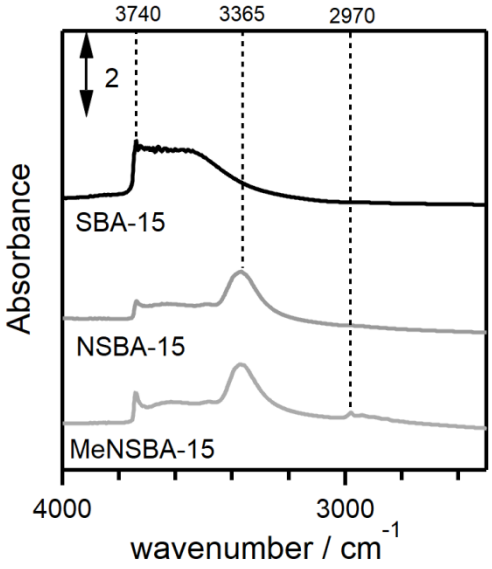

Figure 2-4. IR spectra of a series of SBA-15.

2.4 Cyclic carbonate synthesis from CO_2 and cyclic ether

Cycloaddition of CO_2 to cyclic ethers was carried out using a 5-mL stainless-steel reactor. Typically, 25–100 mg of catalyst and 7.1–35 mmol of cyclic ether were put into the reactor, and the reactor was sealed. CO_2 was then charged into the reactor up to 1.0–5.5 MPa. The reactor was heated in an oil bath at 353–423 K for 1–48 h. After the reactor was cooled and degassed, it was rinsed with acetone to collect all the reactants and products. After adding *n*-decane as an internal standard, the diluted sample was analyzed with a SHIMADZU GC-14B gas chromatograph equipped with a capillary column (ZB-WAX or ZB-1, 30 m × 0.25 mm × 0.50 μm).

The TOF of each catalyst is the number of formed product molecules per number of ideal catalytic sites in one hour. The number of ideal catalytic sites was assumed as the numbers of C- and N-atoms in MeNSBA-15 and NSBA-15, respectively. The activation energy was calculated by an Arrhenius plot measured at 353, 373, 393, and 423 K. All the catalytic tests were conducted under reaction conditions below CO_2 supercritical point (7.38 MPa, 304 K).

2.5 Cyclic carbonate synthesis from CO_2 and unsaturated alcohol

Cyclic carbonate synthesis from CO_2 and unsaturated alcohol was carried out using a 5-mL stainless-steel reactor. Typically, 20 mg of catalyst and 1.5–25 mmol of unsaturated alcohol (2-methyl-3-butyn-2-ol and 3-methyl-1-pentyn-3-ol) were put into the reactor, and the reactor was sealed. CO_2 was then charged into the reactor up to 0.5–5.0 MPa. The reactor was heated in an oil bath at 353-423 K for 24 h. After the reactor was cooled and degassed, it was rinsed with diethyl ether to collect all the reactants and products. After adding mesitylene as an internal standard, the diluted sample was analyzed with the same gas chromatograph as used in cyclic carbonate synthesis from CO_2 and propylene oxide.

The activation energy was calculated by an Arrhenius plot measured at 353, 373, 393, and 423 K. All the catalytic tests were conducted under reaction conditions below CO_2 supercritical point (7.38 MPa, 304 K).

1. Furukawa, Y.; Ogura, M., *Journal of the American Chemical Society* **2014,** 136 (1), 119-121.

2. Sugino, K.; Oya, N.; Yoshie, N.; Ogura, M., *Journal of the American Chemical Society* **2011,** 133 (50), 20030-20032.

3. Zhao, D. Y.; Huo, Q. S.; Feng, J. L.; Chmelka, B. F.; Stucky, G. D., *Journal of the American Chemical Society* **1998,** 120 (24), 6024-6036.

4. Ernst, S.; Hartmann, M.; Sauerbeck, S.; Bongers, T., *Applied Catalysis a-General* **2000,** 200 (1-2), 117-123.

5. Shenderovich, I. G.; Buntkowsky, G.; Schreiber, A.; Gedat, E.; Sharif, S.; Albrecht, J.; Golubev, N. S.; Findenegg, G. H.; Limbach, H. H., *Journal of Physical Chemistry B* **2003,** 107 (43), 11924-11939.

6. Busca, G.; Lorenzelli, V.; Baraton, M. I.; Quintard, P.; Marchand, R., *Journal of Molecular Structure* **1986,** 143, 525-528.

7. Narasimharao, K.; Hartmann, M.; Thiel, H. H.; Ernst, S., *Microporous and Mesoporous Materials* **2006,** 90 (1-3), 377-383.

8. Singh, B.; Mote, K. R.; Gopinath, C. S.; Madhu, P. K.; Polshettiwar, V., *Angewandte Chemie-International Edition* **2015,** 54 (20), 5985-5989.

9. Hruby, S. L.; Shanks, B. H., *Journal of Catalysis* **2009,** 263 (1), 181-188.

3 Catalysis of MeNSBA-15 in cyclic carbonate synthesis from CO_2 and cyclic ether

3.1 Introduction

Synthesis of cyclic carbonates via cycloaddition of CO_2 into cyclic ethers is one of successful processes.[1-3] Cyclic carbonates are industrially important chemicals and these widely used as electrolyte components in lithium batteries[4] and polar solvents.[5] Furthermore, production of cyclic carbonates as precursors of polycarbonates[6] would replace the conventional toxic phosgene process.[7] In the last few decades, both homogeneous (e.g., quaternary ammonium salts,[8] metal halides,[9] metal complexes,[10] and ionic liquids[11, 12]) and heterogeneous (e.g., surface-immobilized ionic liquids,[13] metal oxides,[14] metal modified zeolites,[15] MOFs,[16] and hydroxyapatites[17]) catalysts have been developed and applied to the CO_2 cycloaddition.

MeNSBA-15 was shown to catalyze cyclic carbonate synthesis via cycloaddition of CO_2 with cyclic ether. Among a series of SBA-15 (MeNSBA-15, NSBA-15, and SBA-15), only MeNSBA-15, which was used without any pretreatment for activation, catalyzed the reaction. Kinetic analysis provided deep insights into the reaction mechanism and the catalytic site. In previous cyclic carbonate synthesis studies, many attempts have been made to design the homogeneous and heterogeneous catalysts. These catalysts have unique catalytic site to activate the reactants (CO_2 and/or cyclic ethers) via different types of intermediate activation processes. From the point of view of reaction mechanism, these could be categorized into mainly two different proposed mechanisms, Langmuir–Hinshelwood [18-24] and Eley–Rideal [25-42] mechanisms. Based on our experimental data and discussion, the most plausible mechanism for MeNSBA-15 is proposed to be a Langmuir–Hinshelwood type mechanism with a rate-determining bimolecular reaction step over the methylated-nitrogen pair sites.

3.2 Catalytic performance

Table 3-1 summarizes the results of the catalytic cycloaddition of CO_2 into propylene oxide (PO) over SBA-15-type heterogeneous and well-studied homogeneous base catalysts (3 MPa CO_2, 1.0 MPa PO, reaction temperature 373 K). The reaction did not proceed without catalyst under the conditions applied in this study (Table 3-1). The activation energy was 203 kJ mol^{-1}, determined by DFT calculations.[27] Among the homogeneous and heterogeneous catalysts tested, MeNSBA-15 was found to show a high TOF (6.4 h^{-1}) and selectivity (>99%).Whereas, NSBA-15 showed little catalytic activity (TOF less than 1.0×10^{-3} h^{-1}). The remarkable increase in the catalytic performance caused by methylation could be explained by the enhanced nucleophilicity. Recycling tests were conducted over MeNSBA-15 (3 MPa CO_2, 1.0 MPa PO, 10 mg MeNSBA-15, 373 K, 3 h), and the product yield of second and third uses were 63% and 43% relative to the initial use, respectively.

Table 3-1. Summary of the catalytic performances of direct propylene carbonate synthesis from CO_2 and PO (3 MPa CO_2, 1.0 MPa PO, 373 K reaction temperature). The amounts of catalysts used were 100, 100, 10, and 500 mg for MeNSBA-15, NSBA-15, TBABr, and NMe3, respectively.

Catalyst	TOF[a] [h^{-1}]	Conversion (Selectivity)[b] [%]	E_a [kJ mol^{-1}]
None	-[c]	- (-)	203[d]
MeNSBA-15	6.4	13.3 (>99)	43.2
NSBA-15	$<10^{-3}$	- (-)	-
TBABr	7.5	22.3 (>99)	45.2
NMe_3	0.64	40.8 (83[e])	68.9

a: TOF is calculated at reaction time of 3 h, b: Conversion and selectivity are calculated at reaction time of 6 h, c: Propylene carbonate is not detected by gas chromatograph, d: The value referred to the Reference 27., e: Byproduct is an ether formed via self-reaction of PO

Figure 3-1 shows the TOF of cyclic carbonate synthesis over MeNSBA-15 as a function of CO_2 partial pressure (Fig. 3-1a) and PO partial pressure (Fig. 3-1b). Both plots had a maximum TOF under a certain reactant partial pressure. These results suggest that both adsorbed CO_2 and PO work as reaction inhibitors, and most plausibly, block catalytic active sites under high partial pressure conditions (CO_2 partial pressure over 3 MPa and PO partial pressure over 1.0 MPa). CO_2 is adsorbed on the methylated N-atoms of the catalyst to form a carbamate species. PO also interacts with the basic N-atom through the β-carbon of the molecule to form an alkoxide.[31, 36, 41] Thus, it is suggested that the two reactants, CO_2 and PO, compete to adsorb on the methylated N-atoms of MeNSBA-15 and occupy the sites under excess conditions.

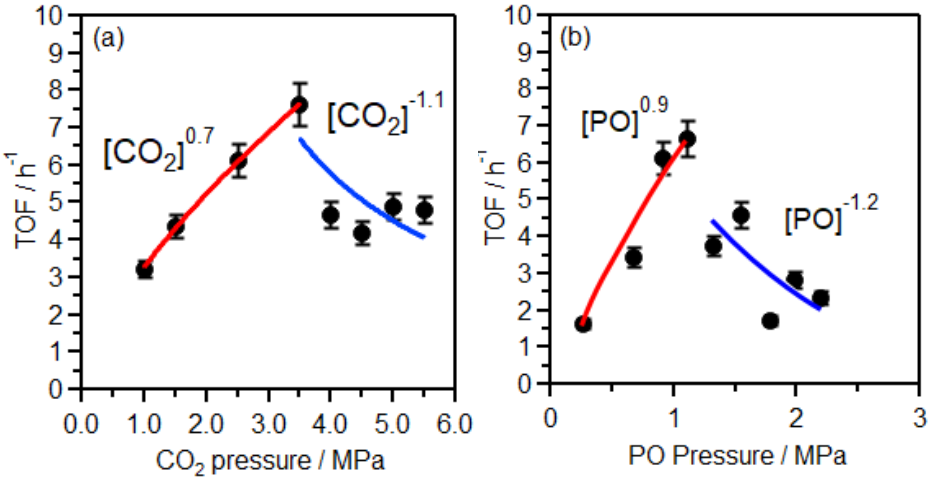

Figure 3-1. Changes in the TOF of propylene carbonate synthesis on MeNSBA-15 (50 mg catalyst, 373 K, 6 h) as a function of (a) CO_2 pressure (1.0 MPa PO) and (b) PO amount (3 MPa CO_2) over 50 mg of catalysts. Red and blue lines are fitting curves.

3.3 Consideration of surface active species

Fig 3-2 shows difference IR spectra of MeNSBA-15 under PO atmosphere. An IR band observed at 3740 cm^{-1} is attributed to the O–H stretching vibration of surface silanol groups[5], and broad peak observed at around 3365 cm^{-1} corresponds to the N–H stretching vibration as mentioned in Chapter 2. Three peaks appeared at 2970, 1490 and 1360 cm^{-1} is due to CH_3 vibration, and three peaks appeared at 2935, 1460 and 1450 cm^{-1} is due to CH_2 vibration. These peaks would be derived from methyl group connected to the nitrogen atom and adsorbed cyclic ether. It is noteworthy that a sharp peak appeared at 1410 cm^{-1}. This peak is attributed to hybrid vibration of $C\text{-}O^-$ stretching and O-H bending, which same type of the peak is observed in IR spectrum of dimer-formed acetic acid. This peak would suggest that ring-opened cyclic carbonate, alkoxide, can be formed on the methylated nitrogen atom.

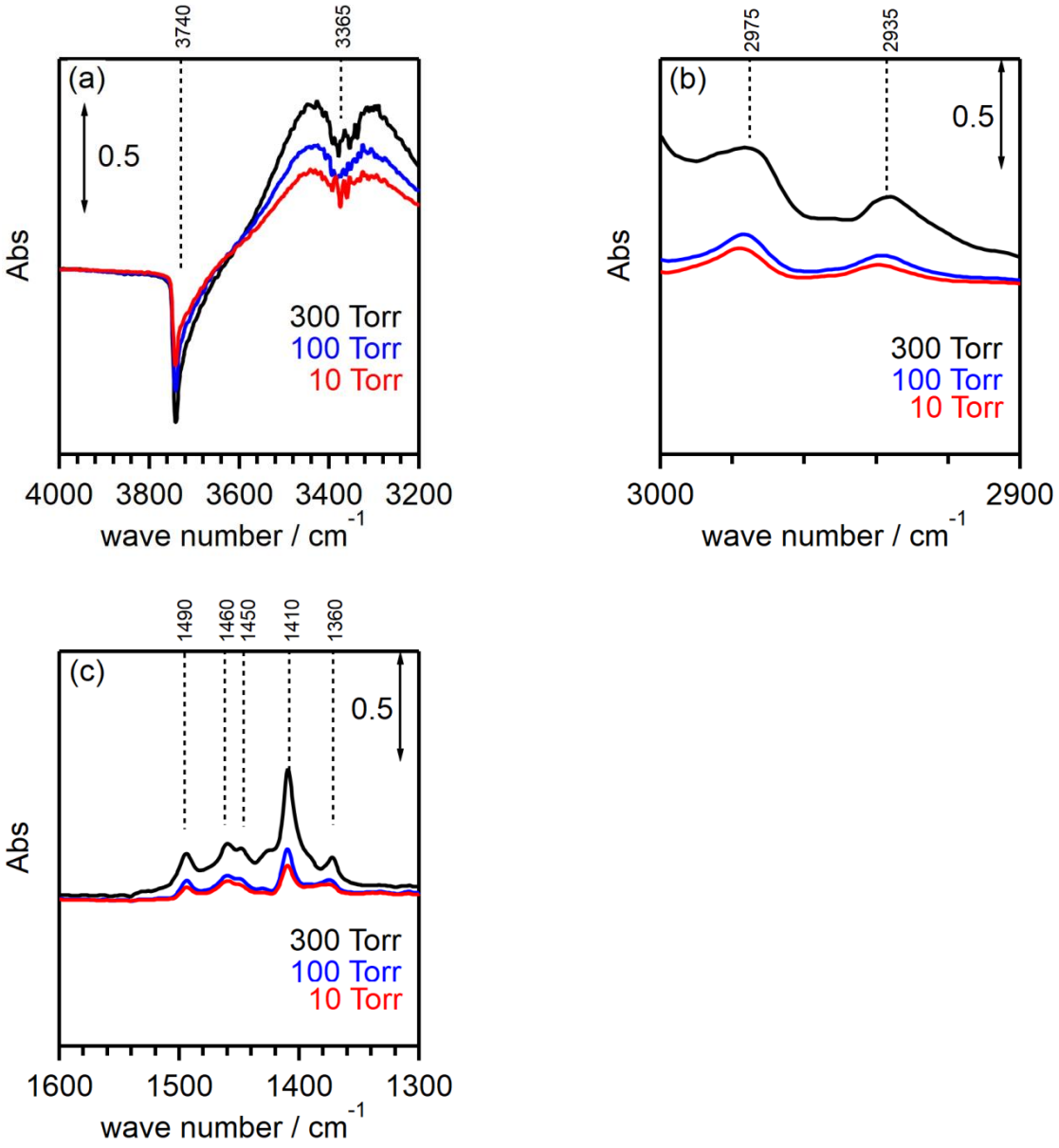

Figure 3-2. Difference IR spectra of MeNSBA-15 under each PO pressure at (a) 4000-3200 cm^{-1} (b) 3000-2900 cm^{-1} (c) 1600-1300 cm^{-1}

Fig 3-3 shows difference IR spectra of NSBA-15 under PO atmosphere. An IR band observed at 3740 cm^{-1} is attributed to the O–H stretching vibration of surface silanol groups[5], and broad peak observed at around 3365 cm^{-1} corresponds to the N–H stretching vibration as well as the one of MeNSBA-15. In this case, a peak at 1550 cm^{-1} is observed, which is attributed to N-H bending vibration. Three peaks appeared at 2975, 1495 and 1360 cm^{-1} is due to CH_3 vibration, and three peaks appeared at 2935, 1460 and 1450 cm^{-1} is due to CH_2 vibration. These peaks would be derived from methyl group connected to the nitrogen atom and adsorbed cyclic ether. It is noteworthy that a sharp peak appeared at 1410 cm^{-1} as well as the one of MeNSBA-15. This peak would suggest that ring-opened cyclic ether, alkoxide, can be formed even on the non-methylated nitrogen atom.

According to above discussion, alkoxide can be formed on both MeNSBA-15 and NSBA-15.

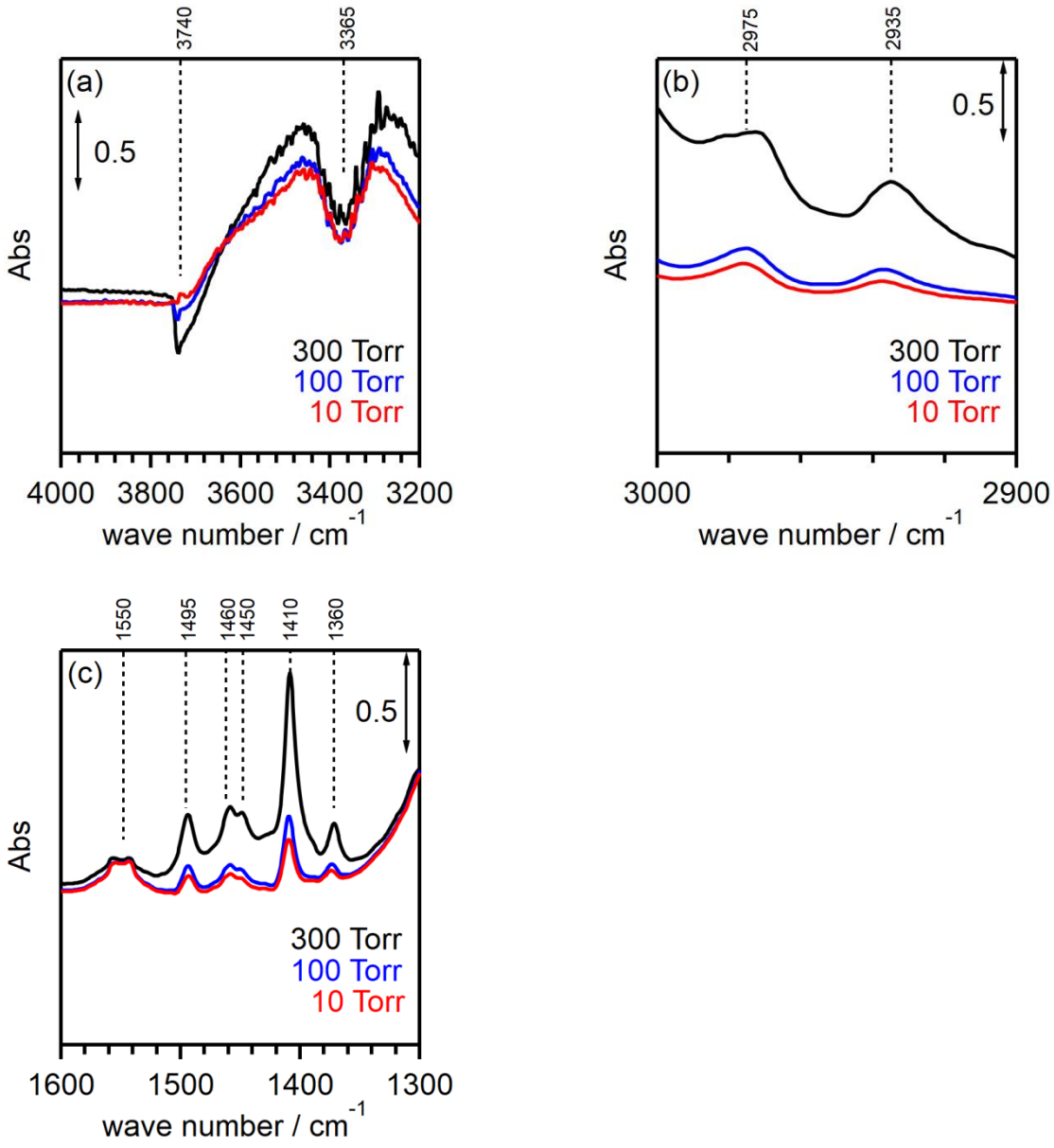

Figure 3-3. Difference IR spectra of MeNSBA-15 under each PO pressure at (a) 4000-3200 cm^{-1} (b) 3000-2900 cm^{-1} (c) 1600-1300 cm^{-1}

3.4 Kinetic analysis

Previously-proposed catalysts (e.g., ammonium salts,[25, 28-34] metal complexes,[18, 24-27, 33, 35-37] ionic liquids,[37-39] and metal oxides[20, 40]) have been designed to possess various types of reaction sites to activate the CO_2 and/or ethers. This variety leads to different reaction mechanisms and rate-determining steps unique to each homogeneous and heterogeneous catalyst. From the point of view of reaction mechanism, these could be roughly categorized into two groups. One assumes that the reaction initiates with the adsorption of two reactants and follows a bimolecular reaction (i.e., Langmuir–Hinshelwood mechanism),[18-24] and the other assumes that one of the adsorbed reactants is activated and attacks the other free (i.e., gas phase) reactant (i.e., Eley–Rideal mechanism).[25-42] It might be straightforward to assume that liquid phase PO molecules initially interact with dissolved homogeneous catalysts or dispersed heterogeneous catalysts, and following a bimolecular reaction with free CO_2 molecules, form cyclic carbonates (i.e., Eley–Rideal model). The derived rate expressions based on any of the cases of the Eley–Rideal mechanism. it might include the case of epoxide ring-opening and CO_2 insertion. Either of these steps is assumed as a rate-determining step (Scheme 3-1). In these cases, adsorption of reactant is the rate-determining step. Thus, the propylene carbonate formation rate (r_{PC}) is proportional to the number of gas phase reactant and open site:

$$r_{PC} = k_1[PO][*] \qquad (1)$$

or $$r_{PC} = k_2[CO_2][*] \qquad (1')$$

where k_1 or k_2 is the rate constant for adsorption of *PO* or *CO_2* in gas phase, respectively, and [*] is the number of unoccupied methylated N-atoms. These rate equations give other forms with using Equation (2):

$$[L] = [*] + [CO_2 *] + [POi] \qquad (2)$$

$$\frac{r_{PC}}{[L]} = k_1 \frac{[PO]}{(1+K_1[PO]+K_2[CO_2])} \qquad (3)$$

or $\frac{r_{PC}}{[L]} = k_2 \frac{[CO_2]}{(1+K_1[PO]+K_2[CO_2])}$ (3')

Both equations (3) and (3') do not explain the experimental data that shows negative dependence in high concentration range.

From the above, it could not explain the observed TOF dependences (Fig. 3-1).

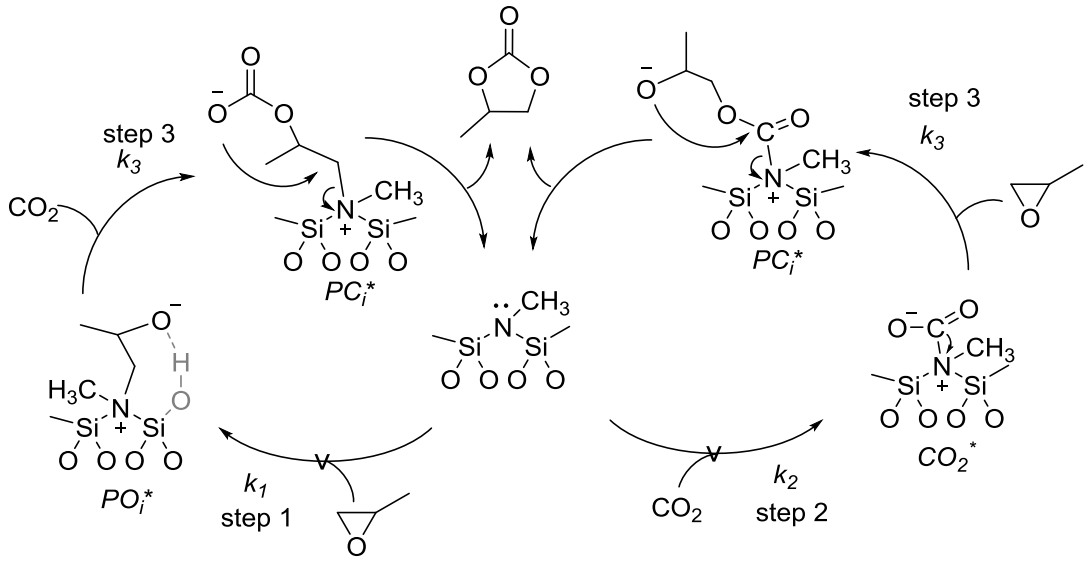

Scheme 3-4. Proposed sequence of reaction steps for propylene carbonate synthesis on MeNSBA-15 in the case adsorption of reactant is the rate-determining step.

Thus, the Eley–Rideal model would not apply to the reaction over MeNSBA-15. Because of the high CO_2 pressure conditions used in this study, CO_2 should be easily dissolved in the liquid PO phase. Hence, the Langmuir–Hinshelwood mechanism was considered. The previously proposed Langmuir–Hinshelwood mechanism can be roughly divided into two cases: 1) CO_2 adsorbs on a basic site and subsequently attacks the PO adsorbed on an acidic site to initiate the ring-opening reaction,[18-23] and 2) the ring-opening reaction of PO proceeds on the basic site followed by a bimolecular reaction with CO_2 adsorbed on the neighboring basic sites.[24] The former mechanism, which involves the reaction between reactants on basic and acidic sites,

does not provide a rate expression that could explain the decrease in TOF at high reactant concentration (Fig. 3-1) because both reactants, PO and CO_2 do not compete to adsorb on catalytic sites and adsorb on basic and acidic sites each other independently.

Thus, it appears that the cyclic carbonate synthesis over MeNSBA-15 follows the Langmuir–Hinshelwood mechanism involving two basic sites. Furthermore, the negative dependence of TOF at high reactant concentration together with very little reactivity of the NSBA-15 (left side of Figure 3-2) suggests that both neighboring basic sites should be methylated N-atoms. However, one can assume that CO_2 adsorbs on a non-functionalized N-atom and reacts with a PO intermediate on a neighboring methylated N-atom (middle of Fig. 3-2). In the case alkoxide intermediate forms on a non-methylated site and carbamate forms on a methylated site, the propylene carbonate synthesis rate (r_{PC}) is proportional to the number of adsorbed PO intermediates ($[POi*]$) and adsorbed CO_2 (carbamate,$[CO_2*]$) on the neighboring methylated N-atom pair sites:

$$r_{PC} = k_3 \frac{[POi*][CO_2*]}{[L_{N-Me}]} \qquad (4)$$

where k_3 is the rate constant for a nucleophilic attack from carbamate to POi, and $[L_{N-Me}]$ is the total number of methylated N-atoms sites. Equation 1 takes a new form after accounting for quasi-equilibrated reactant adsorption in steps 1 and 2.

$$r_{PC} = K_1 K_2 k_3 \frac{[PO][CO_2][*]^2}{[L_{N-Me}]} \qquad (5)$$

Here, K_1 and K_2 are the equilibrium constants for the adsorption of PO and CO_2, respectively. $[*]$ is the number of unoccupied methylated N-atom sites. The total number of available methylated N-atoms ($[L_{N-Me}]$) and available non-methylated N-atoms is equal to the sum of likely surface intermediates:

$$[L_{N-Me}] = [*] + [CO_2*] + [POi*] \qquad (6)$$

$$[L_{N-H}] = [*] + [POi*] \qquad (6')$$

The combination of equations 5, 6, and 6' gives the following rate expression for propylene carbonate synthesis:

$$\frac{r_{PC}}{[L_{N-H}]} = K_1 K_2 k_3 \frac{[PO][CO_2]}{(1+K_1[PO]+K_2[CO_2])(1+K_1[PO])} \quad (7)$$

From the above, this reaction model including the basic site pairs of nitrogen and methylated nitrogen could not provide the rate expression that explains the experimental results (Fig. 3-1). In the case alkoxide intermediate forms on a methylated site and carbamate forms on a non-methylated site, the reaction model is also denied according to the same consideration.

Therefore, the above discussion concludes that the most plausible reaction site on MeNSBA-15 is a neighboring methylated N-atom pair (right side of Fig. 3-2). This further implies that, for the reaction to proceed, CO_2 must be adsorbed on the methylated N-atom, and it would form a more reactive carbamate species due to the stronger basicity of the site.[43] Thus, as a bimolecular reaction step, a nucleophilic attack from a carbamate toward a PO intermediate could be proposed.

Besides basic N-atoms, there would be surface silanol groups that could work as weak Brønsted acid sites on MeNSBA-15. The acidity of the silanol, however, would not be strong enough to adsorb and stabilize PO as in the acidic metal center in metal oxides [20, 21, 25, 40] or metal complexes.[18, 24, 26, 27, 33, 35-37] The hydrogen bond between a silanol group and an oxygen atom of PO would help to stabilize a reaction intermediate.[19, 28, 29, 32, 34, 38, 41]

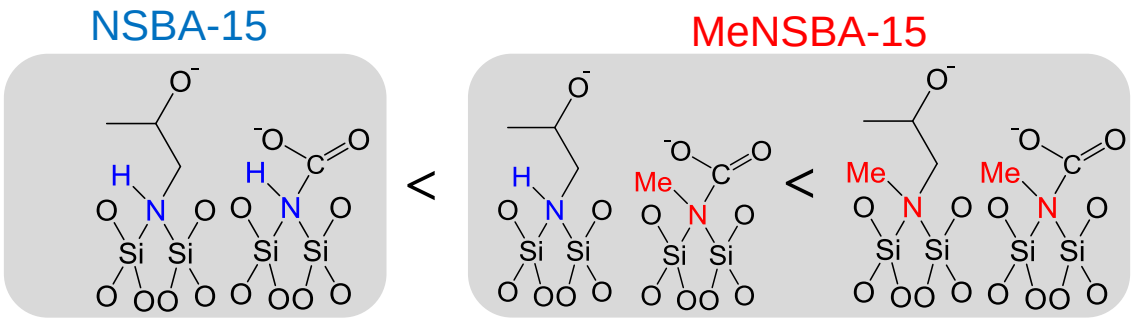

Figure 3-5. Activity order of NSBA-15 and MeNSBA-15

Scheme 3-1 shows a sequence of catalytic reaction steps that accurately describes the effect of CO_2 and PO partial pressure on TOF (Fig. 3-1). The catalytic cycle involves the following steps: 1) ring-opening reaction of PO to form an alkoxide intermediate (POi) on a methylated N-atom, 2) carbamate formation of CO_2 on a neighboring methylated N-atom; 3) nucleophilic attack from an O-atom of carbamate toward a POi forming a propylene carbonate-derived alkoxide intermediate (PCi); and 4) a dissociative ring-closing reaction to form a cyclic propylene carbonate. The bimolecular reaction (step 3) that occurs is kinetically relevant,[22, 44] and the adsorption/desorption of PO and CO_2 (steps 1 and 2) are assumed to be quasi-equilibrated. The neighboring silanol groups (shown in gray in Scheme 3-1) would stabilize a POi (step 1) and a PCi (step 3). This is a typical Langmuir–Hinshelwood mechanism, and following Scheme 3-1, the propylene carbonate synthesis rate (r_{PC}) is proportional to the number of adsorbed PO intermediates ($[POi*]$) and adsorbed CO_2 (carbamate,$[CO_2*]$) on the neighboring methylated N-atom pair sites:

$$r_{PC} = k_3 \frac{[POi*][CO_2*]}{[L]} \qquad (8)$$

where k_3 is the rate constant for a nucleophilic attack from carbamate to POi, and $[L]$ is the total number of methylated N-atoms forming the pair sites. Equation 1 takes a new form after accounting for quasi-equilibrated reactant adsorption in steps 1 and 2.

$$r_{PC} = K_1 K_2 k_3 \frac{[PO][CO_2][*]^2}{[L]} \qquad (9)$$

Here, K_1 and K_2 are the equilibrium constants for the adsorption of PO and CO_2, respectively. $[*]$ is the number of unoccupied methylated N-atoms forming the pair sites. The total number of available methylated N-atoms forming the pair sites ($[L]$) is equal to the sum of all likely surface intermediates:

$$[L] = [*] + [CO_2 *] + [POi *] \qquad (10)$$

The combination of equations 2 and 3 gives the following rate expression for propylene carbonate synthesis:

$$\frac{r_{PC}}{[L]} = K_1 K_2 k_3 \frac{[PO][CO_2]}{(1+K_1[PO]+K_2[CO_2])^2} \qquad (11)$$

On both PO and CO_2, the measured reaction rate shows linear and negative dependences in low and high partial pressure ranges, respectively (Fig. 3-1), which is consistent when POi or carbamate occupies a significant fraction of the methylated N-atoms (Equation 11). Thus, the mechanistic interpretation implies that the bimolecular reaction step is a kinetically relevant step. It should be noted that assuming the step 4 as a rate-determining step also gives a rate equation that mathematically fulfill the experimental result.

In this case, ring-closing reaction of the intermediate is the rate-determining step. Thus, the propylene carbonate formation rate (r_{PC}) is proportional to the number of surface intermediate species:

$$r_{PC} = k_4[PCi] \qquad (12)$$

With using pseudo steady-state hypothesis on the intermediate [*PCi*], assuming reverse reaction

on step 3, and using Equation (10), the rate equation (12) gives another form:

$$\frac{r_{PC}}{[L]} = K_1 K_2 k_3 k_4 \frac{[PO][CO_2]}{(1+K_1[PO]+K_2[CO_2])(k_{-3}+k_4+K_1 k_4[PO]+K_2 k_4[CO_2])} \quad (13)$$

This equation (13) could mathematically explain the experimental results in Fig. 3-1.

Therefore, assuming either step 3 or 4 can mathematically explains the experimental result (Fig. 3-1). The step 4 (ring closing step from intermediate species) is, however, considered as a rate-determining step only in a very limited case[27] among 11 of previous studies[24-28, 30, 32, 34, 37, 38, 42]. Based on these studies, we assumed the step 3 is more plausible, which is proposed in the previous studies[24, 26, 27, 42] The step is, however, considered as a rate-determining step only in a very limited case,[27] and thus, we assumed step 3 as a rate-determining step.[24, 26, 27, 42] This proposed rate determining step is different from what has been proposed in the previous studies (i.e., ring-opening step of cyclic ether),[25, 28, 30, 32, 34, 37, 38] which suggests that MeNSBA-15 would be a unique catalyst that favors the formation of a PO derived ring-opened alkoxide. Moreover, we assume that the higher TOF of MeNSBA-15 compared to that of well-studied homogeneous catalysts (Table 3-1) would be due to the effective stabilization of POi via a hydrogen-bond to the neighboring silanol group.[19, 41]

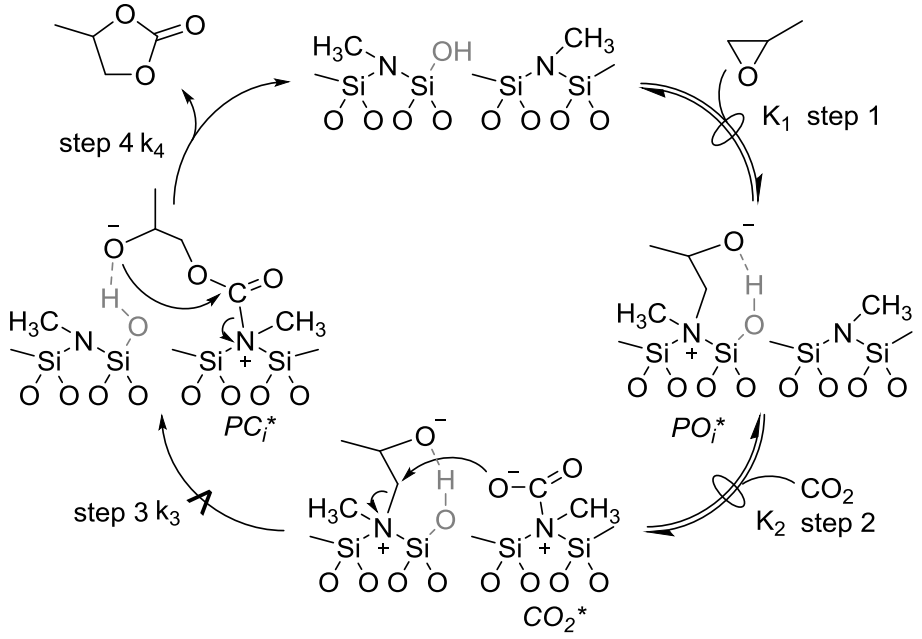

Scheme 3-2. Proposed sequence of reaction steps for propylene carbonate synthesis on MeNSBA-15 catalyst.

3.5 TOF tendency from various cyclic ethers

The catalytic feature of MeNSBA-15 was further investigated by using various cyclic ethers as reactants. Figure 3-3 shows the TOF of cyclic carbonate synthesis between different cyclic ethers and CO_2 (3 MPa CO_2 pressure, 373 K reaction temperature, 1 h reaction time) as a function of the oxygen proton affinity of each cyclic ether.[45, 46] The reactivity of cyclic ether toward attack by a nucleophile is related to the electrophilicity of the C-atom, which is, however, difficult to measure directly. Thus, as an alternative indicator, the proton affinity of the neighboring oxygen is considered, which should reflect the balance of electron donation between the neighboring O- and C-atoms. Over TBABr catalyst, the TOF increased with the increase in the oxygen proton affinity, with the exception of BCMO (Fig. 4, blue triangles). In contrast, there was no clear correlation between the TOF and the oxygen proton affinities over MeNSBA-15 catalyst (Fig. 3-3, red circles). These differences would be explained by their

different reaction mechanisms. Over TBABr catalyst, the reaction has been proposed to proceed through Eley–Rideal mechanism,[29, 33-35] and the ring-opening step of the cyclic ether initiated by the nucleophilic attack toward the C-atom has been considered as the rate-determining step.[34] Therefore, the reaction rate can be assumed to reflect the electron density of the C-atom, and it would roughly correlate with the neighboring oxygen proton affinity. The experimental results (Fig. 3-3) agree with this assumption, in which the TOF of carbonate synthesis increases with the increase in the oxygen proton affinity of the cyclic ether (Fig. 3-3, blue triangles). On the contrary, over MeNSBA-15, the rate-determining step is the bimolecular reaction between ring-opened alkoxide and carbamate on the neighboring methylated nitrogen pair sites (Scheme 3-2). This might cause an irrelevant correlation between the TOF and proton affinity (Fig. 3-3, red circles). The above discussion indirectly supports the proposed reaction mechanism over MeNSBA-15.

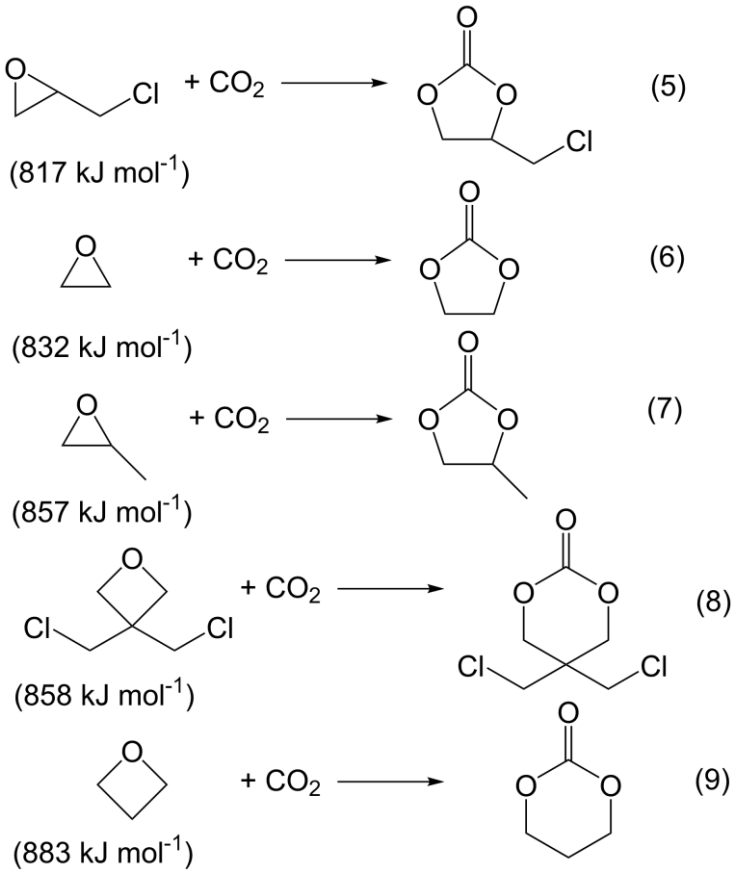

Scheme 3-2. Cyclic carbonate synthesis from CO_2 and (eq. 5) epichlorohydrin, (eq. 6) ethylene oxide, (eq.7) propylene oxide, (eq. 8) 3,3-bischloromethyl oxetane, and (eq. 9) oxetane. The values in the parentheses are proton affinities of the reactant cyclic ethers.

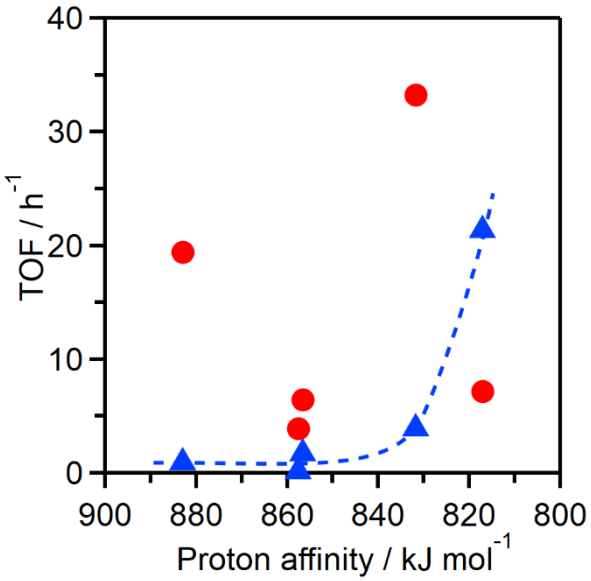

Figure 3-6. Change in the TOF of cyclic carbonate synthesis at 373 K for 6.0 h (3 MPa CO_2, 14 mmol cyclic ether), with epichlorohydrin, ethylene oxide, propylene oxide, 3,3-bischloromethyl oxetane, and oxetane as reactants (corresponding to the equations 5 to 9 in Scheme 3-2) as a function of proton affinity of each reactants (red circles) on MeNSBA-15 (50 mg) and (blue triangles) on TBABr (70 mg). The conversion of each measurement is less than 10%. Blue dashed line is added to guide the eye.

3.6 Conclusions

MeNSBA-15 was shown to catalyze cyclic carbonate synthesis from cyclic ethers and CO_2 for the first time. It catalyzed the reaction without the need for pretreatments. The observation of a drastic increase in the TOF value after the methylation process clearly indicated that the reactivity of the catalyst (i.e., nucleophilicity of the basic N-atom) was enhanced by methylation. The kinetic analysis revealed Langmuir–Hinshelwood mechanism, rather than Eley–Rideal mechanism, with a kinetically relevant bimolecular reaction step between a ring-opened alkoxide intermediate and a carbamate over neighboring methylated nitrogen pair sites. It is further assumed that the silanol of MeNSBA-15 would work as a weak Lewis acid and synergistically stabilize the alkoxide intermediate. The comparison of the observed TOF with the oxygen proton affinity of cyclic ethers over MeNSBA-15 and TBABr further supported the different reaction mechanisms among MeNSBA-15 and the conventional homogeneous catalysts. The detailed understanding of the fundamental reaction mechanism would lead to a rational design of catalysts.

1. Darensbourg, D. J.; Holtcamp, M. W., *Coordination Chemistry Reviews* **1996,** 153, 155-174.

2. Shaikh, A. A. G.; Sivaram, S., *Chemical Reviews* **1996,** 96 (3), 951-976.

3. Yoshida, M.; Ihara, M., *Chemistry-a European Journal* **2004,** 10 (12), 2886-2893.

4. Wakihara, M.; Yamamoto, O., Lithium Ion Batteries-Fundamentals and Performance. Kodansha Ltd.:: Tokyo, 1998

5. Lu, Z.; Schechter, A.; Moshkovich, M.; Aurbach, D., *Journal of Electroanalytical Chemistry* **1999,** 466 (2), 203-217.

6. Suriano, F.; Pratt, R.; Tan, J. P. K.; Wiradharma, N.; Nelson, A.; Yang, Y. Y.; Dubois, P.; Hedrick, J. L., *Biomaterials* **2010,** 31 (9), 2637-2645.

7. Sakakura, T.; Kohno, K., *Chemical Communications* **2009,** (11), 1312-1330.

8. Wang, J. Q.; Dong, K.; Cheng, W. G.; Sun, J.; Zhang, S. J., *Catalysis Science & Technology* **2012,** 2 (7), 1480-1484.

9. Ramidi, P.; Munshi, P.; Gartia, Y.; Pulla, S.; Biris, A. S.; Paul, A.; Ghosh, A., *Chemical Physics Letters* **2011,** 512 (4-6), 273-277.

10. Lang, X. D.; Yu, Y. C.; He, L. N., *Journal of Molecular Catalysis a-Chemical* **2016,** 420, 208-215.

11. Jayakumar, S.; Li, H.; Zhao, Y. P.; Chen, J.; Yang, Q. H., *Chemistry-an Asian Journal* **2017,** 12 (5), 577-585.

12. Saptal, V. B.; Bhanage, B. M., *Chemsuschem* **2017,** 10 (6), 1145-1151.

13. Han, L.; Park, S. W.; Park, D. W., *Energy & Environmental Science* **2009,** 2 (12), 1286-1292.

14. Tomishige, K.; Yasuda, H.; Yoshida, Y.; Nurunnabi, M.; Li, B. T.; Kunimori, K., *Green Chemistry* **2004,** 6 (4), 206-214.

15. Tu, M.; Davis, R. J., *Journal of Catalysis* **2001,** 199 (1), 85-91.

16. Taherimehr, M.; Van de Voorde, B.; Wee, L. H.; Martens, J. A.; De Vos, D. E.; Pescarmona, P. P., *Chemsuschem* **2017,** 10 (6), 1283-1291.

17. Mori, K.; Mitani, Y.; Hara, T.; Mizugaki, T.; Ebitani, K.; Kaneda, K., *Chemical Communications* **2005,** (26), 3331-3333.

18. Kuruppathparambil, R. R.; Jose, T.; Babu, R.; Hwang, G. Y.; Kathalikkattil, A. C.; Kim, D. W.; Park, D. W., *Applied Catalysis B-Environmental* **2016,** 182, 562-569.

19. Lan, D. H.; Chen, L.; Au, C. T.; Yin, S. F., *Carbon* **2015,** 93, 22-31.

20. Yano, T.; Matsui, H.; Koike, T.; Ishiguro, H.; Fujihara, H.; Yoshihara, M.; Maeshima, T., *Chemical Communications* **1997,** (12), 1129-1130.

21. Adeleyea, A. I.; Kellici, S.; Heil, T.; Morgan, D.; Vickers, M.; Saha, B., *Catalysis Today* **2015,** 256, 347-357.

22. Kim, H. U.; Babu, R.; Roshan, R.; Park, D. W., *Applied Catalysis a-General* **2017,** 538, 59-65.

23. Zhong, S. F.; Liang, L.; Liu, M. S.; Liu, B.; Sun, J. M., *Journal of Co2 Utilization* **2015,** 9, 58-65.

24. North, M.; Pasquale, R., *Angewandte Chemie-International Edition* **2009,** 48 (16), 2946-2948.

25. Butera, V.; Russo, N.; Cosentino, U.; Greco, C.; Moro, G.; Pitea, D.; Sicilia, E., *Chemcatchem* **2016,** 8 (6), 1167-1175.

26. Luinstra, G. A.; Haas, G. R.; Molnar, F.; Bernhart, V.; Eberhardt, R.; Rieger, B., *Chemistry-a European Journal* **2005,** 11 (21), 6298-6314.

27. Castro-Gomez, F.; Salassa, G.; Kleij, A. W.; Bo, C., *Chemistry-a European Journal* **2013,** 19 (20), 6289-6298.

28. Foltran, S.; Mereau, R.; Tassaing, T., *Catalysis Science & Technology* **2014,** 4 (6), 1585-1597.

29. Cao, T.; Sun, L. T.; Shi, Y.; Hua, L.; Zhang, R.; Guo, L.; Zhu, W. W.; Hou, Z. S., *Chinese Journal of Catalysis* **2012,** 33 (3), 416-424.

30. Kihara, N.; Hara, N.; Endo, T., *Journal of Organic Chemistry* **1993,** 58 (23), 6198-6202.

31. Cho, W.; Shin, M. S.; Hwang, S.; Kim, H.; Kim, M.; Kim, J. G.; Kim, Y., *Journal of Industrial and Engineering Chemistry* **2016,** 44, 210-215.

32. Rocha, C. C.; Onfroy, T.; Pilme, J.; Denicourt-Nowicki, A.; Roucoux, A.; Launay, F., *Journal of Catalysis* **2016,** 333, 29-39.

33. Tiffner, M.; Gonglach, S.; Haas, M.; Schofberger, W.; Waser, M., *Chemistry-an Asian Journal* **2017,** 12 (10), 1048-1051.

34. Cokoja, M.; Wilhelm, M. E.; Anthofer, M. H.; Herrmann, W. A.; Kuhn, F. E., *Chemsuschem* **2015,** 8 (15), 2436-2454.

35. Montoya, C. A.; Gomez, C. F.; Paninho, A. B.; Nunes, A. V. M.; Mahmudov, K. T.; Najdanovic-Visak, V.; Martins, L.; da Silva, M.; Pombeiro, A. J. L.; da Ponte, M. N., *Journal of Catalysis* **2016,** 335, 135-140.

36. D'Elia, V.; Ghani, A. A.; Monassier, A.; Sofack-Kreutzer, J.; Pelletier, J. D. A.; Drees, M.; Vummaleti, S. V. C.; Poater, A.; Cavallo, L.; Cokoja, M.; Basset, J. M.; Kuhn, F. E., *Chemistry-a European Journal* **2014,** 20 (37), 11870-11882.

37. Pescarmona, P. P.; Taherimehr, M., *Catalysis Science & Technology* **2012,** 2 (11), 2169-2187.

38. Luo, R. C.; Zhou, X. T.; Fang, Y. X.; Ji, H. B., *Carbon* **2015,** 82, 1-11.

39. Yue, S.; Hao, X. J.; Wang, P. P.; Li, J., *Molecular Catalysis* **2017,** 433, 420-429.

40. Yamaguchi, K.; Ebitani, K.; Yoshida, T.; Yoshida, H.; Kaneda, K., *Journal of the American Chemical Society* **1999,** 121 (18), 4526-4527.

41. Sankar, M.; Ajithkumar, T. G.; Sankar, G.; Manikandan, P., *Catalysis Communications* **2015,** 59, 201-205.

42. Hayashi, S.; Yamazoe, S.; Koyasu, K.; Tsukuda, T., *Chemistry-an Asian Journal* **2017,** 12 (13), 1635-1640.

43. Chang, A. C. C.; Chuang, S. S. C.; Gray, M.; Soong, Y., *Energy & Fuels* **2003,** 17 (2), 468-473.

44. Lee, S. D.; Kim, B. M.; Kim, D. W.; Kim, M. I.; Roshan, K. R.; Kim, M. K.; Won, Y. S.; Park, D. W., *Applied Catalysis a-General* **2014,** 486, 69-76.

45. Sasaki, H., TOAGOSEI TREND: 2004; Vol. 7, pp 8-14.

46. Hunter, E. P. L.; Lias, S. G., *Journal of Physical and Chemical Reference Data* **1998,** 27 (3), 413-656.

4 Catalysis of MeNSBA-15 in unsaturated cyclic carbonate synthesis from CO_2 and unsaturated alcohol

4.1 Introduction

Unsaturated cyclic carbonate is useful intermediate for various chemicals such as oxazolidinones[1-4] and and β-oxopropyl carbonates.[5] Enantioselective hydrogenation of α-methylene cyclic carbonates has led to form optically active bicyclic carbonates and 1,2-diols with very high enantioselectivities in the presence of ruthenium catalyst.[6] These facts support that unsaturated cyclic carbonate has a great possibility to be new intermediate towards high-valued chemical products. Typical cyclic carbonate synthesis using unsaturated alcohol is catalyzed by phosphine[7], Tri-n-butylphosphine[8], *t*BuOI[9] and metal complex such as ruthenium[2], cobalt[10], palladium[11], cupper[4], silver[12] and gold[13]. Such conventional syntheses use a highly toxic reagent such as phosphine and organic solvent. Therefore, a novel synthetic route is required to give less and less environmental impact.[8] It is necessary to develop a mild and environmental benign reaction system including a catalyst to capture CO_2 efficiently as the C1 source into a wide variety of substrates, especially fine-chemicals. Using an ionic liquid activated by microwave [14-16] and a silica-supported ionic-liquid[17, 18] as catalysts are reported as a new method of unsaturated cyclic carbonate synthesis. These exhibited various advantages such as high reactivity, and easy purification.

In Chapter 3, MeNSBA-15 was found to catalyze cyclic carbonate synthesis from cyclic ether. Kinetic analysis revealed that this reaction on MeNSBA-15 takes place through Langmuir-Hinshelwood mechanism.[19] Both cyclic ether and CO_2 adsorbed on a neighboring methylated nitrogen pair site and a ring-opened alkoxide intermediate and carbamate intermediate are formed. Subsequently, cyclic carbonate was produced with a kinetically relevant bimolecular reaction.

In this Chapter, MeNSBA-15 was also shown to catalyze cyclic carbonate synthesis from unsaturated alcohol. Among a series of SBA-15 samples (MeNSBA-15, NSBA-15, and SBA-15), only the methylated sample catalyzed the reaction. The catalytic results clearly indicate that formation of methylated nitrogen is essential for the reaction. The changes in the TOF as a function of CO_2 partial pressure and 2-methyl-3-butyn-2-ol concentration reflect the change in the major active surface species. The CO_2 dependence could be plausibly explained by the simple saturation of CO_2 over the active site. This suggested that the formation of carbamate species would be the key for the reaction as same as the case of the reaction with cyclic ether.[19] And the relatively weaker interaction of unsaturated alcohol with the catalytic site as a counter reactant. The difference of pressure dependence of two cyclic carbonate syntheses could be explained by the competing adsorption of the other reactant. The interaction of the methylated nitrogen site with unsaturated alcohol would be much lower compare to that with cyclic ether. The reaction involves the following five steps; carbamate formation, interaction of unsaturated alcohol with the carbamate species, deprotonation and accompanying C-O bond formation, intramolecular cyclization of alkyl hydrogen carbonate acid intermediate and desorption of the unsaturated cyclic carbonate.

4.2 Catalytic performance

Table 4-1 summarizes the results of catalytic cyclic carbonate synthesis from CO_2 and an unsaturated alcohol (2-methyl-3-butyn-2-ol) over heterogeneous SBA-15-type catalysts and well-studied homogeneous catalysts, TBABr and tri-*n*-butylphosphine. TOF and selectivity were 1.82 h^{-1} and >99% on MeNSBA-15 catalyst. In contrast, NSBA-15 showed little catalytic activity (TOF less than 1.0×10^{-3} h^{-1}). The reaction did not proceed without catalyst under the conditions applied in this study. Remarkable increase in the catalytic activity caused by

methylation could be primarily explained by enhanced nucleophilicity of the nitrogen site, similar to the previous example in cyclic carbonate synthesis from cyclic ether in Chapter 3.[19] The observed TOF value over MeNSBA-15 was comparable to that over conventional homogeneous catalysts (Table 2). Recycling tests were conducted over MeNSBA-15 (3 MPa CO2, 5 mmol 2-methyl-3-butyn-2-ol, 20 mg MeNSBA-15, 373 K, 3 h), and the product yield of second and third uses were maintained 100% relative to the initial use.

Table 4-1. Summary of the catalytic performances for cyclic carbonate synthesis from carbon dioxide and unsaturated alcohol

Catalyst	TOF[a] [h^{-1}]	Conversion (Selectivity)[b] [%]	E_a [kJ mol^{-1}]
MeNSBA-15	2.24	4.4 (>99)	66.1
NSBA-15	$<10^{-3}$	(-)[c]	-
TBABr	0.68	2.0	41.6
Tri-n-butylphosphine	2.58	6.1 (>99)	24.4

a: TOF is calculated at reaction time of 24 h, b: Conversion and selectivity are calculated at reaction time of 24 h, c: unsaturated cyclic carbonate is not detected by gas chromatograph

Figure 4-1 shows the changes in the TOF values over MeNSBA-15 as a function of CO_2 partial pressure (Fig. 4-1a) and 2-methyl-3-butyn-2-ol concentration (Fig. 4-2b). As comparison, those with CO_2 and cyclic ether are also shown in Figs. 4-1c and 4-1d, respectively.[19] In Fig. 4-1a, TOF increased linearly with the increase of CO_2 partial pressure, and became constant at around 3.5 MPa. Whereas, TOF kept linear increase as a function of 2-methyl-3-butyn-2-ol concentration in Fig. 4-1b. These observed reactant dependences were different from that of another cyclic carbonate formation from CO_2 and cyclic ether,[19] as shown in Figs. 4-1c and 4-1d.

The observed TOF dependences showed increase and subsequent decrease along with the reactant partial pressure of both CO_2 and cyclic ether. It should be noted that, especially for CO_2, both reactions were conducted in the same pressure range from 1 to 6 MPa, thus their adsorption behavior on the site would be similar. Therefore, the difference in these dependences would reflect the difference of reactants and the resulting reaction mechanism. In another word, the change in the TOF dependence suggested the change in the major active surface species by adsorption of reactants. As have been discussed in the reaction between CO_2 and cyclic ether,[19] the CO_2 pressure dependence (Fig. 4-1c) could be explained by competing the adsorption of both reactants of CO_2 and cyclic ether to the active sites. On the other hand, the CO_2 dependence observed in this study (Fig. 4-1a) could be plausibly explained by the simple saturation of CO_2 over the active site. This also suggested less interaction of unsaturated alcohol with the catalytic active site.

Activation of CO_2 would be the key in these cyclic carbonate syntheses. As shown above, two reactions showed different CO_2 pressure dependences although both were tested in the same CO_2 pressure range of 1 to 6 MPa (Figs 4-1a and 4-1c). The most plausible state of CO_2 on the methylated-nitrogen site would be a carbamate like species (Scheme 4-1), which was observed by the previous spectroscopic study.[20] It has been suggested that the carbamate species only formed on methylated-nitrogen site in MeNSBA-15, and end-on adsorption of CO_2 proceeds over non-methylated nitrogen site of NSBA-15.[20] The catalytic tests (Table 4-1) clearly showed that methylated nitrogen was essential for the reaction and this strongly suggested that the formation of carbamate species would be the key for the reaction, which is the same as the reaction with cyclic ether.[19] Then, based on the formation of the carbamate species, differences of pressure dependence could be explained by the competing adsorption of the other reactants, those are cyclic ether and unsaturated alcohol. In the case of cyclic ether, as described in the

literature, [19] higher CO_2 partial pressure hampered the competing adsorption of cyclic ether, and resulted in the decrease of reaction rate. On the other hand, in the case of unsaturated alcohol, it seemed that CO_2 adsorption simply saturated at around 3.5 MPa and the most abundant surface intermediate would be the carbamate species under the reaction conditions applied here. The interaction of the methylated nitrogen site with unsaturated alcohol would be much less compare with that with cyclic ether because, which accompanied with the ring opening reaction to release the distortion energy of the structure.

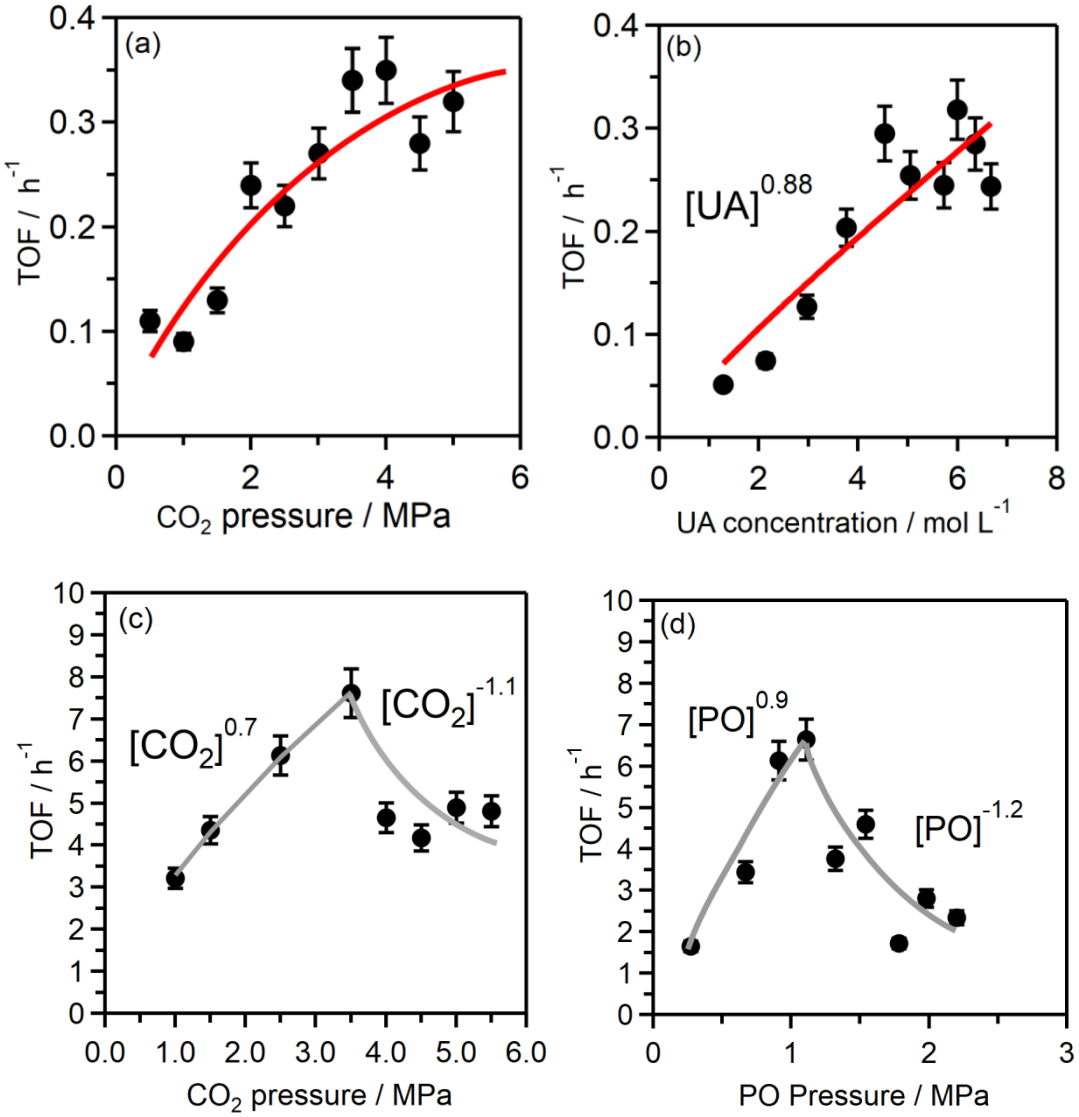

Figure 4-1. TOF values of cyclic carbonate synthesis with 2-methyl-3-butyn-2-ol on MeNSBA-15 as a function of (a) CO_2 pressure and (b) methyl-3-butyn-2-ol concentration. TOF values of propylene carbonate synthesis on MeNSBA-15 as a function of (c) CO_2 pressure and (d) PO amount in Chapter 3.

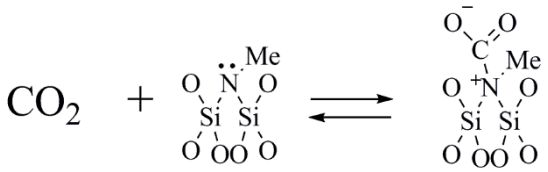

Scheme 4-1. Formation of carbamate on MeNSBA-15

4.3 Consideration of surface active species

Fig 4-2 shows difference IR spectra of MeNSBA-15 under UA atmosphere. An IR band observed at 3740 cm^{-1} is attributed to the O–H stretching vibration of surface silanol groups[5]. A peak observed at 3290 cm^{-1} corresponds to the N^{+}–H stretching vibration. This peak is strong evidence that MeNSBA-15 works as base and abstract proton from UA. Three peaks appeared at 2990, 1490 and 1380 cm^{-1} is due to CH_3 vibration. These peaks would be derived from methyl group connected to the nitrogen atom. A broad peak appeared at 2910 cm^{-1} is attributed to C-H vibration derived from unsaturated bond. A broad peak appeared at 1370 cm^{-1} is attributed to C-N vibration derived from methyl group connected to the nitrogen atom. Above discussion leads that MeNSBA-15 abstracts proton from UA and interact with UA^{-} like Scheme 4-2.

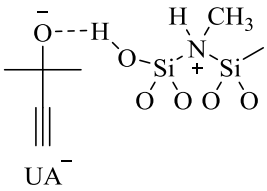

Scheme 4-2. MeNSBA-15 abstracts proton from UA

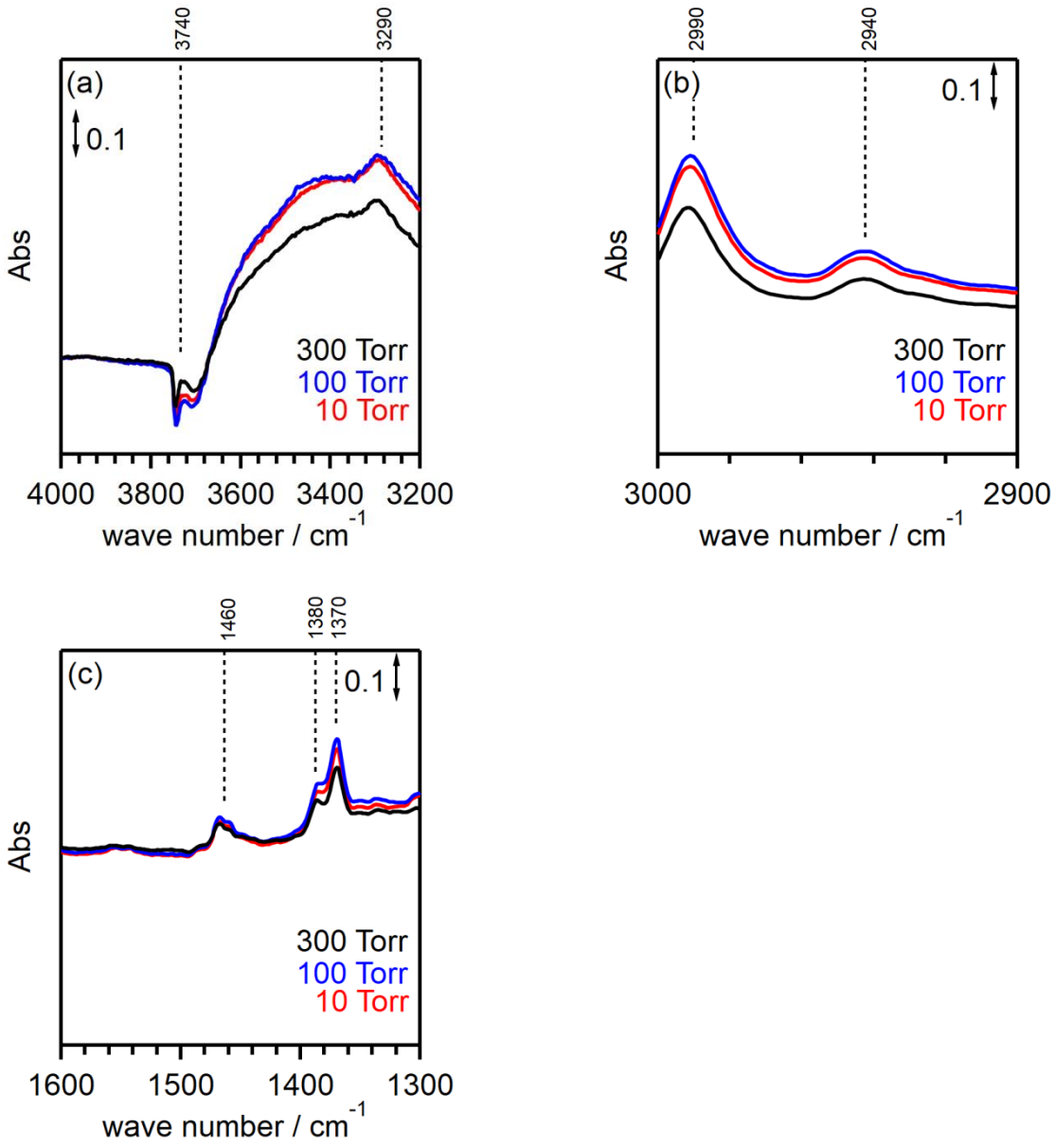

Figure 4-2. Difference IR spectra of MeNSBA-15 under each UA pressure at (a) 4000-3200 cm^{-1} (b) 3000-2900 cm^{-1} (c) 1600-1300 cm^{-1}

Fig 4-3 shows difference IR spectra of MeNSBA-15 under UA atmosphere. An IR band observed at 3740 cm^{-1} is attributed to the O–H stretching vibration of surface silanol groups[5]. A broad peak observed at around 3370 cm^{-1} corresponds to the N–H stretching vibration. The decrease of this peak would mean that bridged amine group (NH) decreased and $N^{+}H_2$ formed by proton abstraction. This is strong evidence that NSBA-15 also works as base and abstract proton from UA. Three peaks appeared at 2990, 1490 and 1380 cm^{-1} is due to CH_3 vibration. These peaks would be derived from methyl group connected to the nitrogen atom. A broad peak appeared at 2910 cm^{-1} is attributed to CH vibration derived from unsaturated bond. Above discussion leads that NSBA-15 also abstracts proton from UA and interact with UA^{-} like Scheme 4-3.

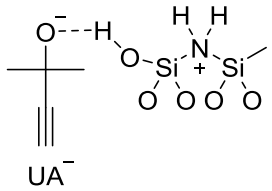

Scheme 4-3. NSBA-15 abstracts proton from UA

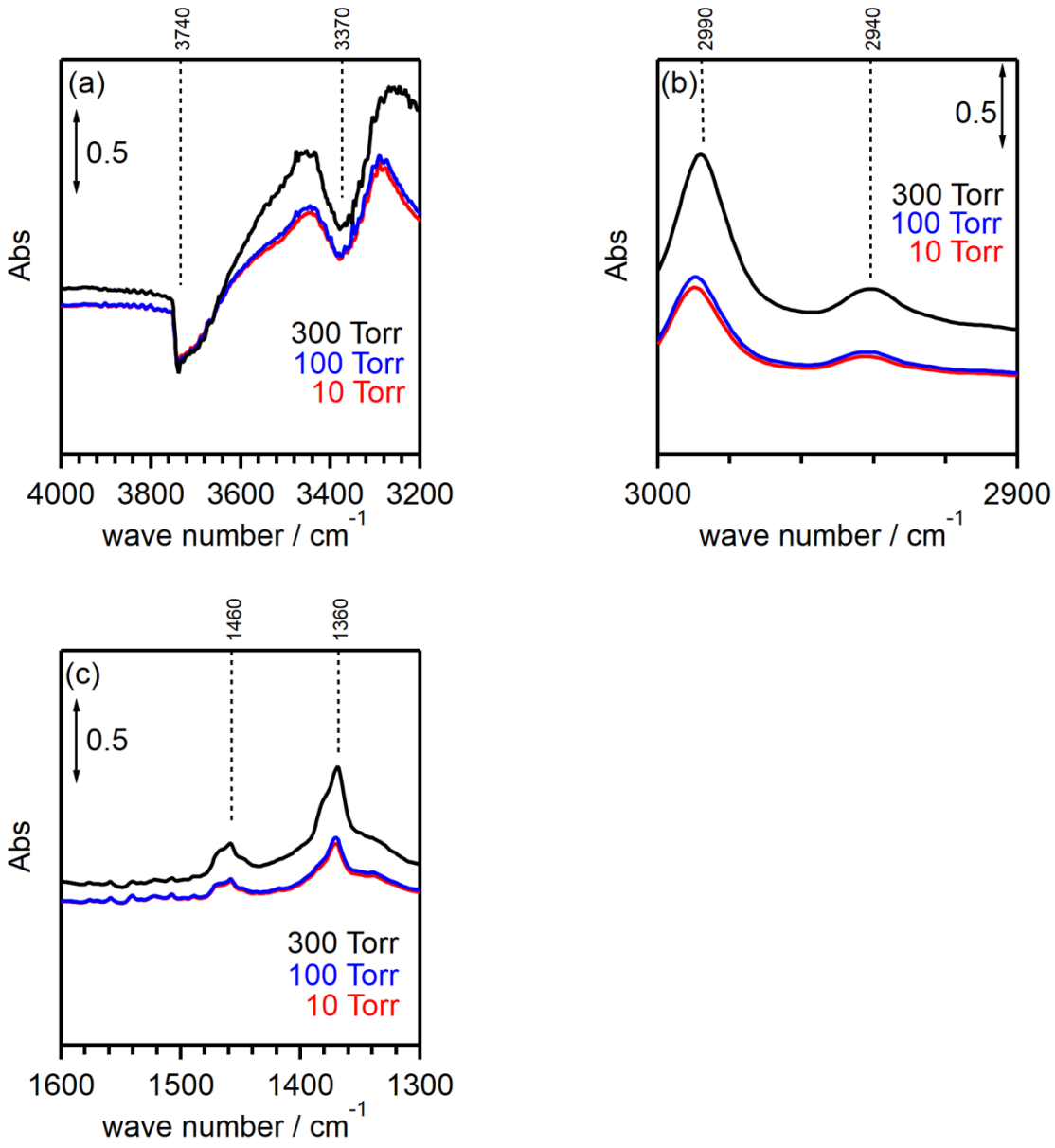

Figure 4-3. Difference IR spectra of NSBA-15 under each UA pressure at (a) 4000-3200 cm^{-1} (b) 3000-2900 cm^{-1} (c) 1600-1300 cm^{-1}

4.4 Kinetic analysis

Based on all above experimental data, discussion, and previous studies,[9, 12, 13] a reaction scheme can be proposed as shown in Scheme 4-4. The reaction involves the following steps: 1) carbamate formation via CO_2 adsorption (*CO_2**) on the methylated nitrogen atom similar to the previous study,[19] 2) interaction of unsaturated alcohol with the carbamate species (*UAC**), 3) deprotonation and simultaneous C–O bond formation between the carbamate and unsaturated alcohol species to form an alkyl hydrogen carbonate acid-like intermediate (*AC**), 4) intramolecular cyclization of the intermediate between hydroxyl and alkyne groups to form an adsorbed cyclic carbonate (*UCC**), and 5) desorption of the unsaturated cyclic carbonate (*UCC*). The adsorption/desorption of CO_2 as the carbamate (Step 1) is assumed to be quasi-equilibrated. Subsequently, unsaturated alcohol interacts with the carbamate, and the hydrogen atom of hydroxyl group in unsaturated alcohol is subject to nucleophilic attack from oxygen atom in the carbamate, and simultaneous C–O bond formation proceeds. (Steps 2 and 3). The other pathway can be considerable at the Step 3, in which the deprotonation and simultaneous C–O bond formation accompanies with the desorption of the molecule (*UAC*'* and subsequent Step 3' in Scheme 3). This step forms a released alkyl hydrogen carbonate acid molecule (*AC*), which has been known to be very unstable and its equilibrium is largely lean to the reactant side (i.e., CO_2 + unsaturated alcohol, as shown in Scheme 4-4).[21] Then, formed intermediate (*AC**) undergoes the intramolecular cyclization between hydroxyl group and unsaturated bond (Step 4). Finally, the formed cyclic carbonate desorbs (Step 5). Among these steps, Step 4, intramolecular cyclization, is the rate-determining step based on the previous studies, in which activation of unsaturated bond by a metal site[12, 13]or formation of active hypoiodite (i.e., R-OI)[9] was conducted to enhance the reaction step. What it should be reminded is the discussion about the correlation between TOF and p*Ka* value of unsaturated alcohol in Fig. 4-2. Because the step

involving unsaturated alcohol itself (Steps 2 and 3) would not be assumed as the rate relevant step, as mentioned above, the observed correlation reflects the correlation between TOF and an intermediate derived from unsaturated alcohol, i.e., alkyl hydrogen carbonate acid intermediate (*AC**). The discussion assumes somewhat linear correlation between the p*Ka* values of unsaturated alcohols and corresponding alkyl hydrogen carbonate, and thus, practical comparison is necessary to confirm the estimation in the future.

According to the Scheme 4-4, formation rate of the unsaturated cyclic carbonate (r_{UCC}) is described as follows, which is proportional to the concentration of alkyl hydrogen carbonate intermediate (*AC**) on the methylated *N*-atom sites:

$$r_{UCC} = k_4[AC^*] \qquad (1)$$

where, k_4 is the rate constant for the formation of the intermediate. Equation 1 takes a new form after accounting for a quasi-equilibrated CO_2 adsorption (Step 1) and a pseudo steady-state hypothesis on the intermediates;

$$\frac{r_{UCC}}{[L]} = \frac{K_1 k_2 k_3}{k_3 + k_3'} \frac{[UA][CO_2]}{(1 + K_1[CO_2])} \qquad (2)$$

where $[L]$ is the total number of methylated N-atoms:

$$[L] = [*] + [CO_2^*] \qquad (3)$$

K_1 is the equilibrium constants for the adsorption of CO_2 and k_2, k_3 and k_3' is the rate constant for the interaction of unsaturated alcohol, the deprotonation to form an alkyl hydrogen carbonate acid-like intermediate and the deprotonation accompanying with the desorption of alkyl hydrogen carbonate acid, respectively. The obtained rate expression in equation (2) could explain the experimental results in Fig. 5. Compared with the previously proposed reaction mechanisms over other catalysts,[9, 12, 13] the formation of adsorbed alkyl hydrogen carbonate acid as an intermediate (*AC**) is newly proposed here. As described above, if the intermediate desorbs and forms alkyl hydrogen carbonate molecule, it will be easily self-decomposed into

CO_2 and unsaturated alcohol. Over MeNSBA-15 catalyst, the key is the formation of adsorbed state of alkyl hydrogen carbonate acid, which works effectively for the subsequent intramolecular cyclization reaction. The formation of the carbamate species is critical to the formation of the intermediate in its adsorbed state via the reaction with unsaturated alcohol.

The cases that other steps are the rate-determining step are also considered. According to Scheme 4-4, in the case step 1 is the rate-determining step, the unsaturated cyclic carbonate formation rate (r_{UCC}) is proportional to the number of CO_2 in liquid phase and open site:

$$r_{UCC} = k_1[CO_2][*] \qquad (1)$$

where k_1 is the rate constant for adsorption of CO_2 in liquid phase and [*] is the number of unoccupied methylated N-atoms. This rate equation gives other forms with using Equation (2):

$$[L] = [*] \qquad (2)$$

$$\frac{r_{UCC}}{[L]} = k_1[CO_2] \qquad (3)$$

Equations 3 do not explain the experimental data (Fig. 4-1) that shows r_{UCC} is proportional to the number of UA in liquid phase. Therefore, this step should not be rate-determining step.

In the case step 2 is the rate-determining step, the unsaturated cyclic carbonate synthesis rate (r_{UCC}) is proportional to concentration of UA in liquid phase and adsorbed CO_2 (carbamate,$[CO_2\ *]$) on the methylated N-atom sites:

$$r_{UCC} = k_2[\mathrm{UA}][CO_2^*] \qquad (1')$$

where k_2 is the rate constant for a nucleophilic attack from carbamate to unsaturated alcohol. Equation 4 takes a new form after accounting for quasi-equilibrated reactant adsorption in step1 with using pseudo steady-state hypothesis on the intermediate$[CO_2^*]$, assuming reverse reaction on step 2, using Equation 2':

$$[L] = [*] + [CO_2^*] \qquad (2')$$

$$\frac{r_{UCC}}{[L]} = K_1 k_2 \frac{[UA][CO_2]}{(1+K_1[CO_2])} \qquad (4)$$

$[L]$ is the total number of methylated N-atoms and K_1 is the equilibrium constants for the adsorption of CO_2. Equation 5 could mathematically explain the experimental results in Fig. 4-1. Therefore, this step should be rate-determining step.

In the case step 3 is the rate-determining step, the unsaturated cyclic carbonate formation rate (r_{UCC}) is proportional to concentration of alkyl hydrogen carbonate acid in liquid phase and the number of surface intermediate species:

$$r_{UCC} = k_2[\mathrm{AC}] \qquad (1'')$$

With using pseudo steady-state hypothesis on the intermediate$[AC]$, assuming reverse reaction on step 2, using Equation 1'' and accounting for quasi-equilibrated reactant adsorption in step 1, the rate equation 1'' gives another form:

$$r_{UCC} = K_1 k_2 k_3 \frac{[\mathrm{UA}][CO_2][L]}{k_3(1+K_1[CO_2])+k_{-2}[L]} \qquad (6)$$

We assume that self-cyclization of alkyl hydrogen carbonate is much slower than reverse reaction of step 2. ($k_3 \ll k_{-2}$) The rate equation 6 gives another form:

$$r_{UCC} = K_1 k_2 k_{-2}^{-1} k_3[\mathrm{UA}][CO_2] \qquad (7)$$

Equations 7 do not explain the experimental data (Fig. 4-1) that shows r_{UCC} hit the ceiling peak as a function of CO_2 partial pressure.

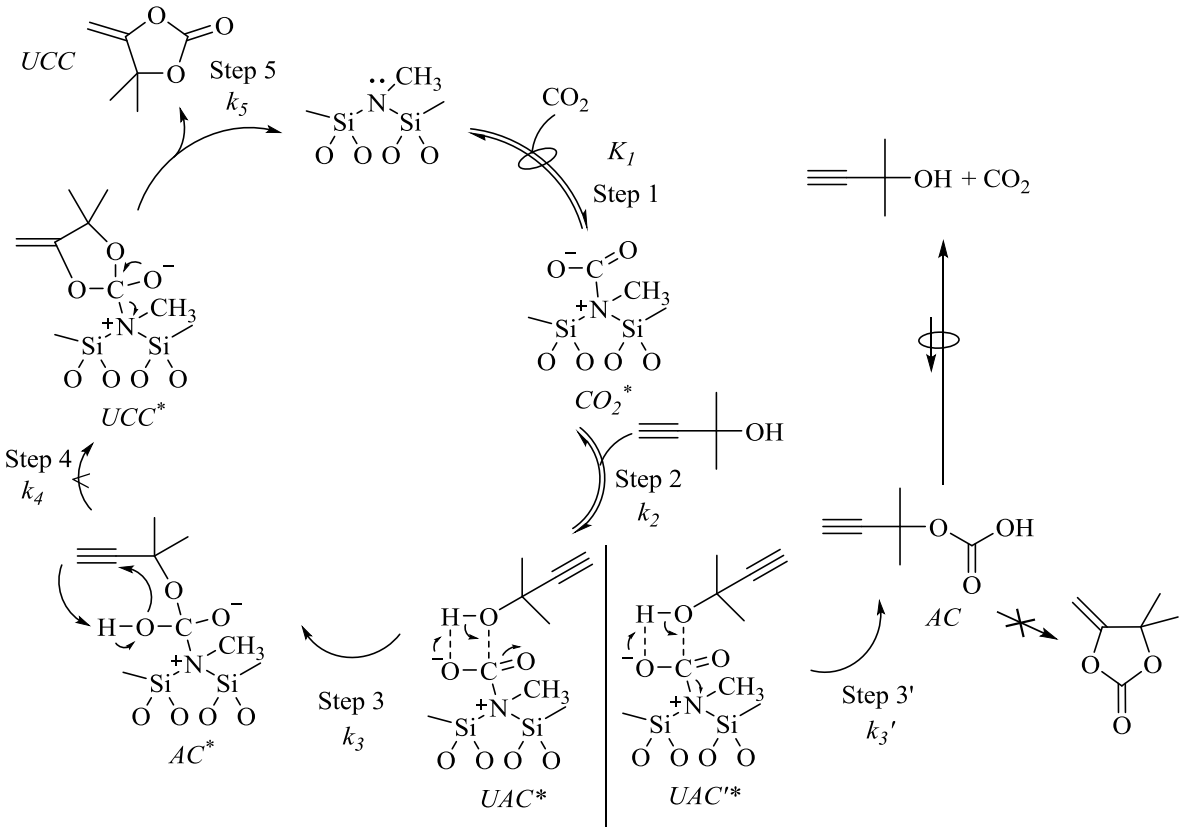

Scheme 4-4. Proposed sequence of reaction steps for cyclic carbonate synthesis from unsaturated alcohol (2-methyl-3-butyn-2-ol) on MeNSBA-15 catalyst

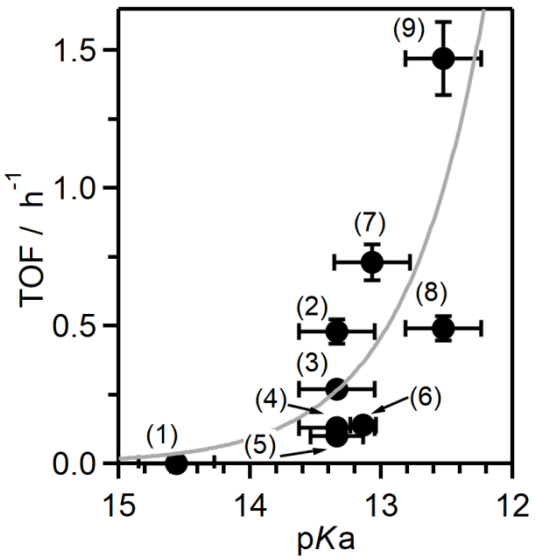

Figure 4-4. TOF values of cyclic carbonate synthesis with various unsaturated alcohols (Scheme 4-6) on MeNSBA-15 as a function of p*K*a of the alcohols. The numbers in parentheses are compatible with those shown in Scheme 4-6.

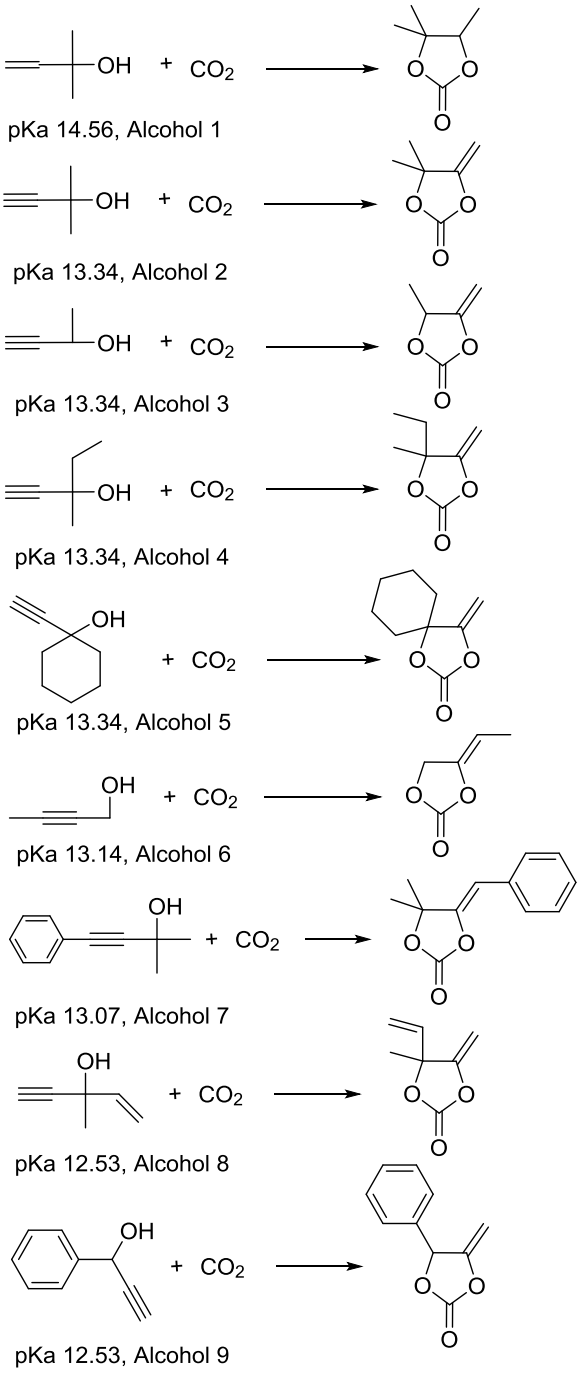

Scheme 4-5. Cyclic carbonate synthesis from CO_2 and unsaturated alcohol The numbers in Fig. 4-2 is compatible with the number shown here.

We also assume that cyclic carbonate synthesis from unsaturated alcohol initiated with abstraction of proton in unsaturated alcohol. Subsequently, nucleophilic addition reaction to CO_2 from alkoxide intermediate, proton-abstracted unsaturated alcohol, proceeds. Catalytic cycle is shown in Scheme 4-5. The rate expressions assuming all steps as rate-determining step is calculated.

1) **Case 1**: Step 1 is the rate-determining step.

In this case, adsorption of UA is the rate-determining step. The unsaturated cyclic carbonate formation rate (r_{UCC}) is proportional to the number of UA in liquid phase and open site:

$$r_{UCC} = k_1[\mathrm{UA}][*] \qquad (8)$$

where k_1 and k_2 is the rate constant for adsorption of UA and CO_2 in liquid phase and [*] is the number of unoccupied methylated N-atoms. This rate equation gives other forms with using Equation 9:

$$[L] = [*] \qquad (9)$$

$$\frac{r_{UCC}}{[L]} = k_1[\mathrm{UA}] \qquad (10)$$

Equations 10 do not explain the experimental data that shows r_{UCC} is related to concentration of CO_2 in liquid phase.

2) **Case 2**: Step 2 is the rate-determining step

In these cases, adsorption of CO_2 is the rate-determining step. Tthe unsaturated cyclic carbonate formation rate (r_{UCC}) is proportional to the number of CO_2 in liquid phase and open site:

$$r_{UCC} = k_2[\mathrm{CO_2}][*] \qquad (8')$$

where k_2 is the rate constant for adsorption of CO_2 in liquid phase and [*] is the number of unoccupied methylated N-atoms. Accounting for quasi-equilibrated reactant adsorption in step 1,

this rate equation gives other forms with using Equation 9' and 10:

$$[L] = [*] + [H*] \qquad (9')$$

$$[H*] = \sqrt{K_1[\mathrm{UA}][*]} \qquad (10)$$

$$r_{UCC} = \frac{1}{4} k_2 [\mathrm{CO_2}] \left(\sqrt{K_1[\mathrm{UA}] + 4[L]} - \sqrt{K_1[\mathrm{UA}]} \right)^2 \qquad (11)$$

Equations 11 do not explain the experimental data that shows r_{UCC} is proportional to concentration of UA in liquid phase.

3) **Case 3**: Step 3 is the rate-determining step

In this case, formation of carbonate intermediate is the rate-determining step. The unsaturated cyclic carbonate formation rate (r_{UCC}) is proportional to concentration of $\mathrm{UA^-}$ in liquid phase and the number of surface intermediate species:

$$r_{UCC} = k_3 [\mathrm{UA^-}][CO_2^*] \qquad (8'')$$

where k_3 is the rate constant for formation of carbonate intermediate in liquid phase. Accounting for quasi-equilibrated reactant adsorption in step 1 and 2, this rate equation gives other forms with using Equation 9'' and 10:

$$[L] = [*] + [\mathrm{H}*] + [CO_2^*] \qquad (9'')$$

and accounting for quasi-equilibrated reactant adsorption in step 1, the rate equation 8'' gives another form:

$$\frac{r_{UCC}}{[L]} = K_2 k_3 \frac{[CO2]\sqrt{K_1[UA]}\left(\sqrt{K_1[UA]+4(1+K_2[CO2])[L]} - \sqrt{K_1[UA]}\right)^3}{8(1+K_1[CO_2])^3} \qquad (12)$$

This equation 12 could not mathematically explain the experimental results in Figure 4-1.

4) **Case 4**: Step 4 is the rate-determining step

In this case, self-cyclization of carbonate intermediate is the rate-determining step. Thus, the

unsaturated cyclic carbonate formation rate (r_{UCC}) is proportional to concentration of intermediate 1 (Im1) in liquid phase:

$r_{UCC} = k_4[\mathrm{Im1}]$ (8’’’)

where k_4 is the rate constant for self-cyclization of carbonate intermediate in liquid phase. Accounting for steady-state approximation of Im1, Equation 8, and quasi-equilibrated reactant adsorption in step 1 and 2, this rate equation gives other forms with using Equation 9’’ and 10:

$k_3[\mathrm{UA^-}][CO_2^*] - k_4[\mathrm{Im1}] - k_{-3}[\mathrm{Im1}] = 0$ (13)

and accounting for quasi-equilibrated reactant adsorption in step 1, the rate equation (8’’’) gives another form:

$\frac{r_{UCC}}{[L]} = K_2 k_3 \frac{[CO2]\sqrt{K_1[UA]}(\sqrt{K_1[UA]+4(1+K_2[CO2])[L]}-\sqrt{K_1[UA]})^3}{8(k_4+k_{-3})(1+K_1[CO_2])^3}$ (14)

This equation 14 could not mathematically explain the experimental results in Figure 4-1.

5) **Case 5**: Step 5 is the rate-determining step

In this case, proton acquisition of intermediate 2 (Im2) is the rate-determining step. Thus, the unsaturated cyclic carbonate formation rate (r_{UCC}) is proportional to concentration of intermediate 2(Im2) in liquid phase and the number of MeNSBA-15 that possesses proton:

$r_{UCC} = k_5[\mathrm{Im2}][\mathrm{H}*]$ (8’’’)

where k_5 is the rate constant for in liquid phase. Accounting for steady-state approximation of Im1 and Im2, Equation 13 and 14, and quasi-equilibrated reactant adsorption in step 1 and 2, this rate equation gives other forms with using Equation 9’’ and 10:

$k_4[\mathrm{Im1}] - k_5[\mathrm{Im2}][H*] = 0$ (14)

and accounting for quasi-equilibrated reactant adsorption in step 1, the rate equation 8’’’ gives another form:

$$\frac{r_{UCC}}{[L]} = K_2 k_3 \frac{[CO2]\sqrt{K_1[UA]}(\sqrt{K_1[UA]+4(1+K_2[CO2])[L]}-\sqrt{K_1[UA]})^3}{8(k_4+k_{-3})(1+K_1[CO_2])^3} \quad (15)$$

This equation 15 could mathematically explain the experimental results in Figure 4-1.

Above discussion led that this reaction proceeds according to the Eley–Rideal mechanism on MeNSBA-15. CO_2 adsorbed on MeNSBA-15 is activated and attacks hydrogen of hydroxyl group in the unsaturated alcohol, and subsequently alkyl hydrogen carbonate acid intermediate forms. This intermediate is cyclized by nucleophilic attack and forms unsaturated cyclic carbonate (UCC).

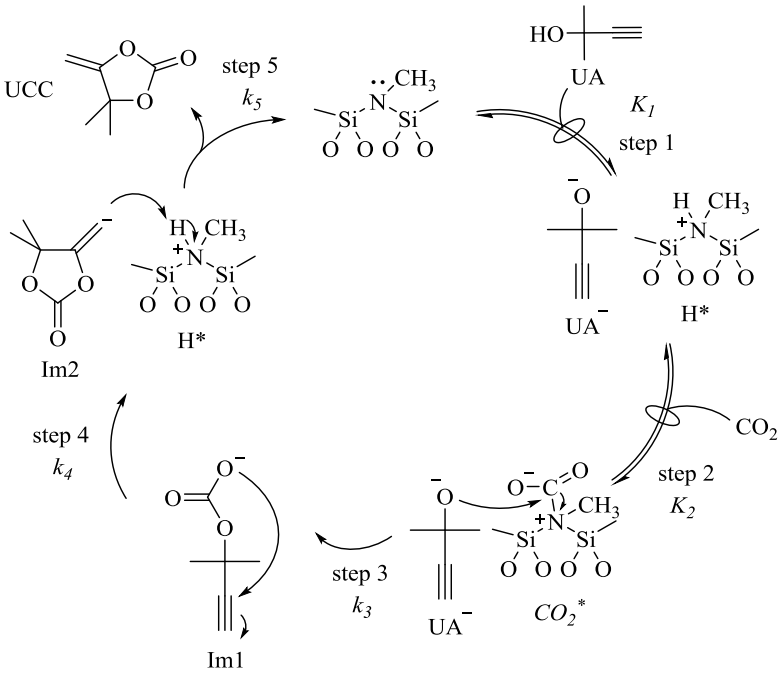

Scheme 4-6. Estimated sequence of reaction steps via proton abstraction reaction for cyclic carbonate synthesis from unsaturated alcohol (UA) on MeNSBA-15.

4.5 TOF tendency from various unsaturated alcohol

The hydroxyl groups in the unsaturated alcohols could be deprotonated by the basic sites of both nitrogen and methylated nitrogen sites). Figure 4-2 shows the TOF of the reaction using different types of unsaturated alcohols as a function of their p*Ka* values. The tested unsaturated alcohols and resulting cyclic carbonates are summarized in Scheme 4-6. The measured TOF increased with the decrease of p*Ka* values. This suggested that the deprotonation from these alcohols or that from intermediate derived from the alcohols reflecting their structural properties would be a rate relevant step. The p*Ka* values of these reactants were roughly ranged from 12.5 to 14.5. Interestingly, it has been known that hydrogen in a methylene group of the active methylene compound with p*Ka* value of around 13 could be deprotonated even by non-methylated nitrogen site, demonstrated as a reactant of Knoevenagel reactions.[22-25] As the plausible active site in the current study is a more basic methylated nitrogen site, deprotonation from hydroxyl group of unsaturated alcohols would be more possible and plausible. Again, the reaction, however, did not proceed over NSBA-15 catalyst (Table 1), indicating the methylation was critical for catalyzing the reaction. Therefore, it can be assumed that deprotonation of the unsaturated alcohol or the intermediate derived from the alcohol by another nucleophile is involved in the rate relevant step although that by surface nitrogen sites can be excluded from the case. Therefore, the deprotonation step relevant to the reaction rate should be written in another scheme (i.e., by another nucleophile), and that by the oxygen atom in the carbamate (i.e., activated CO_2 formed on methylated nitrogen) would be the most plausible. Based on this assumption, a metathesis-like reaction between non-adsorbed unsaturated alcohol and carbamate on the site may proceed, i.e., a deprotonation from hydroxyl group by oxygen in CO_2 and a simultaneous C–O bond formation between oxygen in hydroxyl group and carbon in CO_2

4.6 Conclusions

MeNSBA-15 was shown to catalyze cyclic carbonate synthesis from CO_2 and unsaturated alcohol. The changes in the TOF as a function of CO_2 partial pressure and 2-methyl-3-butyn-2-ol concentration reflect the change in the major active surface species. The difference of pressure dependence of two cyclic carbonate syntheses can be explained by the competing activation of reactants. The interaction of the methylated nitrogen site with unsaturated alcohol would be much lower compare to that with cyclic ether. The reaction involves the following three steps; 1) carbamate formation via CO_2 adsorption on the methylated nitrogen atom 2) interaction of unsaturated alcohol with the carbamate species, 3) deprotonation and simultaneous C–O bond formation between the carbamate and unsaturated alcohol species to form an alkyl hydrogen carbonate acid-like intermediate, 4) intramolecular cyclization of the intermediate between hydroxyl and alkyne groups to form an adsorbed cyclic carbonate, and 5) desorption of the unsaturated cyclic carbonate. The obtained rate expression supported the reaction mechanism and it does not contradict with the previous studies.

1. Fournier, J.; Bruneau, C.; Dixneuf, P. H., *Tetrahedron Letters* **1990,** 31 (12), 1721-1722.

2. Bruneau, C.; Dixneuf, P. H., *Journal of Molecular Catalysis* **1992,** 74 (1-3), 97-107.

3. Costa, M.; Chiusoli, G. P.; Rizzardi, M., *Chemical Communications* **1996,** (14), 1699-1700.

4. Gu, Y. L.; Zhang, Q. H.; Duan, Z. Y.; Zhang, J.; Zhang, S. G.; Deng, Y. Q., *Journal of Organic Chemistry* **2005,** 70 (18), 7376-7380.

5. Li, J. Y.; Song, Q. W.; Zhang, H. X.; Liu, P.; Zhang, K.; Wang, J. W.; Zhang, D. S., *Tetrahedron* **2019,** 75 (15), 2343-2349.

6. Toullec, P.; Martin, A. C.; Gio-Batta, M.; Bruneau, C.; Dixneuf, P. H., *Tetrahedron Letters* **2000,** 41 (29), 5527-5531.

7. Fournier, J.; Bruneau, C.; Dixneuf, P. H., *Tetrahedron Letters* **1989,** 30 (30), 3981-3982.

8. Besse, V.; Camara, F.; Voirin, C.; Auvergne, R.; Caillol, S.; Boutevin, B., *Polymer Chemistry* **2013,** 4 (17), 4545-4561.

9. Minakata, S.; Sasaki, I.; Ide, T., *Angewandte Chemie-International Edition* **2010,** 49 (7), 1309-1311.

10. Inoue, Y.; Ishikawa, J.; Taniguchi, M.; Hashimoto, H., *Bulletin of the Chemical Society of Japan* **1987,** 60 (3), 1204-1206.

11. Inoue, Y.; Ohuchi, K.; Imaizumi, S., *Tetrahedron Letters* **1988,** 29 (46), 5941-5942.

12. Kikuchi, S.; Yoshida, S.; Sugawara, Y.; Yamada, W.; Cheng, H. M.; Fukui, K.; Sekine, K.; Iwakura, I.; Ikeno, T.; Yamada, T., *Bulletin of the Chemical Society of Japan* **2011,** 84 (7), 698-717.

13. Buzas, A. K.; Istrate, F. M.; Gagosz, F., *Tetrahedron* **2009,** 65 (9), 1889-1901.

14. Dharman, M. M.; Choi, H. J.; Park, S. W.; Park, D. W., *Topics in Catalysis* **2010,** 53 (7-10), 462-469.

15. Kim, D. W.; Kim, D. K.; Kim, M. I.; Park, D. W., *Catalysis Today* **2012,** 185 (1), 217-223.

16. Gu, Y. L.; Shi, F.; Deng, Y. Q., *Journal of Organic Chemistry* **2004,** 69 (2), 391-394.

17. Zhao, D. B.; Wu, M.; Kou, Y.; Min, E., *Catalysis Today* **2002,** 74 (1-2), 157-189.

18. Han, L.; Park, S. W.; Park, D. W., *Energy & Environmental Science* **2009,** 2 (12), 1286-1292.

19. Yamazaki, K.; Moteki, T.; Ogura, M., *Molecular Catalysis* **2018,** 454, 38-43.

20. Ogura, M.; Fukuzawa, S.; Fukunaga, S.; Yamazaki, H.; Kondo, J. N.; Morimoto, M.; Guillet-Nicolas, R.; Thommes, M., *Langmuir* **2018,** 34 (4), 1376-1385.

21. Jessop, P. G.; Subramaniam, B., *Chemical Reviews* **2007,** 107 (6), 2666-2694.

22. Sugino, K.; Oya, N.; Yoshie, N.; Ogura, M., *Journal of the American Chemical Society* **2011,** 133 (50), 20030-20032.

23. Hasegawa, T.; Krishnan, C. K.; Ogura, M., *Microporous and Mesoporous Materials* **2010,** 132 (1-2), 290-295.

24. Singh, B.; Mote, K. R.; Gopinath, C. S.; Madhu, P. K.; Polshettiwar, V., *Angewandte Chemie-International Edition* **2015,** 54 (20), 5985-5989.

25. Bouhrara, M.; Ranga, C.; Fihri, A.; Shaikh, R. R.; Sarawade, P.; Emwas, A. H.; Hedhili, M. N.; Polshettiwar, V., *Acs Sustainable Chemistry & Engineering* **2013,** 1 (9), 1192-1199.

5 Consideration of the cyclic carbonate synthesis by quantum chemical calculation

5.1 Introduction

Quantum mechanics has been established in the beginning of 20th century. Microscopic behavior of atom or molecule was found to obey the Schrödinger equation[1]. However, almost all the equation of polyatomic molecule is too complex to be solved if the mechanics strictly applied to polyatomic molecule. Therefore, the mechanics could not develop chemistry for long time.

Theoretical chemists have tried to develop approximate methods to handle the equation by computer and Quantum chemistry is established as study of approximate methods. Progress of computing speed and quality has developed Quantum chemistry. Currently, properties of material and activity can be estimated by only calculation without any experiments. This field is called computational chemistry in contrast to experimental chemistry.

Computational chemistry includes other three types of calculation method in a broad sense. First, dynamic process is estimated based on classical mechanics and it is called molecular dynamics[2]. Second, equilibrium state of molecular assembly is expressed using random number and it is called Monte Carlo Method[3]. Third, properties of materials are predicted by database of similar materials and it is called Quantitative Structure−Activity Relationship (QSAR)[4]. In this study, computational chemistry focuses on quantum chemical calculation.

5.1.1 Molecular orbital theory

Molecular orbital method is approximate solution of the Schrödinger equation of electron in molecule[5-11]. The Schrödinger equation of many-electron wave function is transformed to the one of the product of one-electron wave functions via one-electron approximation. It is called the Hartree-Fock equation[12, 13]. Hartree-Fock equation leads set of one-electron orbital which

constitutes the best approximation of the ground state.

Molecular orbital method is divided into ab initio molecular orbital method, semi-empirical orbital method, extended Hückel method[14, 15]. In 1960s, ab initio molecular orbital method could be applied for only small molecule because computing performance was very low. In semi-empirical orbital method, experimental material properties have supported the calculation to enlarge application scope of the method. Both ab initio and semi-empirical orbital method is developing with improvement of computer performance.

5.1.2 Hartree-Fock(HF) method

The famous representative ab initio molecular orbital method is Hartree-Fock method[12, 13]. Almost all Molecules have multiple electrons and Coulomb repulsion interaction occurs between electrons in molecule. Many-electron wave function which reflects the interaction strictly cannot be identified. Harteree Fock method treats the interaction with adequate approximation and this approximation is called the orbital approximation, one-electron approximation or Hartree-Fock approximation.

Generally, many-electron wave function is defined as the product of one-electron wave functions. The product is called the Hartree product. However, the Hartree product does not consider the fundamental nature of electrons, Pauli Exclusion Principle[16]. The Hartree product is alternated to Slater determinant[11] to reflect Pauli Exclusion Principle. Slater determinant is linear combination of the Hartree product. Slater determinant expresses electronic structure of molecules and the equation that determines Slater determinant is called the Hartree-Fock equation.

Electrons in molecules generate Coulomb field and stabilized in the Coulomb field simultaneously. Therefore, electron orbital that generate Coulomb field is required to match

with electron orbital determined by the Hartree-Fock equation. Analytical solution of the Hartree-Fock equation does not exist for this reason. However, computational techniques are available that give very detailed and reliable numerical solutions for the wave functions and energies. The Hartree-Fock equation gives another form and can be treated as eigenvalue equation with calculating Fock operator from initial electron orbital. Fock operator is approximation of one-electron Hamiltonian. Fock operator considers Coulomb repulsion approximated in mean field and does not consider electron correlation[17]. In general, improved set of orbitals are obtained by solving the eigenvalue equation derived from initial electron orbitals and used in another cycle of calculation. And a second improved set of orbitals is obtained. The recycling continues until the orbitals and energies obtained are insignificantly different from those used at the start of the current cycle. The solutions are then self-consistent and accepted as solutions of the equation. When the set of orbitals converges, Self-Consistent Field is established.

5.1.3 Møller–Plesset perturbation(MP) method

In general, motions of particles cannot be clarified analytically when interactions of more than three particles is considered. This problem is called N-body problem. Perturbation theory is one of approximation for getting approximate solution of N-body problem. In HF method, interaction of electrons, which is called electron correlation, is not considered. Møller–Plesset perturbation method improves such HF method and estimates the effect of electron correlation based on perturbation theory.

In MP method, approximate solution of the Schrödinger equation is regarded to be composed of member which can be strictly calculated (Non-perturbation member) and small correction member (perturbation member). The procedures of MP method are as follows; First,

Hamiltonian ($\widehat{H}$) in the Schrödinger equation is expressed by linear combination of two species, non-perturbation member and perturbation member:

$$\widehat{H} = \widehat{H_0} + \lambda\widehat{W}$$

Next, energy of whole electrons and wave function are expressed by the Hamiltonian using Tailor expansion.

5.1.4 Density functional theory (DFT)

DFT is a computational quantum mechanical modelling method to calculate the energy of the electrons of many-body systems, in particular atoms, molecules from. Using this theory, the properties of a many-electron system can be estimated by using functionals, which in this case is the spatially dependent electron density. Hohenberg and Kohn proved that the spatially dependent electron density determine ground state and the electron energy of the system. The energy of the system is the eigenvalue of the Schrödinger equation and the sum of physical, coulomb, exchange and relation energy.

DFT has been known well for calculations in solid-state physics since the 1970s. However, DFT was not considered accurate enough for calculations in quantum chemistry until the 1990s, when the approximations used in the theory were greatly refined to better model the exchange and correlation interactions. The time required for the calculation is smaller than HF method and DFT is known as simple estimation of the energy and widely used. DFT is among the most popular and versatile methods available in condensed-matter physics, computational physics, and computational chemistry.

Despite recent improvements, some difficulties still remain in using density functional theory. It is noteworthy that Hohenberg and Kohn did not lead strict function of the each energy member. Therefore, the accuracy and credibility of Hamiltonian is inferior to HF or MP method.

Especially, intermolecular interactions (of critical importance to understanding chemical reactions), van der Waals forces, charge transfer excitations, transition states and global potential energy surfaces are difficult to describe properly. The incomplete treatment of dispersion can adversely affect the accuracy of DFT. The development of new DFT methods designed to overcome this problem, by alterations to the functional[18] or by the inclusion of additive terms,[19-22] is a current research topic.

5.1.5 Basis function

The Schrödinger equation of many-electron wave function is transformed to the one of the product of one-electron wave functions via one-electron approximation in molecular orbital method. Basis function is used to express molecular orbital. Molecular orbital is expressed by linear combination of basis functions:

$$\psi_i(\mathbf{r}) = \sum_{\mu=1}^{N} C_{\mu i}\varphi_\mu(\mathbf{r})$$

where, $C_{\mu i}$ is molecular orbital constant showing contribution of μ-th basis function to i-th molecular orbital, $\mathbf{r}$ is position coordinates of the electrons and N is the amount of basis functions. The accuracy of the calculation is improved with increasing N, however the time required for the calculation also increase. Therefore Basis function which expressed molecular orbital accurately with fewer N is desirable. Thus, molecular orbital is shown by linear combination of atom of atomic orbitals and this method is called LCAO-MO (Linear Combination of Atomic Orbitals-Molecular Orbital).

Basis function is based on the solution of the Schrödinger equation over hydrogen atom, which is strictly calculated.

5.2 Clarification of energy diagram in cyclic carbonate synthesis

The formation of carbamate intermediate and interaction of MeNSBA-15 and unsaturated alcohol were considered by ab initio molecular orbital calculation (MP2/6-31g(d) or MP2/6-31+g(d,p) over Gaussian16) In the proposed reaction mechanism in Chapter 3 and 4, adsorbed cyclic ether and solved unsaturated alcohol in DMF were involved, respectively. The interaction of unsaturated alcohol with methylated N-atom is, however, also probable. Therefore, heat of reaction between critical states in cyclic carbonate synthesis from unsaturated alcohol was calculated to consider the interaction of unsaturated alcohol with methylated N-atom.

Figure 5-1 shows potential energy of critical state in cyclic carbonate synthesis from unsaturated alcohol. Almost all unsaturated alcohol seems to be extracted proton in hydroxyl groups because CO2 adsorption on MeNSBA-15 is endothermic process on the other hand proton extraction on MeNSBA-15 is exothermic process. However, it is difficult to form cyclic carbonate via proton extraction because formation of alkylcarboxylic anion is required several times larger energy than formation of carbamate intermediate. Therefore, it seems that this reaction proceeds via formation of carbamate intermediate as mentioned in Chapter 4.

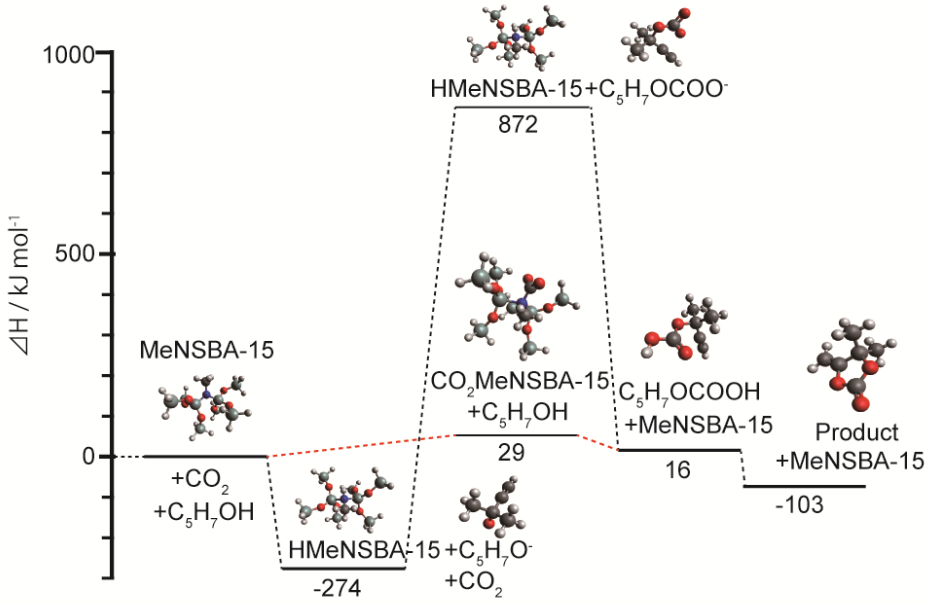

Figure 5-1. Potential energy diagram of cyclic carbonate synthesis from unsaturated alcohol on MeNSBA-15.Light gray=Si, deep gray=C, Red=O, White=H, Blue=N.

5.3 Conclusions

The differences of reaction mechanism might be explained by the difference of maximum energy barrier derived from the higher potential energy state of alkylcarboxylic anion. CO_2 adsorbs on MeNSBA-15 and forms carbamate intermediate via endothermic process, and formed bent conformation. This bent CO_2 is unstable and more active than gaseous CO_2, which is a linear molecule. Therefore, it seems that MeNSBA-15 catalyze both two cyclic carbonate syntheses by forming bent CO_2

1. Schrodinger, E., *Physical Review* **1926,** 28 (6), 1049-1070.

2. Alder, B. J.; Wainwright, T. E., *Journal of Chemical Physics* **1959,** 31 (2), 459-466.

3. Binder, K., *Topics in Applied Physics* **1992,** 71, 1-22.

4. Cherkasov, A.; Muratov, E. N.; Fourches, D.; Varnek, A.; Baskin, II; Cronin, M.; Dearden, J.; Gramatica, P.; Martin, Y. C.; Todeschini, R.; Consonni, V.; Kuz'min, V. E.; Cramer, R.; Benigni, R.; Yang, C. H.; Rathman, J.; Terfloth, L.; Gasteiger, J.; Richard, A.; Tropsha, A., *Journal of Medicinal Chemistry* **2014,** 57 (12), 4977-5010.

5. Hartree, D. R., *Proceedings of the Cambridge Philosophical Society* **1928,** 24, 89-110.

6. Hartree, D. R., *Proceedings of the Cambridge Philosophical Society* **1928,** 24, 111-132.

7. Hartree, D. R., *Proceedings of the Cambridge Philosophical Society* **1928,** 24, 426-437.

8. Slater, J. C., *Physical Review* **1928,** 32 (3), 0339-0348.

9. Hund, F., *Zeitschrift Fur Physik* **1926,** 36 (9/10), 657-674.

10. Mulliken, R. S., *Physical Review* **1927,** 29 (5), 0637-0649.

11. Slater, J. C., *Physical Review* **1929,** 34 (10), 1293-1322.

12. Fock, V., *Zeitschrift Fur Physik* **1930,** 61 (1-2), 126-148.

13. Slater, J. C., *Physical Review* **1930,** 35 (2), 0210-0211.

14. Huckel, E., *Zeitschrift Fur Physik* **1930,** 60 (7-8), 423-456.

15. Hoffmann, R., *Journal of Chemical Physics* **1963,** 39 (6), 1397-&.

16. Pauli, W., *Zeitschrift Fur Physik* **1925,** 31, 765-783.

17. Lowdin, P. O., *Physical Review* **1955,** 97 (6), 1509-1520.

18. Grimme, S., *Journal of Chemical Physics* **2006,** 124 (3), 16.

19. Zimmerli, U.; Parrinello, M.; Koumoutsakos, P., *Journal of Chemical Physics* **2004,** 120 (6), 2693-2699.

20. Grimme, S., *Journal of Computational Chemistry* **2004,** 25 (12), 1463-1473.

21. von Lilienfeld, O. A.; Tavernelli, I.; Rothlisberger, U.; Sebastiani, D., *Physical Review Letters* **2004,** 93 (15), 4.

22. Tkatchenko, A.; Scheffler, M., *Physical Review Letters* **2009,** 102 (7), 4.

6 General Conclusions

6.1 Summary in this study

In this dissertation, methylated nitrogen-substituted SBA-15(MeNSBA-15) was applied as a catalyst in some cyclic carbonate syntheses. The catalysis of MeNSBA-15 in the CO_2 transformation is clarified in order to elucidate mechanisms of CO_2 activation and lay out theoretical plan for development of catalyst for CO_2 transformation. The best laid plan let us select an optimal catalyst for each CO_2 transformation catalyzed by an acid or base function.

In Chapter 3 MeNSBA-15 was shown to catalyze cyclic carbonate synthesis from cyclic ethers and CO_2 for the first time. It catalyzed the reaction without the need for pretreatments. The observation of a drastic increase in the TOF value after the methylation process clearly indicated that the reactivity of the catalyst (i.e., nucleophilicity of the basic N-atom) was enhanced by methylation. The kinetic analysis revealed Langmuir–Hinshelwood mechanism, rather than Eley–Rideal mechanism, with a kinetically relevant bimolecular reaction step between a ring-opened alkoxide intermediate and a carbamate over neighboring methylated nitrogen pair sites. It is further assumed that the silanol of MeNSBA-15 would work as a weak Lewis acid and synergistically stabilize the alkoxide intermediate. The comparison of the observed TOF with the oxygen proton affinity of cyclic ethers over MeNSBA-15 and TBABr further supported the different reaction mechanisms among MeNSBA-15 and the conventional homogeneous catalysts. The detailed understanding of the fundamental reaction mechanism would lead to a rational design of catalysts.

In Chapter 4, MeNSBA-15 was shown to catalyze cyclic carbonate synthesis from CO_2 and unsaturated alcohol. The changes in the TOF as a function of CO_2 partial pressure

and 2-methyl-3-butyn-2-ol concentration reflect the change in the major active surface species. The difference of pressure dependence of two cyclic carbonate syntheses can be explained by the competing activation of reactants. The interaction of the methylated nitrogen site with unsaturated alcohol would be much lower compare to that with cyclic ether. The reaction involves the following three steps; 1) carbamate formation via CO_2 adsorption on the methylated nitrogen atom 2) interaction of unsaturated alcohol with the carbamate species, 3) deprotonation and simultaneous C–O bond formation between the carbamate and unsaturated alcohol species to form an alkylcarboxylic acid-like intermediate, 4) intramolecular cyclization of the intermediate between hydroxyl and alkyne groups to form an adsorbed cyclic carbonate, and 5) desorption of the unsaturated cyclic carbonate. The obtained rate expression supported the reaction mechanism and it does not contradict with the previous studies.

In Chapter 5, The differences of reaction mechanism might be explained by the difference of maximum energy barrier derived from the higher potential energy state of alkylcarboxylic anion. CO_2 adsorbs on MeNSBA-15 and forms carbamate intermediate via endothermic process, and formed bent conformation. This bent CO_2 is unstable and more active than gaseous CO_2, which is a linear molecule. Therefore, it seems that MeNSBA-15 catalyze both two cyclic carbonate syntheses by forming bent CO_2

Through the studies in the dissertation, it was found that the reaction mechanism of cyclic carbonate synthesis from CO_2 and propylene oxide was the Langmuir-Hinshelwood mechanism and the reaction mechanism of cyclic carbonate synthesis from CO_2 and unsaturated alcohol was the Eley-Rideal mechanism. MeNSBA-15 catalyzes both two cyclic carbonate syntheses by forming a bent CO_2. The bent CO_2 seems unstable and more active than a linear-shaped CO_2.

For development of a solid base catalyst for CO_2 transformation, this dissertation indicates that solid material is required to adsorb CO_2 with endothermic process for CO_2 activation.

Acknowledgements

I appreciate Professor Masaru Ogura and Assistant Professor Takahiko Moteki for their supervising my doctoral dissertation. And I thank all members in ogura Lab. for their helping in various situations.

In the Chapter 5, I thank supervisor Dr. Hiroshi Ushiyama and the supercomputer system ITO in Kyushu University.